Department Chemie und Pharmazie

FRIEDRICH-ALEXANDER UNIVERSITÄT ERLANGEN-NÜRNBERG
NATURWISSENSCHAFTLICHE FAKULTÄT

On the Adsorption Behavior of Different Porphyrinoids on Cu(111):

a Comparative Scanning Tunneling Microscopy Study

Adsorptionsverhalten unterschiedlicher Porphyrinoide auf Cu(111):

Eine vergleichende STM Studie

Der Naturwissenschaftlichen Fakultät
der Friedrich-Alexander-Universität Erlangen-Nürnberg

zur Erlangung des Doktorgrades Dr. rer. nat.

vorgelegt von

Michael Stark

aus Ansbach

Als Dissertation genehmigt von der Naturwissenschaftliche Fakultät
der Friedrich-Alexander-Universität Erlangen-Nürnberg

Tag der mündlichen Prüfung:

Vorsitzender des Promotionsorgans:	Prof. Dr. Jörn Wilms
Gutachter:	PD Dr. Hubertus Marbach
	Prof. Dr. Alexander Schneider

Table of Contents

1 Introduction

1.1 Motivation

Miniaturization is one of the most prominent buzzwords in modern technology and is closely related to nanotechnology. The term nanotechnology basically refers to the fabrication, development, manipulation and utilization of well-defined structures with dimensions smaller than 100 nm.[1]

The main aim of the miniaturization process is to increase the density of functional elements[2-4], and/or to access new areas of physical or chemical properties and functionalities, like antibacterial paint[5-7] or self-cleaning coatings[8-9]. The miniaturization trend can be illustrated by Moore's law which quantitatively states that the number of transistors per area of integrated circuits doubles every two years.[10] Miniaturization can be achieved in two ways: the top-down approach is probably up to now the industrial more relevant one and is technically realized via lithographic methods. As the minimum size of these structures and devices further decreases and reaches the molecular or atomic level, the second strategy, the so-called bottom-up approach becomes more and more important.

In the bottom-up approach, the fabrication of nanostructures is mainly targeted by the self-assembly or controlled manipulation of basic building blocks like atoms or molecules. One main strategy of the bottom-up approach is inspired by a basic principle found in nature, which is the molecular recognition and results in the mentioned self-assembly. For self-assembling systems, the formation of desired nanostructures out of the basic building blocks occurs by a spontaneous assembly of the latter, due to the mutual interactions in-between all involved building blocks. This opens up the perspective for tailoring functionalities of supramolecular architectures. In order to do so, a detailed understanding of the underlying processes during self-assembly is vital, and suitable means to investigate the self-assembly are required. For the detailed characterization of adsorbates on surfaces, the scanning tunneling microscope (STM), invented in 1982 by G. Binnig and H. Rohrer[11-12], has proven to be a very powerful tool.

Currently, a vivid branch of science focuses on the research of molecular building-blocks with easily tunable electronic and chemical properties. Within the different molecule classes that match this description, porphyrinoids seems to be particularly promising for several reasons like a high thermal stability, allowing for intact sublimation of the molecules, well investigated and established synthesis routes, and the large variety of intrinsic functionalities.

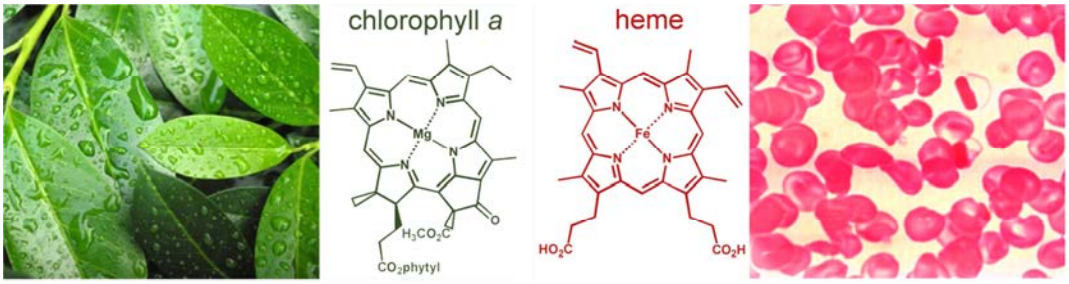

Figure 1.1: *Illustration of the two most prominent metalloporphyrins in nature. Modified from* [13].

The versatility of porphyrinoids is also documented by their abundance in nature as main functional building blocks in biological systems. The two most prominent functions of porphyrins in nature are shown in Figure 1.1. These are iron porphyrin as the main functional building block of hemoglobin (shown on the right side of Figure 1.1), enabling the oxygen transport in the blood stream of mammals, while magnesium porphyrin is responsible for light harvesting in chlorophyll *a* (shown on the left side of Figure 1.1). Thereby the functionalities of the porphyrins are largely determined by the central metal atom, the attached substituents, and the chemical environment.[14]

This thesis aims to expand the knowledge and understanding of the adsorption behavior and formation of supramolecular aggregates on surfaces by analyzing the different interactions occurring in the investigated systems by STM. In particular, the structures formed on a Cu(111) surface upon adsorption of free-base tetrephenylporphyrin (2HTPP), free-base tetraphenylporphycene (2HTPPc), free-base and Co tetrakisditertbutylphenylporphyrin (2HTTBPP and CoTTBPP) were studied in detail. Besides an analysis of molecular conformations and interactions at room temperature (RT), the temperature and coverage dependent changes of the systems have been investigated with a particular focus on surface diffusion, molecular rotation, disorder-order transition, conformational changes, molecular dynamics and chemical modification of the molecules.

1.2 Literature Review

One of the main topics of interest concerning the investigation of structures fabricated with the bottom-up approach is the detailed understanding of the factors influencing the molecular self-assembly. Molecular self-assembly is defined as the "spontaneous association of molecules under equilibrium conditions into stable, structurally well-defined aggregates joined by non-covalent bonds".[15]

In order to gain this understanding, molecular self-assembly on well-defined single crystalline surfaces is studied to identify the specific molecule-substrate interactions, as well as the corresponding intermolecular interactions. Thereby, the conformation of the molecule, its chemical structure and the influence of the substrate were major points of interest and intensively investigated in the past.[16-26] In this context, porphyrins and tetrapyrroles in general received much attention by scientists due to the outstanding properties these classes of molecules exhibit.[16, 27-30] In this respect, properties like the coordination of a large variety of different metal atoms to the center of the macrocycle, as well as the possibility to attach various functional groups to the meso- and β-positions of the molecules lead to a wide range of different electronic, steric and chemical properties, which can be tailored in a controlled manner.[16, 18-19, 31] So far, the present understanding of porphyrinoids was used to design porphyrin-based applications like biosensors[32], molecular electronics[33], surface functionalization[34], and heterogeneous asymmetric catalysis[35].

In most cases, porphyrinoids adsorb in a geometry where the plane of the macrocycle is oriented parallel to the surface.[19] Despite this general trend, numerous investigations showed that the substituents attached to the macrocycle strongly influence the self-assembly of supramolecular aggregates of porphyinoids. For example, although 2H-tetraphenylporphyrin (2HTPP) and 2H-tetrapyridylporphyrin (2HTPyP) exhibit only subtle differences in their chemical structure, i.e. in the periphery of the molecule one carbon atom per substituent is replaced by a nitrogen atom, this modification results in substantially different supramolecular arrangements when adsorbed on Ag(111): while 2HTPP forms square ordered domains[36], 2HTPyP forms hexagonal arrangements[37]. This demonstrative example

proofs the sensitivity of the adsorption behavior towards subtle structural changes of the molecule and offers a route for tailoring these properties.

Another important factor influencing the adsorption behavior of molecules, and thus the resulting supramolecular assembly, is the nature of the substrate. As already mentioned, 2HTPP and 2HTPyP adsorbed on Ag(111) form regular and well-ordered patterns at RT. However, on Cu(111) both molecular species adsorb at low coverage as individual molecules and appear to be distributed randomly on the surface without supramolecular ordering.[38-41] This observation indicates that the adsorption behavior of molecules on surfaces always results from a complex interplay of molecule-substrate or molecule-molecule interactions.

If a system is dominated by molecule-substrate interactions, the molecules show a stronger confinement to the substrate and are more influenced by specific adsorption sites and the substrate symmetry. This is often reflected by a lower mobility of the molecules, i.e. less and slower diffusion and rotation, as well as the hindrance to form supramolecular aggregates. If the system is dominated by molecule-molecule interactions, a strong trend for the formation of supramolecular aggregates is observed. For 2HTPP on Ag(111), it was shown that the square arrangements are stabilized by so-called T-type interactions between the peripheral phenyl substituents of neighboring molecules.[36] Although the self-assembly is dominated by molecule-molecule interactions, it is also influenced by the substrate, as the orientation of the molecular islands is determined by the symmetry of the substrate. The adsorption as individual molecules of 2HTPP on Cu(111) and the dominance of molecule-substrate interactions can be explained by the formation of a strong coordinative bond between the iminic nitrogen atoms of the porphyrin and Cu substrate atoms.[42] A similar interaction was postulated for 2HTPyP on Cu(111) between the nitrogen atoms of the pyridyl groups and the substrate, mediated by the lone pairs of the nitrogen.[43] From the similarity in the observed one-dimensional diffusion behavior for both molecules on Cu(111), an analogy in the type of molecule-substrate interactions and thus a minor influence of the pyridyl groups is deduced.[40]

In addition, the intramolecular conformation of the adsorbed molecules is of interest as it is an indicator for the strength of the molecule-substrate and molecule-molecule interactions. For example, it was found that the arrangement and conformation of Cu(II)-tetrakisditert-butylphenylporphyrin (CuTTBPP) strongly depends on the substrate.[44] Although CuTTBPP forms square ordered domains on Cu(100)[44], Au(110)[44] and Ag(110)[44], the molecular conformation and the intermolecular interactions are different for each case.[44] Another

example for such a system is Co(II)-tetrakisditertbutylphenylporphyrin (CoTTBPP) on Ag(111) where up to four different supramolecular arrangements were found, each accompanied by a different, distinct molecular conformation.[45] A similar behavior is observed when investigating systems like Ni(II)-tetraphenylbenzoporphyrin (NiTPBP) on Cu(111) where up to three different arrangements were found coexisting at RT and depending on factors like temperature and coverage.[46] Interestingly, in this example the three supramolecular structures are formed by only two intramolecular conformations. With these systems it was demonstrated that the subtle balance between molecule-molecule and molecule-substrate interactions can also be strongly influenced by factors like sample temperature or molecular coverage.

Finally, there is also the possibility to influence the self-assembly by chemical functionalization of the molecules. The easiest way to achieve this is the metalation of free-base porphyrins with metal atoms on solid surfaces.[17] This possibility has gained significant interest over the last decade, especially due to the role of metalloporphyrins in natural processes. In nature, the role and functionality of the porphyrin compound is basically defined by the corresponding metal atom coordinated to the porphyrin. Inspired by this natural versatility several technological applications for metalloporphyrins have been developed, like colorimetric[47] and transistor-based sensors[48], dye-sensitized solar cells[49], or as support for heterogeneous catalysts[50]. For metalation of free-base porphyrins on solid surfaces, there are currently three main routes known[17, 51]: (i) by adsorbing porphyrins on a surface precovered with metal atoms,[52-54] (ii) by deposition of metal atoms onto a porphyrin layer,[52, 55-57] or (iii) by so-called self-metalation of molecules with substrate atoms[18, 58-64]. The first two routes are well established for quite some time and have been investigated extensively by STM, scanning tunneling spectroscopy (STS), X-ray photoelectron spectroscopy (XPS) and near edge X-ray absorption fine structure (NEXAFS). During these investigations, 2HTPP was metalated on Au(111) with Ni[65] and on Ag(111) with Co[19, 57, 66-67], Fe[52-53, 55-56, 68-69], Zn[54, 66, 70], and Ce[71-72].

The self-metalation was first observed for 2H-protoporphyrin IX (2HPPIX) on Cu(110) and Cu(100)[58]. Other self-metalating systems were found to be 2H-tetrabromophenylporphyrin on Cu(111)[59], 2H-diphenylporphyrin and 2H-porphyrin on Cu(110)[64] and 2HTPP on Cu(111)[60-61], and 2HTPP on Fe(110) and Ni(111)[73]. DFT calculations in the gas phase suggest that the metalation reaction is a step wise process where initially the metal atom is coordinated to the nitrogen atoms, then the hydrogen atoms are transferred one after the other from the nitrogen

atoms to the metal, and finally H_2 is released from the molecule.[66] Recent temperature programmed desorption (TPD) investigations for deuterated 2DTPP suggest that the metalation reaction on the substrate is different from that in the gas phase, since a surface mediated exchange of the deuterim with hydrogen atoms from the carbon backbone of the molecules was observed.[74]

Although the main focus of most investigations on the metalation of porphyrins was on the reactivity and reaction path ways of the reaction, they also demonstrated that the metalation can change the molecule-substrate and molecule-molecule interaction balance in a way that the metalation reaction is accompanied by massive changes in the intramolecular conformation and/or in the supramolecular ordering.[16, 60, 67, 75-76]

2 Theoretical and Experimental Background

2.1 Principle of STM

Scanning tunneling microscopy is an experimental method that allows for imaging conducting and semi-conducting surfaces in real space on a molecular or atomic scale.

Although the basic idea for the scanning tunneling microscope was already proposed by Young et al. in 1972[77], the first working microscope was presented in 1982 by Binnig and Rohrer.[11-12] Soon after, STM revealed its potential and versatility and became an important technique in chemistry, physics, biology, and material science for imaging and analysis of surfaces. As STM is the main method used to obtain the results presented in the thesis at hand the basic principles will be reviewed here. For a more detailed description the reader is referred to [78-79].

STM is based on the quantum-mechanical tunneling effect, which allows a particle (an electron in the case of STM) to tunnel through a potential well, although in a classical physical model its kinetic energy is insufficient to overcome the potential barrier. In STM, the gap between tip and sample practically establishes this potential barrier. For STM measurements, a sharp conducting, ideally monoatomic tip is used to probe the topographic and electronic structure of the sample surface. Typical tip materials are tungsten or a 90:10 platinum:iridium alloy. The STM tip is fixed on a scanning unit that allows for a position and motion control of the tip in in the three dimensions of space, i.e. x, y and z, with a precision in the picometer regime, using piezo actuators. Piezo actuators are crystalline materials, which reversibly change their spatial dimensions using the reverse piezoelectric effect, i.e. they generate mechanical motion when an external electrical field is applied.

If the distance between tip and sample is in a range that allows for electron tunneling, i.e. typically in the sub nm regime, the dependency of the tunneling current I on this distance d is simplified given by the proportional correlation[80]:

$$I \propto U \cdot e^{\frac{-2d}{\hbar}\sqrt{2m_e\Phi}} \tag{2.1}$$

U is the bias voltage applied between sample and tip, Φ the barrier height between sample and tip, and m_e the mass of an electron.

This exponential term shows the extreme height (distance) sensitivity and thus high resolution of surface corrugations in STM in the vertical z direction and allows for a resolution in the sub Å regime in this direction. On the other hand, this term also shows the dependency of the tunneling process on the barrier height Φ which to a first approximation is the averaged value of the work functions of tip and sample. The property of the sample which is primarily probed by STM is the local density of states, often reflecting the topography of the investigated structure, but sometimes also the electronic structure of the object might strongly contribute to the appearance in STM.[69, 81] Utilizing this, for STM measurements, the samples are raster-scanned in order to obtain a map of the sample surface. There are two different operation modes to conduct these raster scans: the constant-current and the constant-height mode.

In constant-height mode, the vertical z position of the tip is kept constant during the measurements and the tunneling current is recorded vs. the lateral tip position to obtain an I(x,y) map. While this operation mode allows for high scanning speeds by disabling the feedback loop, it is only applicable to very flat surfaces, since there is a severe risk of crashes between tip and surface for higher surface corrugations. Due to this drawback, the second operation mode is the primarily used one: In constant-current mode, the tunneling current is kept constant by means of a feedback loop constantly adjusting the vertical position of the tip. In this mode, the vertical tip position (z) vs. the lateral one (x,y) is used as representation of the surface structure. Although measurements in this operation mode are slightly more time consuming than for the constant-height mode, this drawback is compensated by the capability of imaging much rougher surfaces.

All STM measurements presented in the thesis at hand were conducted in constant-current mode, and the bias voltages given refer to the sample, i.e. when negative bias voltages are applied, the STM is sensitive to the highest occupied molecular orbitals (HOMOs) of the

sample. The STM images were processed with WSxM[82] in a way that linear background subtraction and Gaussian smooth has been applied for noise reduction.

2.2 The Substrate: Cu(111)

In order to understand the adsorption behavior of molecules on surfaces, the detailed knowledge of the atomic arrangement and the electronic and chemical structure of the substrate is crucial. For the studies presented in the thesis at hand, a Cu(111) surface of a single crystalline Cu sample was used. Copper follows the general trend for coinage metals to crystallize in a face-centered cubic (fcc) lattice (see Figure 2.1a). With a bulk lattice parameter of 0.361 nm, the next neighbor distance of Cu atoms in the (111) plane is 0.255 nm, as shown in Figure 2.1b.

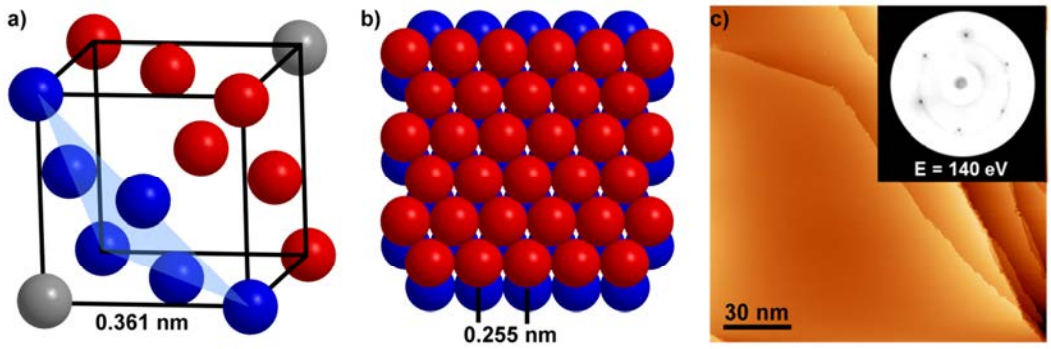

Figure 2.1: *a) Face centered cubic (fcc) crystal unit cell of copper with indicated (111) cutting plane. b) Top view on the resulting Cu(111) arrangement. c) STM image of a freshly cleaned Cu(111) surface and a corresponding LEED pattern (inlet).*

The Cu(111) single crystal used in this thesis was purchased from MaTeck with a purity >99.99 % and an alignment of <0.1° with respect to the nominal orientation. The cleaning of the surface in UHV was achieved by repeated cycles of sputtering and annealing: Ar^+-ion bombardment with a kinetic energy of 500 eV at a background pressure of 5 x 10^{-5} mbar for 0.5 to 3 h, resulting in a sample current between 2 and 3 µA, was followed by an annealing cycle; thereby the sample temperature was ramped up with 1 K/s to 850 K, held for 10 min and ramped down to RT with 1/3 K/s. This rather slow preparation procedure was applied

successfully to achieve larger terraces and fewer step edges. In addition, during the annealing cycle cooling had to be applied to the manipulator to keep its temperature below 170 K in order to prevent contamination of the Cu(111) surface by desorbing species from the manipulator. A representative STM image of a freshly cleaned Cu(111) surface is depicted in Figure 2.1c, together with a corresponding low energy electron diffraction (LEED) pattern with six spots in a hexagonal arrangement, characteristic for the three-fold symmetry of fcc (111) surfaces.

2.3 The Porphyrinoids

Porphyrinoids or tetrapyrroles are a class of molecules which are composed of four pyrrole groups, usually bridged by methine groups. These four groups are linked in a way that a polycyclic aromatic structure is formed that obeys Hückel's rule for aromaticity and thus show extended, highly conjugated π-systems.[83] This complex polycyclic nature of the tetrapyrroles results in a very complex IUPAC nomenclature, which explains the common usage of trivial or semi-systematic names for these molecules. In general, the nomenclature follows this scheme: the last part of the name describes the main macrocycle of the molecule. In this thesis the two types of macrocycle used are porphyrin and porphycene. The difference between both types is the linkage of the pyrrole groups. Within porphyrins, the four pyrrole groups are connected in a highly symmetrical fashion via four methin-bridges. In contrast, within porphycenes, the linkage of the pyrrole groups occurs asymmetrically. Here, two pyrrole groups each are linked directly together, and the two resulting pairs of pyrrole groups are linked via ethylene-bridges. Thus porphycenes and porphyrins are constitutional isomers.

One important aspect for the versatility of the molecules is the numerous possibilities for attachment of peripheral substituents. At least for porphyrins and porphycenes these substitution sites can be reduced to two types of sites: One is the substitution at the bridges between the pyrrole groups. These are referred to as the meso-sites. The second possibility is the substitution at the pyrrole groups themselves. While the α-sites are occupied by the bonds forming the macrocycle, the β-positions are available for substitution.[84]

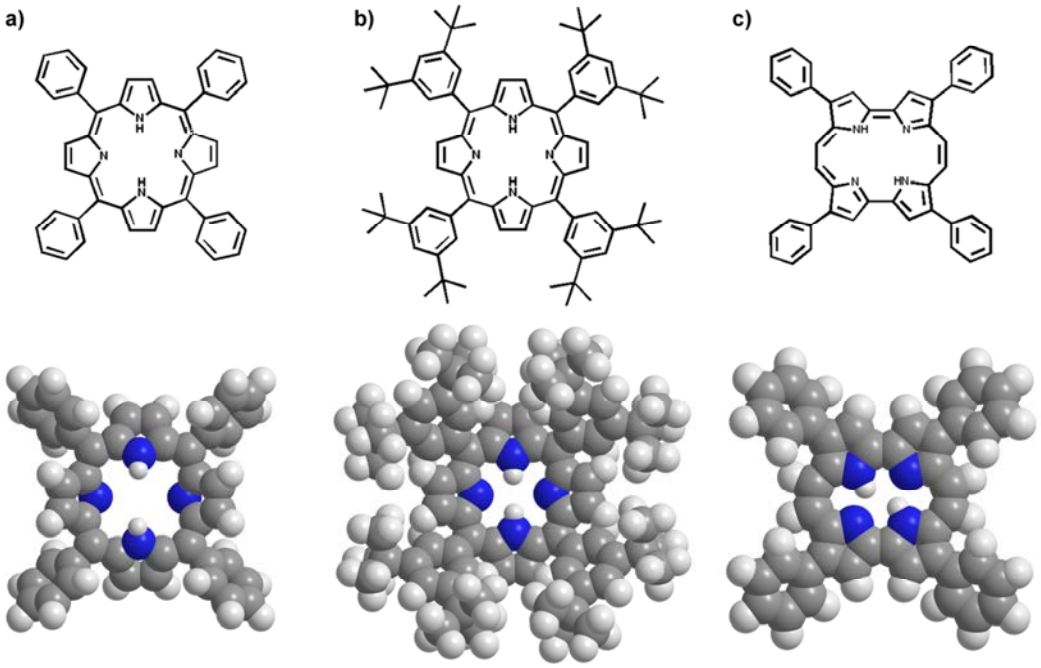

Figure 2.2: *Models of different molecules relevant for this thesis a) 2HTPP, b) 2HTTBPP, c) 2HTPPc.*

All molecules used in the thesis at hand are highly symmetrically substituted. For the porphyrins, the substitution was done at the meso-positions, while the substitution of the used porphycene was done at one *β*-position of each pyrrole group. Models with the substitutions relevant for this thesis are shown in Figure 2.2. One substitution of the porphyrin (Figure 2.2a) and the porphycene core (Figure 2.2c) was done with four phenyl substituents. Consequently, the molecules are referred to as tetraphenyporphyrin (TPP, see Figure 2.2a) and tetraphenylporphycene (TPPc, see Figure 2.2c). The third type of molecule is a porphyrin core substituted at the meso-positions with di-*tert*-butylphenyl groups (see Figure 2.2b) and are thus referred to as tetrakis-di-*tert*-butylphenylporphyrin (TTBPP). These molecules can also be described as TPPs substituted with additional *tert*-butyl groups at the 3 and 5 positions of each phenyl ring.

Another possibility for functionalization of these molecules is at the center of the macrocycles. Here, the tetrapyrroles can either host two hydrogen atoms and are thus referred to either as free-base or as 2H-porphyrins or 2H-porphycenes. In these cases, the macrocycle consists of two pyrrole groups with attached hydrogens at the nitrogen atoms, forming an

aminic functionality, and two pyrrole groups with nitrogen atoms without hydrogen, forming an iminic functionality (see Figure 2.2 and 2.3a). The second possibility for these molecules is the complexation of a metal atom. In this case, a metal atom is coordinated equally to all four nitrogen atoms in the center of the molecule as shown in Figure 2.3b and c, and the molecules are referred to as metal-porphyrin or metal-porphycene.

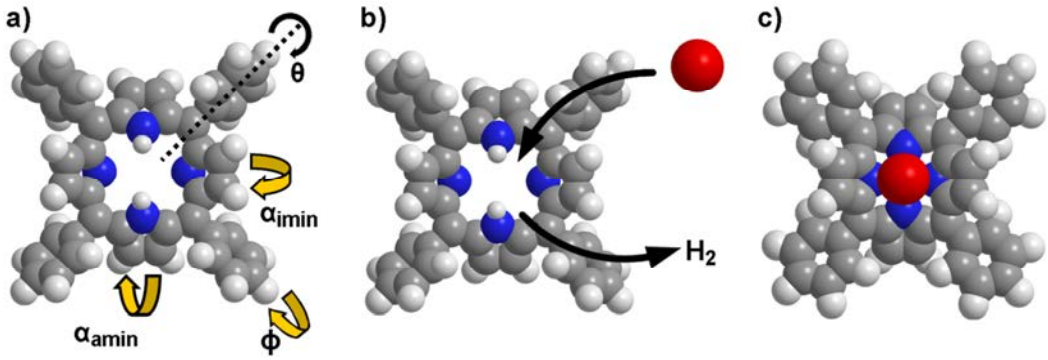

Figure 2.3: *a) Model of a 2HTPP molecule. The angles* α_{imin} *and* α_{amin} *describe the inclination of the respective pyrrole rings out of the macrocycle plane, while* θ *refers to the twist angle and* ϕ *to the tilt angle of the substituted groups. b) and c) show the metalation or complexation of a metal atom into the central cavity of a 2HTPP molecule.*

The sketches in Figure 2.2 suggest a completely planar conformation; however, the real conformation of the molecules is non-planar and close inspection shows that it cannot be planar due to the steric hindrance of the ortho-hydrogen atoms of the phenyl rings and the β-hydrogen atoms and, in case of the TPPc, the meso-hydrogen atoms. Hence, although the molecules are rather rigid, they show certain degrees of freedom for deformation. These deformation possibilities are indicated in Figure 2.3 and describe the actual conformation of the molecules very well. In particular these are the rotation of the pyrrole groups out of the molecular plane α_{pyr}, or in the case of the free-base molecules α_{imin} and α_{amin}, differentiated for the iminic and the aminic pyrrole group. Besides these angles for the pyrrole groups, there are also the tilt angle ϕ and the twist θ that describe the tilt of the phenyl side group out of the macrocycle plane, or the rotation of the side group around the σ-bond between macrocycle and side group, respectively.[45, 85-87] For a completely planar molecule all angles would be 0°

For the adsorption of porphyrins on metal surfaces, a so-called saddle shape conformation of the macrocycle is often reported. This saddle is formed by a deformation of the porphyrin macrocycle in a way that two opposite pyrrole groups are tilted upwards, while the other two are tilted downwards.[36, 55, 69, 71, 88]

The TPPs investigated in this thesis were purchased from Porphyrin Systems with a specified purity of 98 %, while the TPPc and TTBPPs were synthesized in the group of Prof. Norbert Jux of the Chair of Organic Chemistry II at the Friedrich-Alexander-Universität Erlangen-Nürnberg. The sufficiently low vapor pressure of tetrapyrroles along with their stability allows for the preparation of clean molecule layers by sublimation at high temperatures under UHV conditions, without decomposition of the molecules. The investigated molecular layers were prepared by thermal sublimation form a home build Knudsen cell onto the substrate held at RT. The intactness of the sublimated molecules was checked with a quadrupole mass spectrometer (QMS).

2.4 The UHV-instrument

The UHV system used in the thesis at hand consists of two main chambers with one chamber dedicated to sample preparation and the second one dedicated to the STM operation. Both chambers are separated by a gate valve and operated at a base presser in the low 10^{-10} mbar regime. Here the setup will be described briefly and the reader is referred to [89-90] and [91] for more details. The whole setup is isolated against low frequency vibrations by three Newport I-2000 laminar flow stabilizers.

The preparation chamber is equipped with various options for sample preparation like a SPECS IQE 11/12 sputter gun, an electron bombardment heating and two Knudsen cell evaporators for organic materials. Both evaporators can be individually pumped and separated from the preparation chamber by gate valves, which allows for fast load exchange without breaking the vacuum of the main system. Additionally, for sample characterization the preparation chamber is equipped with a *SPECS ErLEED* optics for low energy electron diffraction (LEED) and a *Pfeiffer HiQuad QMG700* quadrupole mass spectrometer (QMS) with a mass limit of $m/z = 2000$.

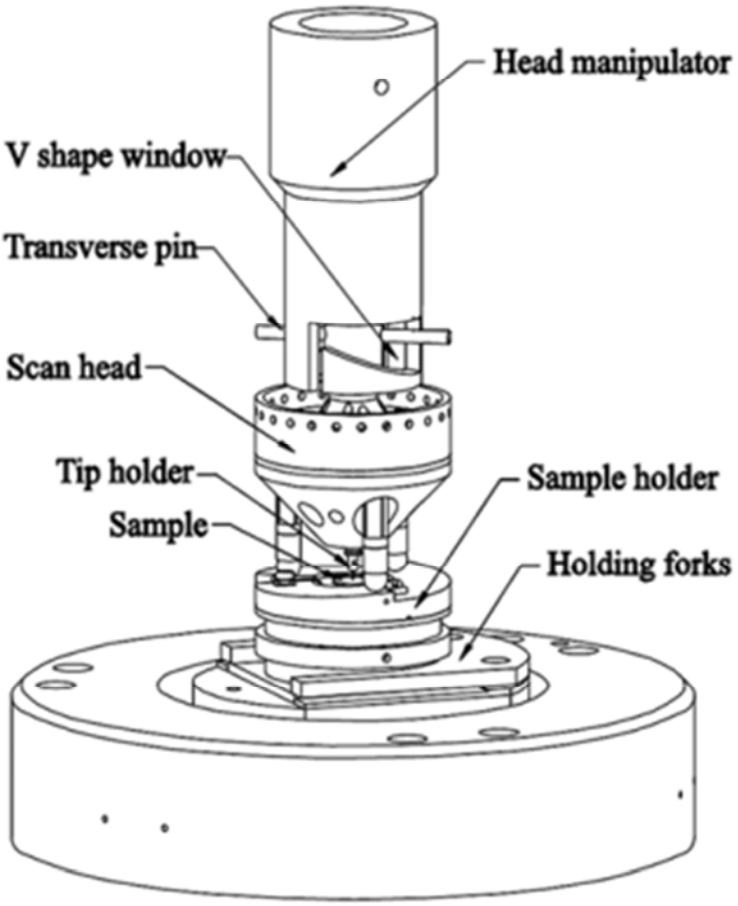

Figure 2.4: *Scheme of the scan head touched down to the sample. Reprinted from* [91].

The second chamber houses an *RHK UHV VT STM 300* STM, which is constructed based on the Besocke STM design[92]. A scheme of the STM, with the scan head located on the sample is shown in Figure 2.4. The sample temperature can be controlled via radiative heating and a flow cryostat in a temperature range from ~200 up to 500 K. The STM is equipped with an *RHK SPM 1000* electronics and a variable gain low noise *FEMTO DLPCA-200* pre-amplifier for measuring tunneling currents in the range of 10 to 50 pA

3 Results & Discussion

In this chapter the most important results of the investigated systems will be discussed. A more detailed discussion for these systems is given in the publications used for this cumulative PhD thesis [P1-P4]. The publications are attached to the appendix. The aim of this work is to identify general trends and effects of the adsorption behavior of porphyrinoids in order to predict the influence of different modifications. To achieve this, first, a peculiar aspect of the adsorption behavior of the prominent 2HTPP on Cu(111) will be investigated, which is the coverage induced disorder/order transition [P1] (see Chapter 3.1). Next, the influence of a modification of the central porphyrin macrocycle on the adsorption is investigated. For example, row based supramolecular aggregates of 2HTPPc on Cu(111) were explored and investigated, with the goal to unravel the specific interactions responsible for the assembly in rows [P2] (see Chapter 3.2). Afterwards, the temperature induced conformational and structural changes of the initially bimodal aggregates of 2HTTBPP on Cu(111) will be addressed, with particular focus on the changes induced by the self-metalation. [P3] (see Chapter 3.3). Finally, the thermally induced, reversible phase transition of the metalated CoTTBPP on Cu(111) will be addressed [P4] (see Chapter 3.4).

3.1 Coverage induced Disorder/Order Transition of 2HTPP on Cu(111) [P1]

This chapter addresses, the adsorption behavior of 2HTPP on Cu(111) at RT, with a focus on the peculiar disorder/order transition at coverages in the regime of a closed molecular layer.

In numerous publications on the structures formed by TPPs adsorbed on (111) fcc coinage metal single crystal surfaces, the formation of square ordered islands was found. [31, 37, 44-45, 52, 55, 66, 69, 93-95] It was shown that these structures are stabilized by specific attractive intermolecular interactions[31, 36], the so called T-type interactions. T-type interaction describes a situation where a C-H group of a phenyl substituent of the TPP points edge-to-face towards the center of the π-system of a phenyl substituent of a neighboring molecule.[31, 36] A

schematic drawing of this interaction pattern is given in Figure 3.1a. For the adsorption situations described before, typically a twist angle θ of about 60° [36, 69] is observed.

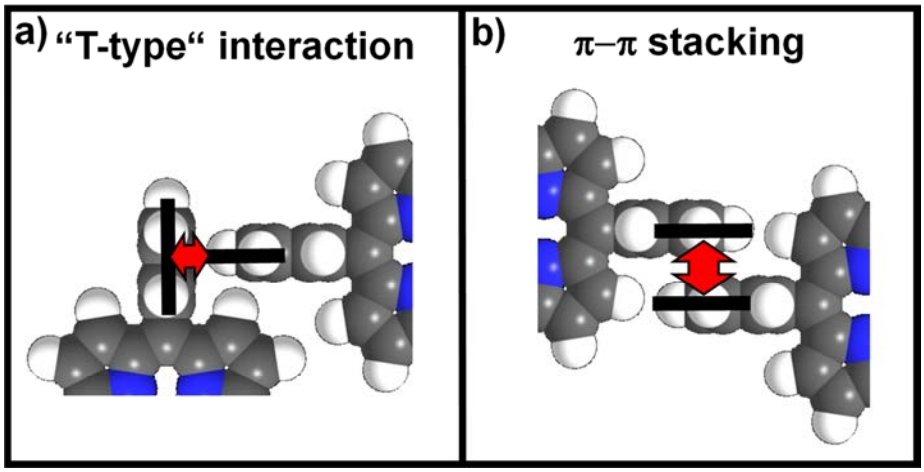

Figure 3.1: *Schematic drawings of the two possible interaction patterns for intermolecular phenyl-phenyl interactions.*

For the phenyl groups, a second type of interaction pattern is conceivable, the so called π-π stacking.[96-97] For this aromatic interaction, the π-systems of the phenyl groups of two neighboring molecules have to be oriented in a way that the planes of the phenyl groups are almost parallel. The schematic drawing of this interaction pattern can be found in Figure 3.1b.

Previous studies on the adsorption of 2HTPP on Cu(111) reported on an adsorption behavior dominated by molecule-substrate interactions.[38, 41-42, 60, 98-99] A clear indication for this is the observation of individual, isolated molecules on the Cu(111) surface at RT even at very low coverages. This behavior is illustrated in Figure 3.2a, where each molecule appears as two longish parallel protrusions, with a depression in-between, which will be referred to as "molecular axis".

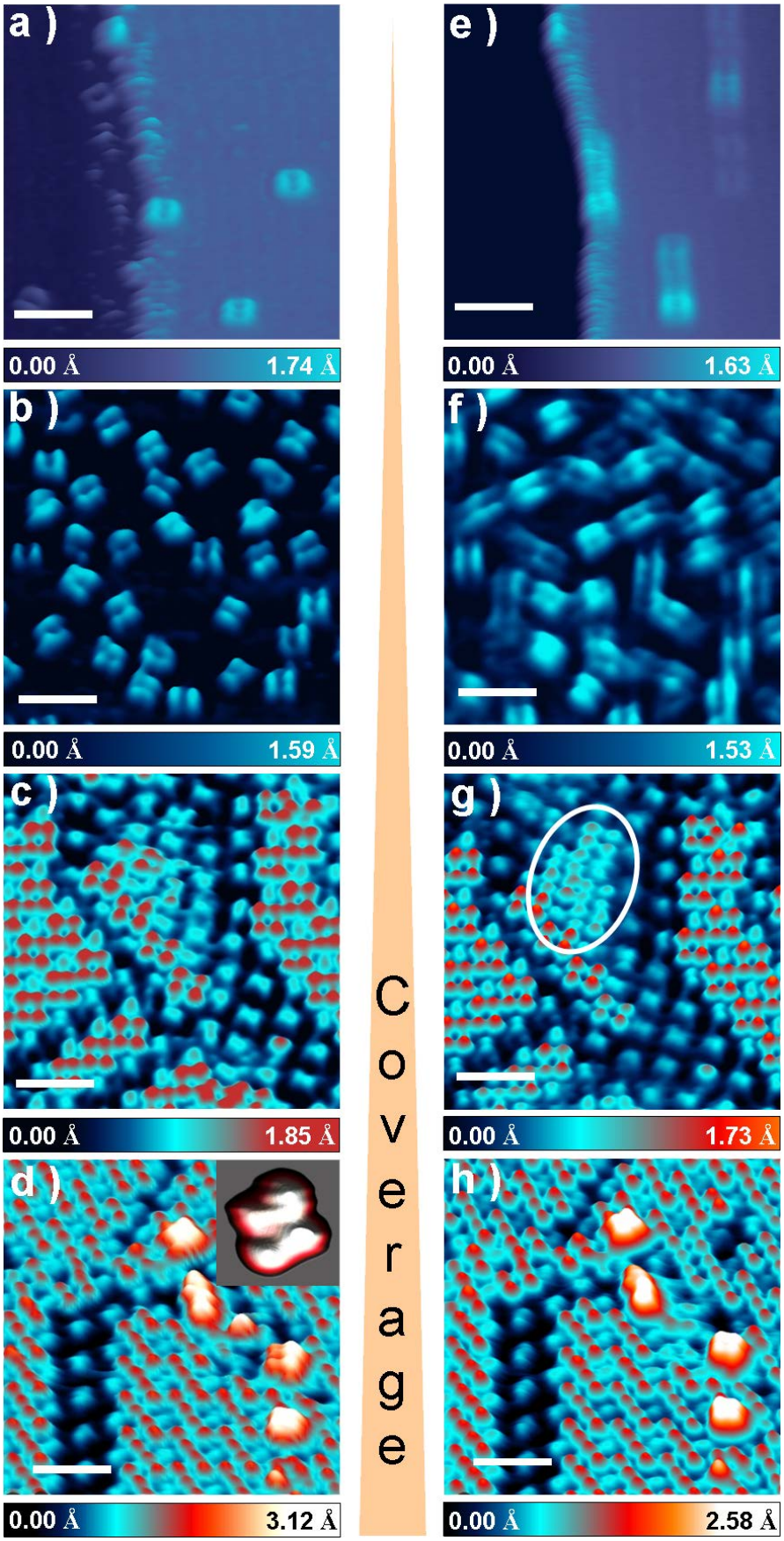
a)
0.00 Å
1.74 Å
b)
0.00 Å
1.59 Å
c)
0.00 Å
1.85 Å
d)
0.00 Å
3.12 Å
Coverage
e)
0.00 Å
1.63 Å
f)
0.00 Å
1.53 Å
g)
0.00 Å
1.73 Å
h)
0.00 Å
2.58 Å

Figure 3.2: *Constant current STM images of 2HTPP on Cu(111) at different coverages; the turquoise molecules represent 1st layer molecules, the red ones 2nd layer molecules and the white ones 3rd layer molecules. a) Isolated molecules at very low coverage (U_{bias} = -1.49 V, I_{set} = 30 pA), b) 0.009 ML of 2HTPP (U_{bias} = -0.193 V, I_{set} = 11 pA), c) formation of checkerboard structure involving 1st and 2nd layer molecules (U_{bias} = -1.05 V, I_{set} = 30 pA), d) almost completely covered surface with checkerboard domains and some 3rd layer molecules present (U_{bias} = +1.35 V, I_{set} = 22 pA), e) average frame of a 39 image (13 min) STM movie, where 1D diffusion is visible (U_{bias} = -1.49 V, I_{set} = 30 pA), f) average frame of a 51 image (22 min) STM movie, where besides the 1D diffusion rotation of the molecules is visible (U_{bias} = -193 mV, I_{set} = 11 pA), g) average frame of a 60 image (23 min) STM movie, where the dynamics of the checkerboard structure is visible. The white oval marks a region where frequent molecular movements occur during the movie (U_{bias} = -1.05 V, I_{set} = 30 pA), h) average frame of a 26 image (10 min) STM movie; here the average frame is identical to each of the single frames of the movie (U_{bias} = +1.35 V, I_{set} = 22 pA). a)-d) are individual frames of the movies averaged in e)-h). The scale bars correspond to 4 nm.*

This dark molecule axis intersects the molecules along the two aminic pyrrole groups and is aligned to one high symmetry direction of the substrate.[42] In addition, the molecules were found to slowly diffuse along these directions at RT, which becomes evident from the elongated shape of the molecules along the molecular axis in the average frame of a time lapse series of STM images shown in Figure 3.2e. It was shown that the molecules can change their orientation to another high symmetry direction at elevated temperatures. The resulting activation energy barriers were determined by Buchner et al. to be $E_m = 0.71 \pm 0.08$ eV for diffusion and $E_r = 1.28 \pm 0.12$eV for rotation.[42]

Increasing the coverage to 0.009 ML of 2HTPP (1 ML defined as 1 molecule per surface atom) results in the situation shown in Figure 3.2b and f. The situation is similar to the previous coverage, i.e. adsorption as individual molecules, no supramolecular ordering, and diffusion along the close packed substrate rows. However, the increased coverage reduces the free surface area per molecule, resulting in a hindered one-dimensional diffusion and a reduced average diffusion length. Occasional collisions of molecules allow for sufficient momentum transfer to some molecules to overcome the energy barrier E_r even at RT and change their orientation towards another high symmetry direction of the substrate. This

becomes evident from the average frame of a time lapse series of STM images, shown in Figure 3.2f, where the diffusion paths of some molecules are not completely linear and changes in the diffusion direction are present.

For the adsorption situations discussed so far, it was found that the molecules are lying almost flat on the surface with a twist angle θ of the phenyl rings of only 20° [60], which does not allow for intermolecular T-type interactions[38].

When the total coverage exceeds ~ 0.020 ML, molecules with increased apparent height and a different molecular appearance are observed (see Figure 3.2c). These molecules, which will be referred to as 2nd layer molecules, no longer show the parallel rod like shape, but appear as four protrusions (color-coded red in Figure 3.2) Further increase of the coverage results in the formation of a well ordered checkerboard like structure, as depicted in Figure 3.2c, d, g and h and in Figure 3.3.

Within these ordered domains 2nd layer molecules (4 red protrusions per molecule, indicated by the solid circle in Figure 3.3) and 1st layer molecules (turquoise, indicated by the dashed circle in Figure 3.3) arrange in a checkerboard-like structure, where each molecule is surrounded by four molecules of the other type. The lattice vectors for this peculiar superstructure are shown in Figure 3.3 and were determined to be a = 2.12 ± 0.03 nm and b = 1.74 ± 0.05 nm, with an angle of γ= 90° ± 5°. Another interesting feature of the checkerboard structure is that within one domain all molecules, i.e. 1st and 2nd layer ones, are oriented with their molecular axes along the same high symmetry direction of the substrate (cf. Figure 3.3). A detailed analysis shows that there are a total of three pairs of chiral domains existing. [P1] Assuming that the 1st layer molecules within the checkerboard domains persist the orientation of the individual ones at low coverage, the substrate rows can be represented by the parallel orange lines in Figure 3.3d), showing that all molecules (1st and 2nd layer ones) adopt an equivalent position towards a substrate row. The next aspect to be addressed is the number of molecules per unit cell. Two scenarios could be possible: one, where a 2nd layer molecule sits on top of a first layer one (porphyrin “sandwich”, see Figure 3.4a) and the other one, where a 2nd layer molecule bridges four 1st layer molecules (see Figure 3.4b).

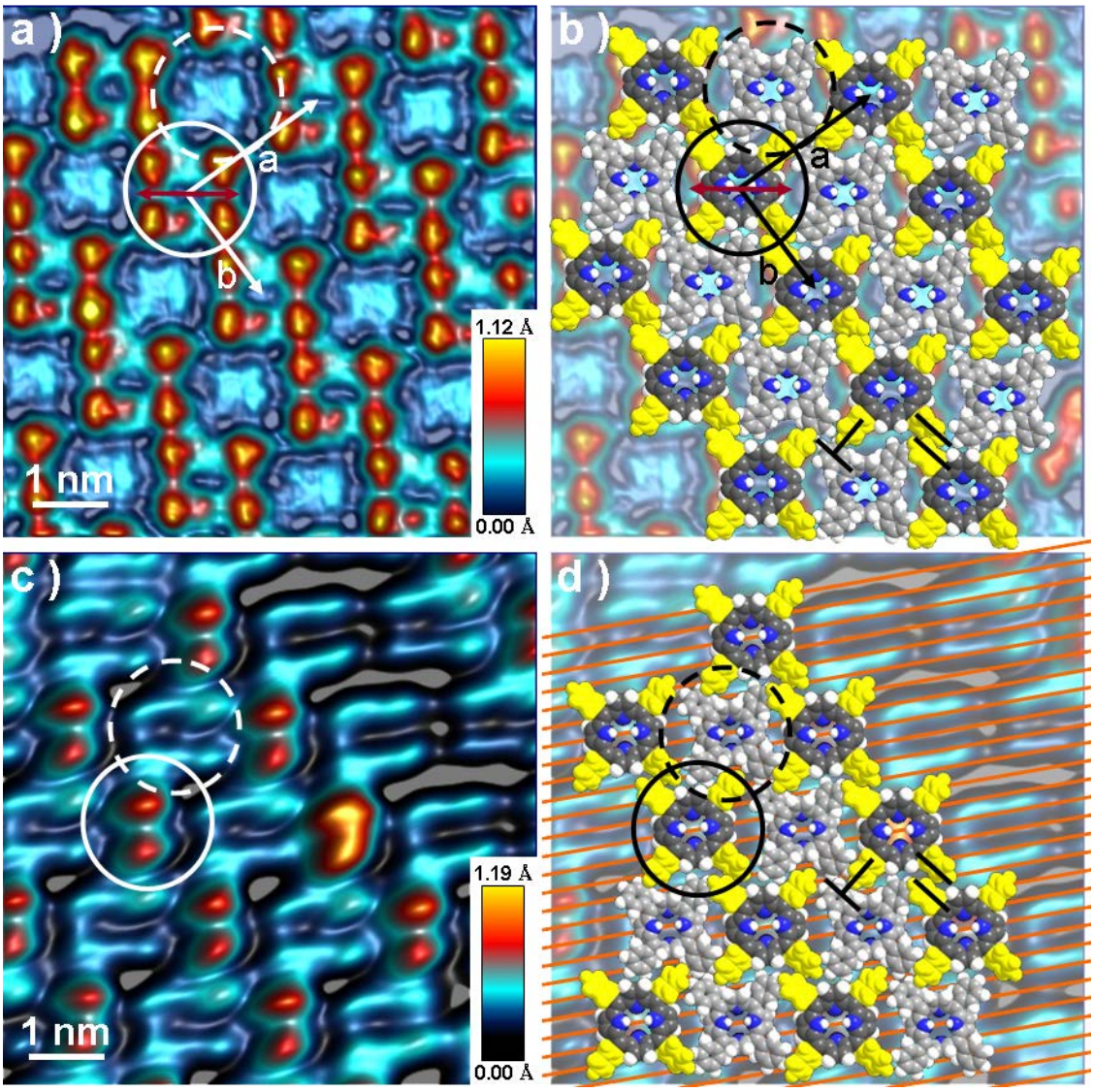

Figure 3.3: *Constant current STM images of a checkerboard domain in (a, b) 'normal' contrast (U_{bias} = -1.14 V, I_{set} = 46 pA) and (c, d) in a contrast adjusted to depict the turquoise 1st layer molecules with their typical two parallel rod like shape (U_{bias} = -0.92 V, I_{set} = 19 pA). b) and d) show superimposed scaled space filling models to the STM images. The model visualizes the stabilization of the checkerboard structure by T-type interactions (indicated by a black T) and π-π-stacking (black parallel lines). The solid circles mark a 2nd layer molecule and the dashed circles a 1st layer one. The orange lines in d) represent neighboring close packed atomic rows of the substrate in one high symmetry direction.*

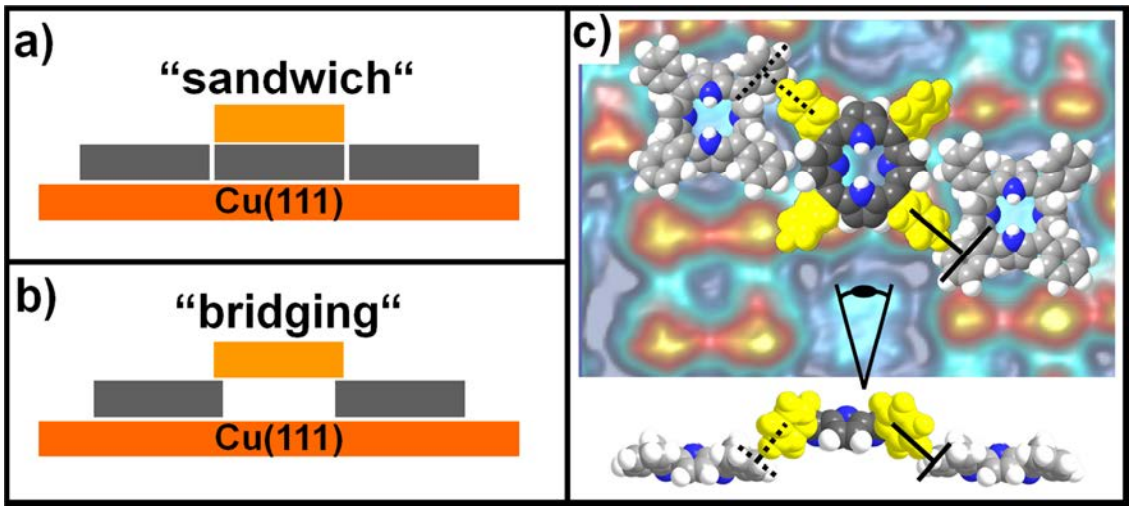

Figure 3.4: *a) and b) schematically show the two possible arrangements of 2HTPP molecules in checkerboard domains. c) gives a top and a side view of scaled models of the 1st and 2nd layer molecules in the checkerboard structure, highlighting the T-type interactions.*

Due to the missing contributions of the molecule below the 2nd layer one in case of the "sandwich" arrangement, and the height difference of only 0.8 Å between 1st and 2nd layer molecules, the "sandwich" arrangement can be ruled out. (For a more detailed discussion see [P1].) Additional proof for the bridging arrangement of the checkerboard domains stems from metalation experiments. Upon heating 2HTPP adsorbed on a Cu(111) surface, in-situ self-metalation with Cu substrate atoms to CuTPP occurs.[60-61, 98-99] In Figure 3.5a, the situation is shown after deposition of about 0.030 ML of 2HTPP, which resulted in a surface completely covered with checkerboard domains. After annealing to 400 K for 33 min, the surface is almost completely covered with large, square ordered domains that can be assigned to the formed CuTPP (see Figure 3.5b). Please note that the nominal coverage for a closed layer of CuTPP on Cu(111) is 0.033 ML. The insufficient coverage for a closed layer of the "sandwich" structure (0.045 ML would be required) and the perfect agreement in coverage after metalation proofs the existence of the bridging arrangement.

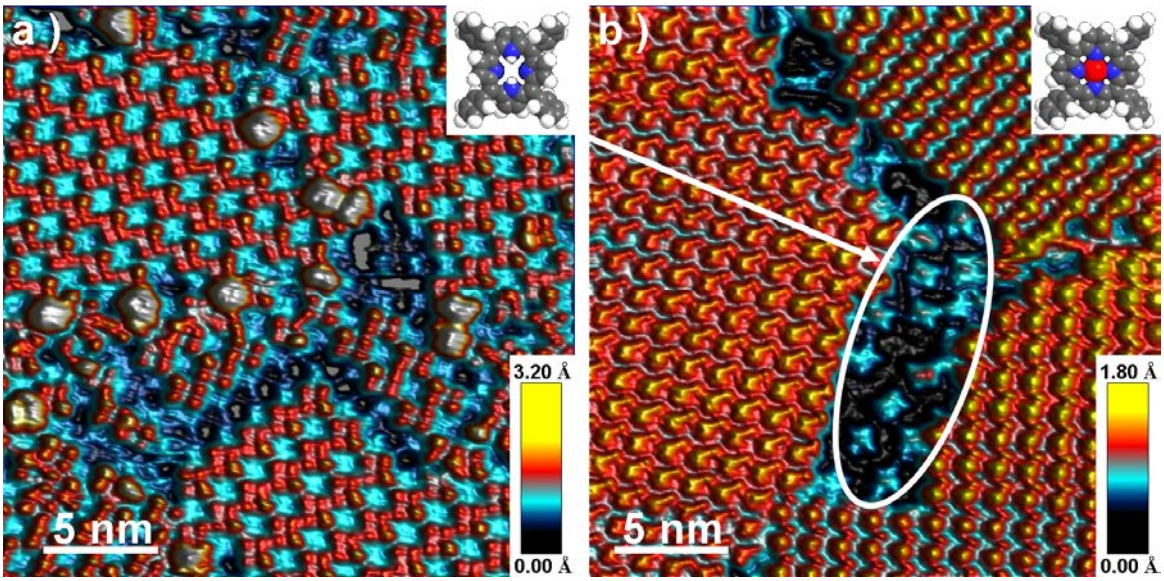

Figure 3.5: *Constant current STM image of 0.030 ML 2HTPP on Cu(111) a) before and b) after annealing to 400 K. a) 2HTPP in 1st (turquoise), 2nd (red) and 3rd layer (white) (U_{bias} = 1.35 V, I_{set} = 22 pA), b) the metalated CuTPP (red and yellow) forming square ordered islands. The turquoise molecules especially in the region marked with the white oval are residual non-metalated 2HTPPs (U_{bias} = -1.05 V, I_{set} = 28 pA).*

In order to obtain a deeper understanding of the interactions stabilizing the checkerboard arrangement, the STM image in Figure 3.3a was superimposed with molecule models of 2HTPP in Figure 3.3b. Thereby, the yellow species represents the 2nd layer molecules (indicated by the solid circle) and the light gray species the 1st layer molecules (indicated by the dashed circles). For the intermolecular conformations of the 1st and 2nd layer molecules in the checkerboard structure, the intramolecular conformations determined by Diller et al.[60] for submonolayer 2HTPP on Cu(111) (θ = 20°, α_{py} = 40° and α_{im} = 60°) and multilayer 2HTPP molecules (θ = 55-60°, α_{py} = 40° and α_{im} = 40°) were used. Inspection of the models in Figure 3.3 reveals that the 2nd layer molecules are arranged such that the phenyl groups of neighboring molecules along the short lattice direction *b* are oriented almost parallel, with only a small intersecting angle between the planes of the two phenyl rings. This geometry suggests that the supramolecular structure within the 2nd layer is stabilized via π-π-stacking interactions. The other two phenyl groups of the 2nd layer molecules, oriented along the long lattice vector *a* are arranged towards phenyl groups of 1st layer molecules in a way common for T-type interactions, i.e. the C-H bond in meta position of the 2nd layer phenyl ring points

perpendicular towards the center of the 1st layer phenyl ring. This postulated stabilization via π-π-stacking between 2nd layer molecules and T-type interactions between 1st and 2nd layer molecules is supported by the dynamic behavior of the checkerboard domains at RT (see Figure 3.2g and h). In these average frames of time lapse series, the areas of larger, well-ordered checkerboard domains appear as sharp as in the corresponding single frames (see Figure 3.2c and d), indicating that the situation is static. In contrast, the lower coordinated and thus less stabilized 2nd layer molecules are still mobile, as can be seen by the reduced intensity of the 2nd layer molecules in the marked region in Figure 3.2g.

Finally, at coverages higher than ~0.030 ML, molecules in the 3rd layer can be observed as depicted in Figure 3.2d, where they are color-coded as white spots at the void locations between checkerboard domains. The contrast-optimized magnification (Figure 3.2d, inlet) shows that these molecules maintain the four spot appearance of the 2nd layer molecules and that the ordering of the checkerboard domains is not continued towards higher layers. Interestingly, the average frame shown in Figure 3.2h is identical to each single frame of the corresponding STM movie, indicating that the 3rd layer molecules are pinned and do not diffuse over the surface.

In conclusion, upon increasing the coverage of 2HTPP on a Cu(111) surface, the transition from a disordered phase towards a highly ordered phase stabilized by a peculiar interaction pattern is found. This ordered checkerboard phase is stabilized by π-π stacking interactions between 2nd layer molecules and T-type interactions between 1st and 2nd layer molecules.

3.2 Ordering of 2H-tetraphenylporphycene on Cu(111) [P2]

After discussing the adsorption behavior and the structures formed by 2HTPP adsorbed on Cu(111) (see previous section) the influence of variations of the macrocycle shall be addressed. The molecule of choice is 2H-tetraphenylporphycene (see Figure 2.2c), a structural isomer of 2HTPP. Recent low temperature STM studies on the unsubstituted porphycene backbone on Cu(110) revealed a situation, where the molecules adsorb with the molecule plane parallel to the substrate surface plane and develop strong interactions between the iminic N atoms of the molecules and Cu atoms of the substrate.[100-101] Thus similarities in the adsorption behavior of 2HTPPc and 2HTPP are to be expected.

Initially, at low coverage the step edges of the Cu substrate are decorated with molecules, as shown in Figure 3.6a.

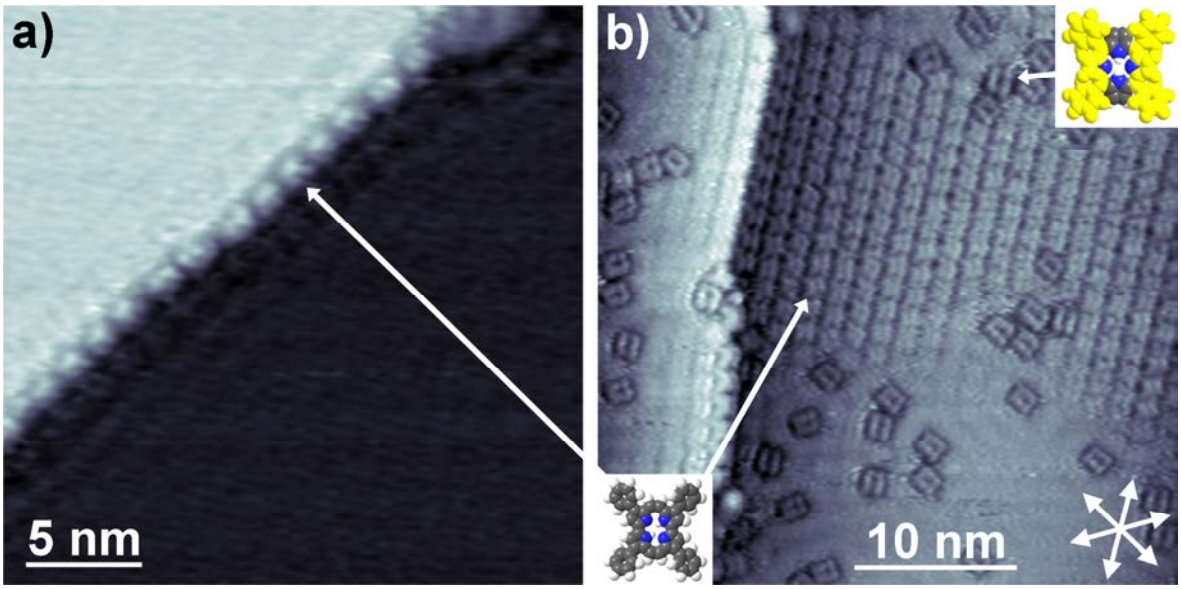

Figure 3.6: *a) Constant current STM image at low coverage of 2HTPPc on Cu(111), displaying step decoration (U_{bias} = -0.77 V, I_{set} = 30 pA); b) Medium coverage of 2HTPPc (lower left inlay) with co-deposited 2HTPP (top right inlay) on Cu(111). 2HTPPc forms islands while 2HTPP adsorbs mainly as individual isolated molecules (U_{bias} = -1.14 V, I_{set} = 30 pA).*

Such an adsorption behavior is common for systems with rather weak molecule-substrate interactions and molecules diffusing over the surface, as e.g. 2HTPP on Ag(111)[36]. The step decoration is a strong indication for the adsorption at the step edges being energetically favorable due to the increased coordination at the lower side of the step. The accumulation of molecules at the step edges in combination with the fact that no isolated molecules are found on the terraces is a strong indication towards fast diffusion on the surface. The fact that no supramolecular arrangements are found on the terraces indicates that the molecule-substrate interactions are insufficient for the stabilization of such arrangements at RT[36, 38, 102].

At higher coverages, 2HTPPc forms ordered supramolecular arrangements on the terraces, as shown in Figure 3.6b. Note that the situation shown in Figure 3.6b is a coadsorption of 2HTPPc and a low fraction of 2HTPP. As discussed in section 3.1 and reported in literature[38, 41], 2HTPP appears as two elongated parallel protrusions that are oriented along the high symmetry directions of the substrate. Thus, 2HTPP is a good indicator for the crystallographic directions of the surface (red arrows in Figure 3.6b).

Inspection of the 2HTPPc island reveals that it consists of parallel molecular rows along one of the main crystallographic directions and is surrounded by surface areas with elevated height. This observation, which is made for similar adsorption systems as well[36, 38, 62, 102], can be explained by molecules diffusing over the surface much faster than the scanning speed of the STM tip. In this regard, the supramolecular assembly into islands can be interpreted as a condensation process[38, 102].

Before discussing the supramolecular arrangement in detail, the appearance of a molecule has to be analyzed first: A close-up STM image of a 2HTPPc molecule within a supramolecular arrangement is shown in Figure 3.7, along with a scaled model overlay.

Each molecule appears as a pair of bow-shaped protrusions connecting two more intense protrusions each. The two bows frame a depression through the center of the molecule, which will be referred to as the molecular axis in the following. A common observation for STM investigations of similar molecules is the independence of the molecular appearance on the bias voltage in a range of several volts.[42]

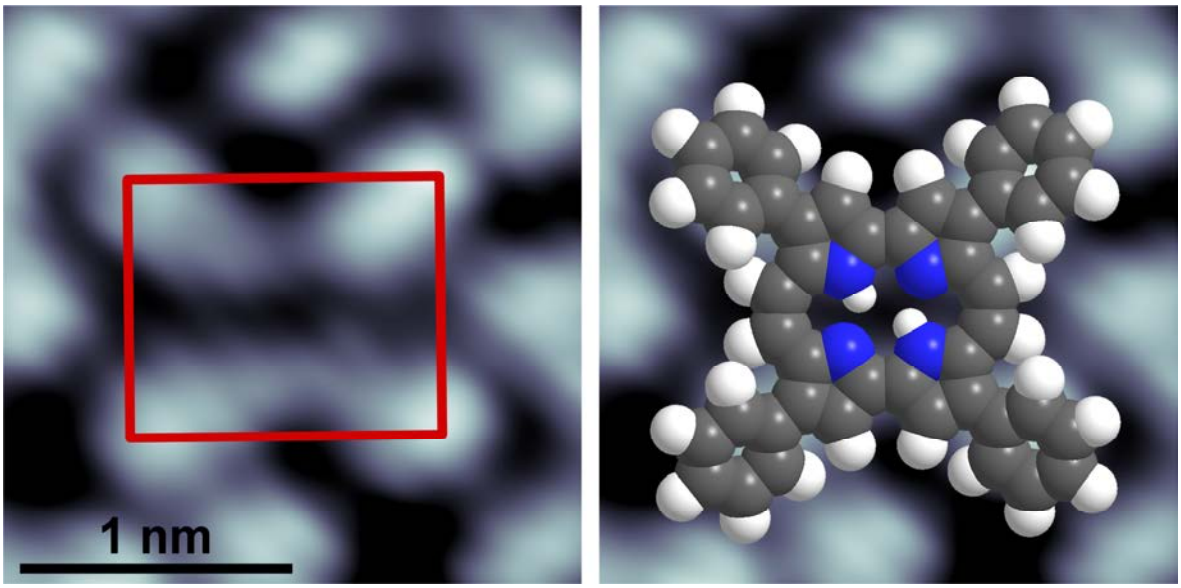

Figure 3.7: *Close up constant current STM image of one 2HTPPc molecule (left), and the same image overlaid with the corresponding, scaled space filling model (right). (U_{bias} = -229 mV, I_{set} = 30 pA)*

As this effect is observed for 2HTPPc on Cu(111) too, it is safe to assume that the STM images reflect to a large extent the actual topography of the molecules. The overall appearance of the molecules represents a rectangular shape, as indicated in red in the left panel of Figure 3.7. Since this shape is in good agreement with the diameter and the aspect ratio of a molecule model with a flat macrocycle, it is possible to attribute the different protrusions to different parts of the molecule: The four intense protrusions in the periphery of the molecule are caused by the four phenyl groups of the 2HTPPc. The less intense links between these protrusions are assigned to the pyrrole groups, and the central cavity represents the molecular axis intersecting the ethylene bridges. This assignment is represented in the right panel of Figure 3.7. Due to some minor deviations between the completely flat model and the dimensions derived from STM images a slight kinking of ~5° along the molecular axis is deduced.

In the next step, the supramolecular arrangement will be discussed. A representative STM image of a supramolecular arrangement is shown in Figure 3.8, together with the results of the following analysis.

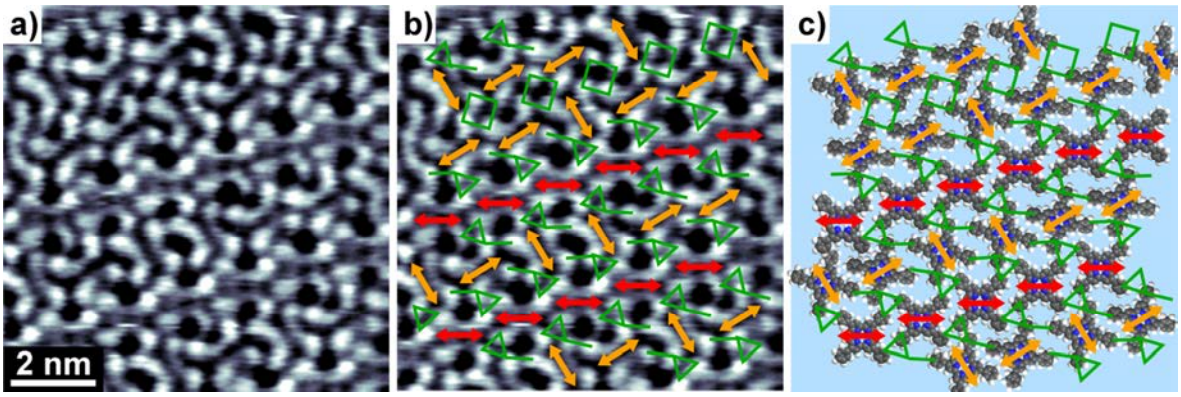

Figure 3.8: *Constant current STM image of a typical supramolecular 2HTPPc assembly. The molecules in the highly ordered rows are indicated by red arrows and the ones of the less ordered rows with orange arrows. The intermolecular T-type interactions are indicated by the green squares and rectangles, giving rise to the two different structural motives. For further illustration the arrangement is shown with space filling models. (U_{bias} = -229 mV, I_{set} = 30 pA)*

For illustration of the orientations of the molecules, their molecular axes are indicated with arrows. As pointed out before, the molecules are arranged in parallel rows. Figure 3.8 reveals that there are different types of rows: Some rows are highly ordered (indicated by red arrows), i.e. all molecules within such rows are oriented the same way, which is an orientation of the molecular axes of 15° towards the rows main direction. Please note that for each domain all molecules in all highly ordered rows are oriented identically. This peculiar behavior automatically results in the existence of mirror domains, where the molecular axes are oriented 15° clockwise in one domain and 15° counterclockwise in the mirror domain. These highly ordered rows are separated by less ordered rows (indicated with orange arrows), where the molecules adopt two different azimuthal orientations.

In the less ordered rows, two different orientations can be found, which depend on the azimuthal orientation of the molecules in the highly ordered rows: Considering that the molecules in the highly ordered rows are oriented 15° clockwise towards the primary direction of the rows, then the orientations found in the less ordered rows are 15° counterclockwise and 75° clockwise. For the orientations of the corresponding mirror domain clockwise and counterclockwise would be inverted. As the main direction of the rows coincides with one high symmetry direction of the substrate, and due to the threefold

symmetry of the substrate lattice, all molecules are oriented 15° towards one high symmetry direction of the substrate. In addition, the two orientations present in the less ordered rows occur in a ratio close to 1:1, indicating the energetic equivalence of both orientations.

Detailed analysis on the distribution of the different rows within one domain shows that highly ordered rows are never found next to each other. They are always separated by either one or two less ordered rows. In order to understand this peculiar arrangement a detailed inspection of the molecule-substrate interactions and the intermolecular interactions is necessary. The molecule-substrate interactions were partially discussed above. However, if the orientation of the molecular axis of 15° towards the high symmetry direction of the substrate would be the only contribution, one would anticipate finding all six possible orientations for molecules within one domain. As this is not the case, the limitation to only three orientations per domain must be caused by the intermolecular contributions. The scaled model of the supramolecular arrangement in Figure 3.8c shows that these intermolecular interactions are mediated via the periphery of the molecules, which are the phenyl substituents. For phenyl groups, in general two types of aromatic interactions are possible (see illustration in Figure 3.1). Simple π-π-stacking[96-97] can be ruled out, as the geometry of the phenyl groups in the STM images in Figure 3.8 does not fit this type of interaction. Instead, T-type interactions are proposed, which were previously found to be the main contribution to intermolecular interactions in similar adsorption systems[31, 36, [P1]]. Burley et al. reported typical distances of 4.5 to 7 Å and intersection angles of 50 to 90° for T-type interactions in biomolecules[103]. Upon close inspection of the supramolecular arrangement, two interactions pattern were found (see Figure 3.8): At the junctions of a less and a highly ordered row, a triangular T-type interaction pattern with one additional interaction is found as indicated by the triangle with one leg in Figure 3.8b and c. With distances of 5.0 to 6.5 Å and an intersection angle of 60° this geometry is indeed suitable for T-type interactions[103]. In contrast, at the junctions of two less ordered rows, a rectangular T-type arrangement is found, as indicated by the squares in Figure 3.8b and c. This pattern with distances between 5.5 and 6.5 Å and an intersection angle of 90° is well suited for T-type interactions, too.

Another interesting fact of this peculiar arrangement is the dynamic behavior of the 2HTPPc molecules within the domains: In the highly ordered rows the molecules are static, while the molecules in the less ordered rows can occasionally switch between the two orientations. This is illustrated in Figure 3.9 where three consecutively recorded STM images of the same region of the surface are shown. While the molecules in the highly ordered rows (indicated

with red arrows) always exhibit the same orientation, the molecules in the less ordered rows (indicated with orange arrows) occasionally change their orientation from image to image.

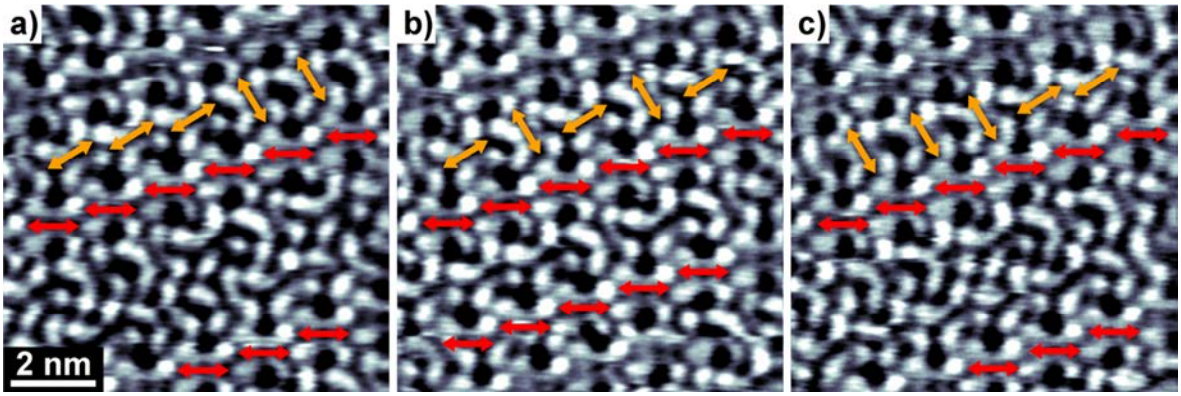

Figure 3.9: *Three consecutive STM images of the same surface area. The molecules in the highly ordered rows are indicated with red arrows, while the orange arrows indicate molecules of the less ordered rows. From a to c each indicated molecule in a less ordered row changes its orientation once. Additionally the separation of the higher ordered rows (red arrows) changes from a to b and from b to c. (U_{bias} = -229 mV, I_{set} = 30 pA, Δt = 14 s)*

The series of STM images also documents another dynamic aspect of the 2HTPPc domains, namely the systematic rearrangement of whole rows. This effect can be identified by the varying distance between the two highly ordered rows marked in red in the different images. Although this rearrangement occurs very rarely, it has to be a fast process, as it occurs in-between two scans and in the images the situation always appears to be static, i.e. there are no distorted molecules or intersections of rows visible.

When following the dynamic evolution of the 2HTPPc domains at RT over time, a clear systematic trend is identified: while shortly after deposition, the highly ordered rows are predominantly separated by one less ordered row (see situation in Figure 3.10a), after a few days, the highly ordered rows are predominantly separated by two less ordered rows (see situation in Figure 3.10b).

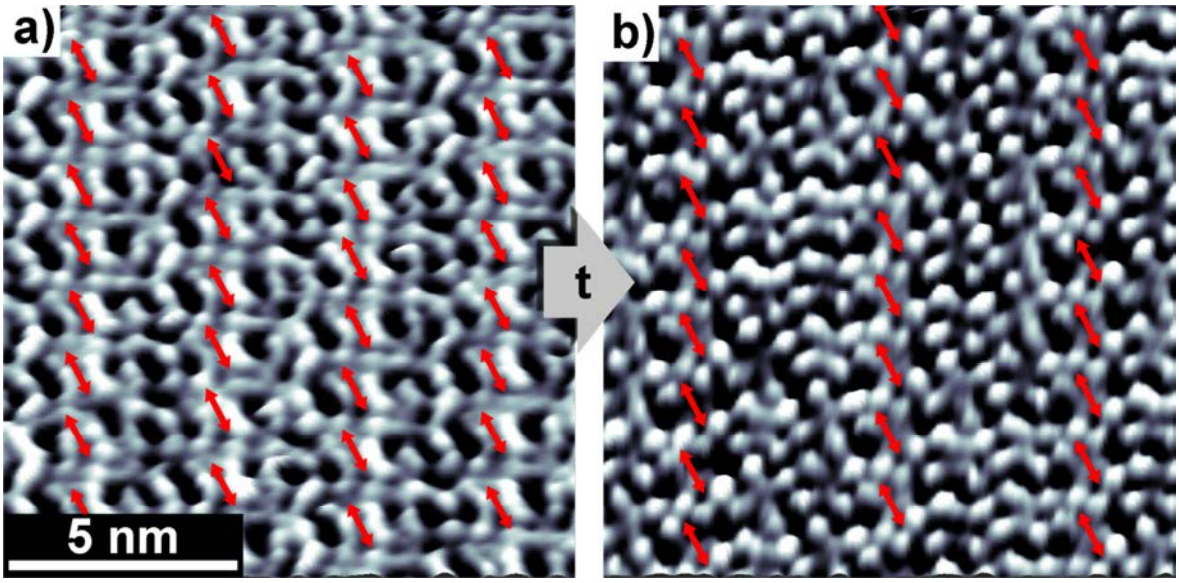

Figure 3.10: *Representative constant current STM images of 2HTPPc domains right after deposition (a, U_{bias} = -0.89 V, I_{set} = 30 pA) and after storage at RT for 1 week (b, U_{bias} = -113 mV, I_{set} = 33 pA). The red arrows indicate the molecules of the highly ordered molecular rows.*

This temporal evolution (one less ordered row separation changing to two rows separation) indicates a rather small energy difference between both structures and a kinetic stabilization (at least partially) of the initial situation with a separation of one less ordered row. One explanation for this peculiar behavior can be found in the registry with the substrate: While the distance of two highly ordered rows separated by one less ordered row was found to be 2.96 ± 0.06 nm, which corresponds to 13.5 Cu substrate rows, the distance increases for the two rows separation situation to 4.44 ± 0.07 nm, which corresponds to 20.0 Cu substrate rows. Hence, the better registry for the latter case, where every highly ordered row adopts a similar adsorption site, compared to only every second one for the first case, could be responsible for the structural rearrangement. In addition, it is likely, that the quadratic T-type interaction motive is energetically more favorable than the triangular one (90° vs. 60°). As the quadratic motive only exists for two neighboring less ordered rows this would also favor the structural rearrangement towards the situation where highly ordered rows are separated by two less ordered ones.

In conclusion, 2HTPPc forms supramolecular arrangements consisting of parallel rows oriented along one high symmetry direction of the substrate. The uncommon aspect of the formed arrangements is the presence of several orientations of 2HTPPc within one domain, resulting in the formation of molecular rows with different degrees of order. This adsorption behavior is explained by a subtle interplay of intermolecular T-type interactions and attractive molecule-substrate interactions.

3.3 Temperature Dependent Supramolecular and Conformational Changes of 2HTTBPP on Cu(111) [P3]

In this chapter, the changes of conformation and long-range order of 2HTTBPP upon metalation to CuTTBPP on Cu(111) will be discussed. Upon metalation, the molecules are subjected to massive conformational changes together with changes of the distance between molecule and substrate due to altered molecule-substrate interactions.

The adsorption of free base porphyrinoids on Cu(111) often results in very peculiar molecular conformations and supramolecular arrangements due to the strong interaction between the iminic nitrogen atoms of the molecules and Cu atoms from the substrate[40-42, 59, 64]. Figure 3.11a shows the result for adsorption of 2HTTBPP on Cu(111) at RT.

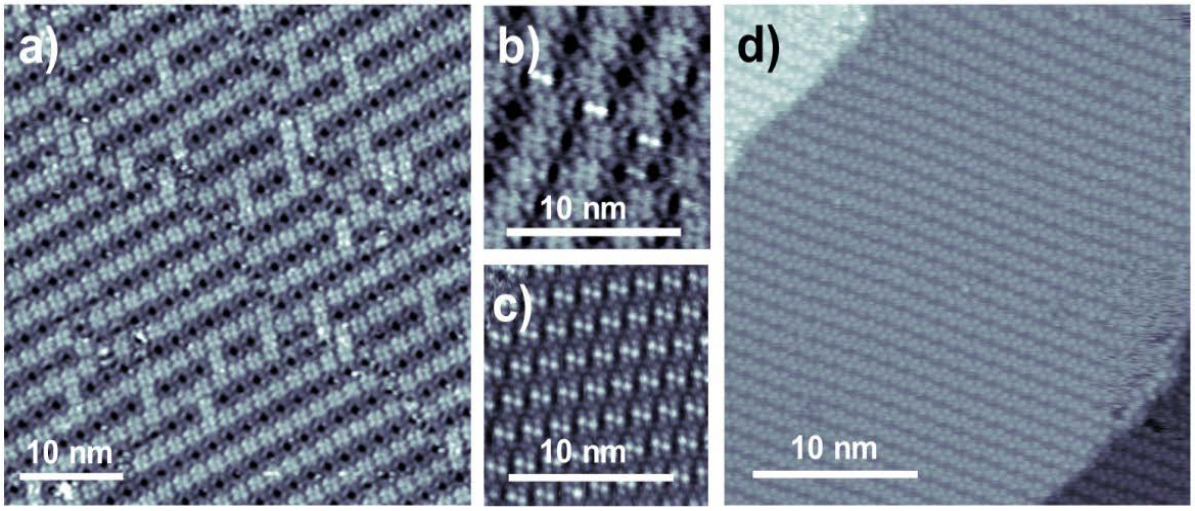

Figure 3.11: *Constant current RT STM images of ordered islands of a monolayer of 2HTTBPP on Cu(111) prepared at RT, after different heat treatments: (a) bimodal appearance observed for the as prepared layer (U=+1.3 V, I=30 pA); (b) transition phase from bimodal to monomodal hex A phase after heating for 10 minutes at 330 K (U=+1.3 V, I=30 pA); (c) fully developed hex A phase after heating for 2 minutes at 360 K (U=+1.8 V, I=30 pA); (d) monomodal hex B phase (U=-1.8 V, I=30 pA).*

The obtained supramolecular arrangement exhibits a bimodal appearance formed by alternating rows of molecules with a convex or concave intramolecular conformation[87]. Upon heating, the supramolecular arrangement undergoes massive transformations as shown in Figure 3.11b-d. After heating to 330 K for 10 min, the onset for the transformation of the bimodal to a monomodal structure (referred to as hex A) is found, as shown in Figure 3.11b. After this first conformational change, the molecules appear as two pairs of protrusions with different intensity. The first molecules adopting this new conformation are found at dislocations of the bimodal row structure. Prolonged heating to 330 K or increased heating temperature (e.g. heating to 360 K for 2 min) result in a total conversion of the bimodal to the hex A structure. This situation is shown in Figure 3.11c. After heating to 450 K for 2 min, another supramolecular arrangement (referred to as hex B) is formed, which is shown in Figure 3.11d.

The following analysis will address the reasons for the observed transformations. One important feature of free base porphyrins on a Cu substrate is the so-called self-metalation reaction.[58, 60-62] The smaller 2HTPP was found to metalate on a Cu(111) surface to CuTPP, already at temperatures slightly below 400 K[61]. Hence a similar reaction is to be expected for 2HTTBPP, too.

In this respect X-ray photoelectron spectroscopy (XPS) is a helpful tool as it can monitor the changes of the chemical nature of the N atoms in the N 1s region. The XPS measurements reveal that upon heating the sample to 350 K and above, metalation of 2HTTBPP to CuTTBPP occurs. (For details see [P3].) The correlation of XPS and STM data shows that the hex B phase, which is found to be the exclusive structure after heating to 450 K for 2 min, where a total conversion to CuTTBPP occurred, consists of pure CuTTBPP. For situations, where partial metalation is observed in XPS, coexisting domains are found. In these situations, the ratio of hex B found in STM is in good agreement with the degree of metalation determined by XPS.

In order to gain a better understanding of the nature of the observed supramolecular arrangements, the structures will be investigated using high resolution STM images, partially overlaid with scaled molecular models exhibiting the deduced molecular conformations. The results are shown in Figure 3.12.

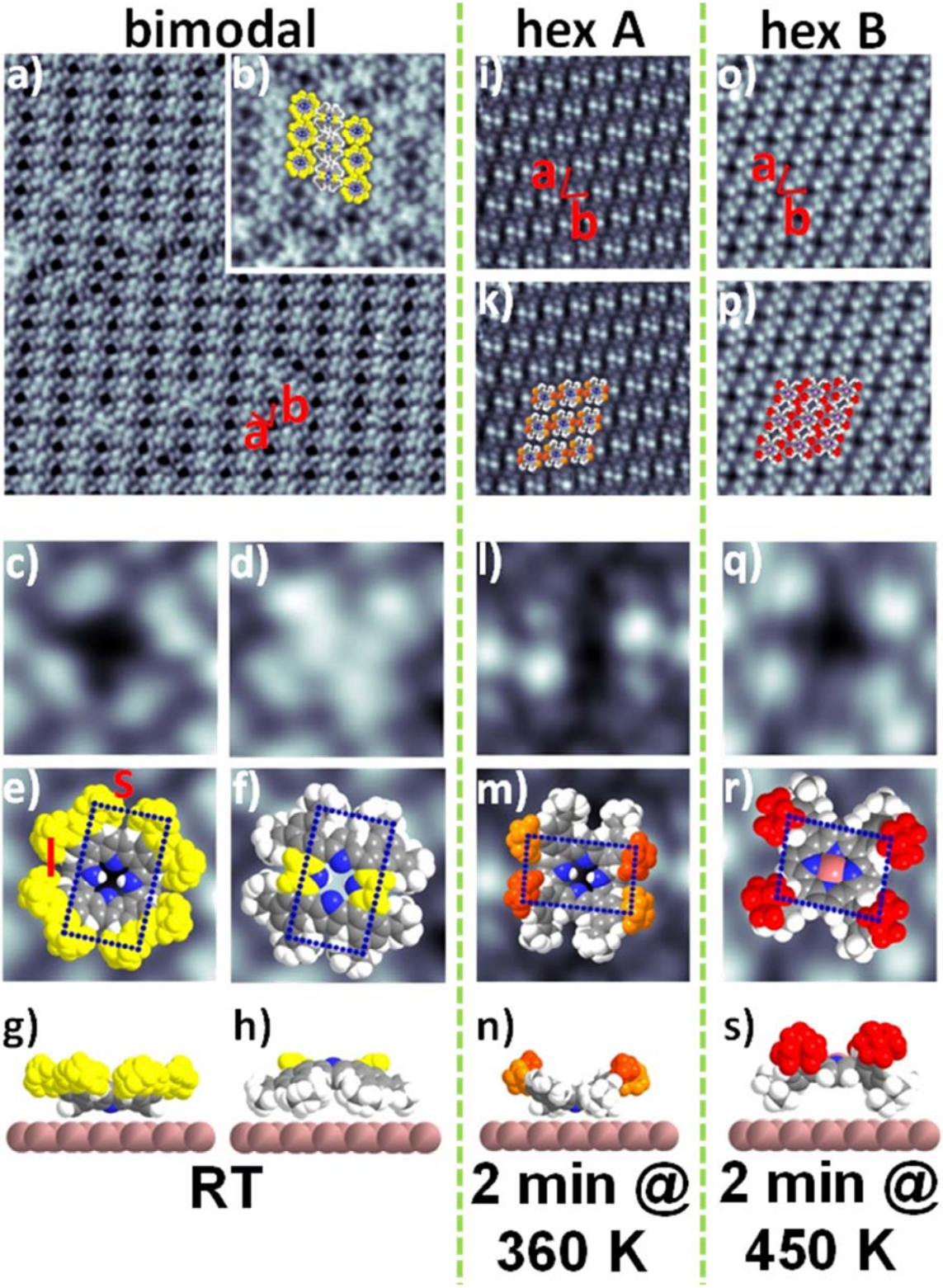

Figure 3.12: *Overview of the observed supramolecular porphyrin phases and the derived molecular models on Cu(111): (a-h) bimodal phase of 2HTTBPP as prepared at room temperature. (i-n) hex A phase of 2HTTBPP after heating to 360 K for 2 minutes. (o-s) hex B*

phase of CuTTBPP after metalation. The scanning parameters are: (a) U=+1.3 V, I=30 pA; (b-f) U=+1.8 V, I=25 pA; (i-m, o-r), U=+1.8 V, I=30 pA; (a) 35.0x35.0 nm^2; (b, i, k, o, p) 13.5x13.5 nm^2; (c, d, f, g, l, m, q, r) 2.5x2.5 nm^2.

It is well known for TTBPP molecules on different substrates that their appearance in STM is dominated by the four upper most *tert*-butyl groups.[44-45, 85-86, 104] These *tert*-butyl groups form a rectangle that allows to deduce the twist angle θ based on the aspect ratio of the rectangle and the tilt angle ϕ based on the perimeter of the rectangle. More details on this method can be found in [45, 87]. The parameters deduced for the supramolecular arrangements are given in Table 3.1. In addition, the two intramolecular conformations in the bimodal phase were confirmed by STM simulations[87].

Table 3.1: *Summary of the supramolecular and intramolecular geometrical values extracted from STM data; a, b: lattice parameters, α: angle between lattice vectors, ρ: molecular density, s and l experimentally determined s and l values, θ: the twist angle of the phenyl groups, ϕ: the corresponding tilt angle.*

Phase ↓	*a* [nm]	*b* [nm]	*α* [°]	*ρ* [molecules/ nm^2]	*s* [nm]	*l* [nm]	*θ* [°]	*ϕ* [°]
bimodal	1.90±0.10	2.00±0.06	60±5	0.30	0.70±0.1	1.25±0.1	5 ±5	35 ±5
hex A	1.75±0.10	1.92±0.10	68±5	0.32	0.57±0.1	1.07±0.1	35/10 ±5	35 ±5
hex B	1.81±0.10	1.85±0.05	60±5	0.35	0.87±0.05	1.12±0.05	75 ±5	5 ±5

Ditze et al. recently investigated the bimodal structure in great detail[87]: Within the bimodal structure all molecules, i.e. the convex and the concave ones, adopt the same molecular conformation with θ = 5 ± 5° and ϕ = 35 ± 5°. The resulting conformation resembles the shape of a bowl. Whether a molecule is a convex or concave one is determined by the orientation of the molecule towards the substrate: upright standing molecules resemble the concave conformation (Figure 3.12c, e, g), while upside down molecules resemble the

convex conformation (Figure 3.12d, f, h). While the concave conformation is in line with the strong attractive interaction between iminic nitrogen atoms and the Cu substrate, i.e. the nitrogen atoms are positioned close to the substrate, this is not the case for the convex conformation. The energetic analysis of the bimodal structure instead revealed that the convex conformation is stabilized by entropic contributions[87].

After the transformation to the monomodal hex A structure, conformation and orientation of the molecules, especially their macrocycle, are very similar to the concave conformation. The main difference is that for the hex A structure the *tert*-butyl phenyl groups are significantly twisted out of the porphyrin plane up to $\theta = 35 \pm 5°$. Figure 3.12n suggests that the distance of the N atoms of molecules in the hex A conformation to the substrate is similar compared to the concave conformation in the bimodal phase. As the molecules in the hex A phase are not yet metalated, the center of the molecule can be assumed to be similar to the concave situation, too. Thus the interactions between hex A molecules and the substrate should be similar to the interactions for the concave molecules. Besides that, the stronger rotation of the sidegroups allows for a better interlocking of the sidegroups of neighboring molecules. This also results in a reduced molecule-molecule distance and a higher packing density (bimodal: ρ = 0.30 molecules/nm^2, hex A: ρ = 0.32 molecules/nm^2). These findings indicate an additional stabilization of the supramolecular arrangement by attractive interactions between the *tert*-butyl groups of neighboring molecules. Due to the irreversibility of the conformational transition to hex A, this structure seems to be energetically more favorite than the bimodal arrangement, but the transition is an activated process, i.e. an activation barrier has to be overcome.

Further heating results in the metalation of the 2HTTBPP and the transformation into the hex B structure, as shown in Figure 3.11d and Figure 3.12o, p. Unlike the previous conformations, the macrocycle of the CuTTBPP molecule in the hex B phase is almost flat, while the *tert*-butylphenyl groups are rotated almost perpendicular ($\theta = 75 \pm 5°$) to the molecule plane. This results in a larger distance of the porphyrin core from the surface (cf. Figure 3.12s), indicating reduced molecule-substrate interactions compared to the concave or hex A conformation. Interestingly, the intramolecular conformation found for hex B is very similar to the one expected for the isolated molecule in the gas phase ($\theta = 70$; $\phi = 0$)[104].

In conclusion the bimodal structure formed by 2HTTBPP upon adsorption on Cu(111) at RT transforms into the more stable hex A phase upon mild annealing. Further annealing results in the self-metalation with Cu substrate atoms to CuTTBPP, which is accompanied by drastic reduction of the attractive molecule-substrate interactions resulting in a conformation where the molecule is lifted from the substrate.

3.4 Temperature Dependent Reversible Phase Transitions of CoTTBPP on Cu(111) [P4]

In the following, the adsorbate structures formed by CoTTBPP on Cu(111) will be discussed, with particular focus on the changes upon temperature variations. The results will also be compared to the ones obtained for the same molecule on Ag(111).[45]

The adsorption behavior of CoTTBPP upon coverage variations follows a well-known scheme: Initially, at low coverage the step edges of the substrate are decorated with molecules first. A representative STM image of molecules decorating a step edge is shown in Figure 3.13a. The preferred adsorption can be explained by the step edges representing energetically favorable adsorption sites due to the lower coordination of the substrate atoms there, compared to the ones of the terraces.

The close up view on three CoTTBPP molecules adsorbed at a step edge shown in Figure 3.13b demonstrates the actual conformation of the molecules: For the tunneling parameters applied for recording this image the molecules appear with a central protrusion, caused by the d_{z^2} orbital of the Co atom. (For a more detailed discussion of the voltage dependent appearance of CoTTBPP in STM see [P4].) Each central protrusion is surrounded by eight smaller protrusions originating from the eight *tert*-butyl groups of the molecule. The position of the Co atom right at the step edge and the reduced intensity of the *tert*-butyl groups on the lower side of the step suggest that the CoTTBPP molecules bridge the lower and upper terrace. A similar bridging behavior was observed for the similar tertiary-butyl-metoxyphenyl-porphyrin before.[105]

In addition, Figure 3.13a and d show clear indications for fast diffusing molecules on the terraces, i.e. the stripy features in a and the elevated background in d are due to molecules diffusing much faster over the surface than the movement speed of the STM tip. This observation is a strong indication for not very site specific molecule-substrate interactions resulting in a low diffusion barrier for the molecules on the terraces.

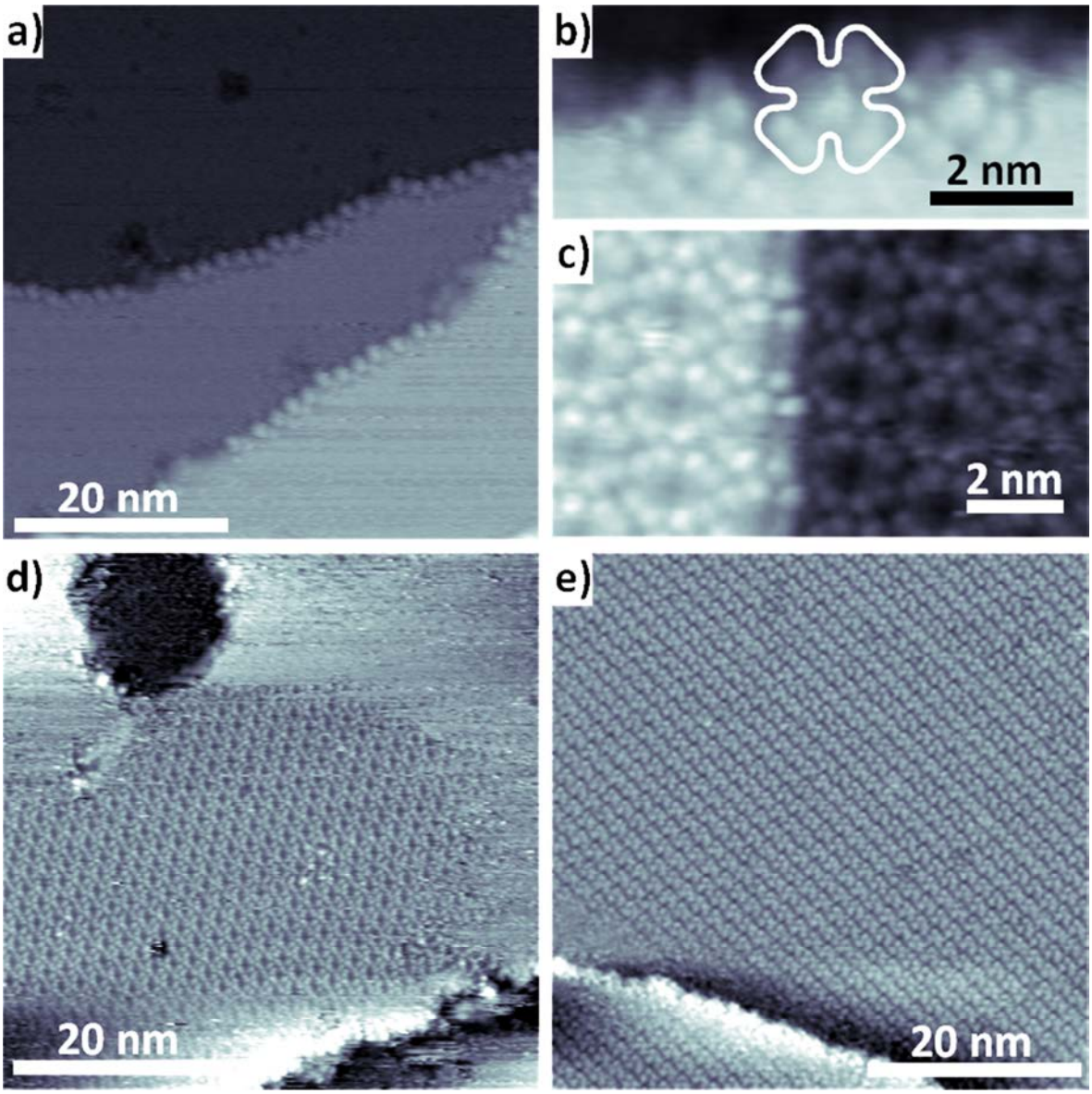

Figure 3.13: *Coverage dependent adsorption behavior of CoTTBPP on Cu(111):* ***a)*** *step decoration at low coverage (U = +1.03 V, I = 29 pA);* ***b)*** *close up on three molecules decorating a step edge; the center molecule is indicated by a white frame (U = -0.4 V, I = 29 pA).* ***c)*** *close up on a supramolecular arrangement pursuing over a step edge (U = +1.30, I = 36 pA).* ***d)*** *island formation at medium coverage (U = +1.22 V, I = 23 pA);* ***e)*** *completely covered surface at low resolution (U = +1.34 V, I = 35 pA).*

Higher coverages result in situations as shown in Figure 3.13c and d where the formation of well-ordered supramolecular hexagonal arrangements of molecules is observed. Since all

molecular islands were found to be in contact with at least one step edge, it can be assumed that the step edges act as nucleation site for the formation of the islands and also contribute to their stabilization. Another peculiar observation is shown in Figure 3.13c, where the hexagonal arrangement of a molecular island persists across a step edge. Due to the threefold symmetry of substrate and adsorbate domains, and the alignment of the latter according to the substrate (c.f. the step edges acting as nucleation sites for the island formation), all islands exhibit the same supramolecular hexagonal arrangement at RT up to a coverage of a closed layer. This situation is shown in Figure 3.13e.

Next, the supramolecular arrangement, and the molecular conformation will be discussed: High resolution STM images of CoTTBPP molecules in this hexagonal arrangement at RT, partially overlaid with scaled models are shown in Figure 3.14a-d.

As the images shown in this figure are recorded at a bias voltage of about +1 V, the molecules appear with a central depression and only the eight protrusions of the *tert*-butyl groups, surrounding the central depression, are visible. All eight protrusions appearing with similar height suggests an adsorption geometry of the molecule with the phenyl groups parallel to the surface plane. Further, two more, less intense protrusions closer the center of the molecule are visible in Figure 3.14c, which can be assigned to upward bent pyrrole groups. This conformational feature indicates a so called saddle-shaped distortion of the macrocycle, which is observed for phenyl meso-substituted porphyrin derivates[36, 38, 106-108].

From the STM images, the conformation of a TTBPP molecule, more precisely the tilt (ϕ) and twist (θ) of the di-*tert*-butyl-phenyl substituents can be evaluated, based on aspect ratio and circumference of the rectangle formed by the four most intense *tert*-butyl protrusions of each molecule. For details on this method the reader is referred to Section 3.3 and [56, 87]. Such rectangles used for analysis are shown in red in Figure 3.14b and f. The results of the analysis are reproduced in Table 3.2 and are represented in the models overlaid to the STM images in Figure 3.14.

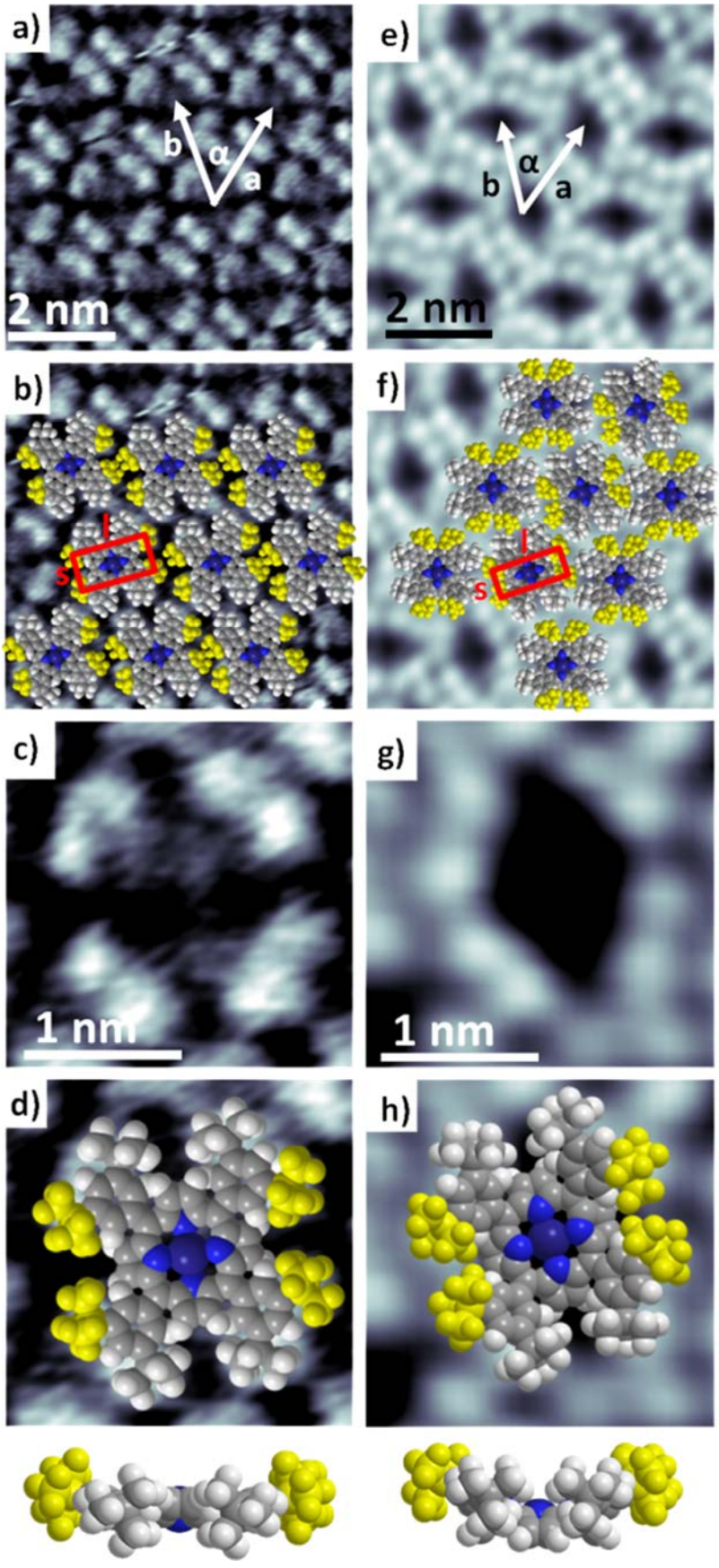
a)
b
α
a
2 nm
e)
b
α
a
2 nm
b)
l
s
f)
l
s
c)
1 nm
g)
1 nm
d)
h)

Figure 3.14**: High resolution STM images of the two observed arrangements demonstrating the different supramolecular arrangements and molecular conformations:* ***a) *hexagonal arrangement,* ***b)*** *overlaid with space filling models;* ***c)*** *single molecule of the hexagonal phase,* ***d)*** *overlaid with a space filling model and additional side view of the molecular conformation (a)-d): U = +1.31 V, I = 36 pA, T = RT).* ***e)*** *herringbone arrangement,* ***f)*** *overlaid with space filling models;* ***g)*** *single molecule of the herringbone phase,* ***h)*** *overlaid with a space filling model and additional side view of the molecular conformation (e)-h): U = +1.26 V, I = 23 pA, T = 180 K).*

***Table 3.2:** Summary of the supramolecular and intramolecular geometrical values extracted from STM data; a, b: lattice parameters, α: angle between lattice vectors, ρ: molecular density, s and l experimentally determined s and l values, θ: the twist angle of the phenyl groups, ϕ: the corresponding tilt angle.*

	a [nm]	*b* [nm]	*α* [°]	*ρ* [Mol/nm^2]	*l* [nm]	*s* [nm]	*θ* [°]	*ϕ* [°]
Hexagonal	1.97±0.04	2.07±0.02	59±1	0.28	1.37±0.05	0.7±0.05	10	5
Herringbone	1.9±0.06	1.77±0.04	60±1	0.34	1.25±0.07	0.63±0.06	10	30

The derived values of a tilt of 5° and a twist of 10° confirm the first impression of an almost flat molecule mentioned earlier. As the interactions between molecule and substrate are not very site specific, the formation and stabilization of the supramolecular arrangements has to be driven by intermolecular interactions. Judging from the close proximity of *tert*-butyl groups or protrusions of neighboring molecules in the STM images and the scaled model overlay shown in Figure 3.14b, the stabilizing interactions are proposed to be van der Waals forces.

In the next step, the influence of the sample temperature on the adsorbed molecules and the formed supramolecular structures will be discussed. Starting with the hexagonal arrangement obtained at RT, the mobility of the molecules increases upon heating as the total energy increases. This process continues up to about 440 K, where the molecular ordering is destroyed irreversibly. Most likely, dehydrogenation occurs at this temperature, which was reported to occur at similar temperatures for related systems[99, 108-109]. Such a dehydrogenation

reaction usually occurs on the energetically unfavorable, sterically hindered positions first, resulting in drastically different conformations due to the formation of additional bonds. With this new conformation the mutual stabilization observed for the hexagonal arrangement at RT is no longer possible.

Interestingly, the reduction of the sample temperature below 220 K results in the formation of a new herringbone structure that coexists with the hexagonal one between 180 and 220 K. This coexistence of phases, as well as the reversibility of this phase transition is shown in Figure 3.15. Please note that 180 K is the minimal achievable operating temperature for the STM setup used to obtain these results and thus the investigation and analysis of the thermal evolution could not be expanded to lower temperatures.

The ratio of hexagonal and herringbone phase depends on the actual temperature, which is to be expected. With reduced temperature the herringbone phase fraction increases. At 180 K approximately 65 ± 5 % of all molecules forming supramolecular structures are in the herringbone phase.

Details on the herringbone structure are shown in Figure 3.14e-h. Although the general appearance of a molecule is similar to the one already discussed for the hexagonal phase, i.e. eight protrusions surrounding a central cavity, the intramolecular conformation is very different from the hexagonal one. While the twist angle of θ = 10° is similar, the tilt angle of ϕ = 30° is much larger (c.f. Figure 3.14d vs. h).

This change in conformation, especially the larger tilt angle, results in a smaller surface area per molecule and allows for a higher packing density (0.34 molecules/nm^2 for the herringbone and 0.28 molecules/nm^2 for the hexagonal phase). In contrast to the hexagonal appearance, the herringbone one does not show any protrusions at the pyrrole positions, suggesting that the saddle-shaped distortion is less pronounced or not present at all (cf. Figure 3.14c and g). Indeed, DFT calculations for CoTTBPP on Ag(111) show a local minimum in the potential energy surface for the combination of angles representing the herringbone conformation[110]. The calculated structure shows no saddle-shape, but a bowl-like distortion, i.e. all four pyrrole groups are bent by 30° to one side of the molecular plane, while the *tert*-butylphenyl groups are tilted towards the other side.

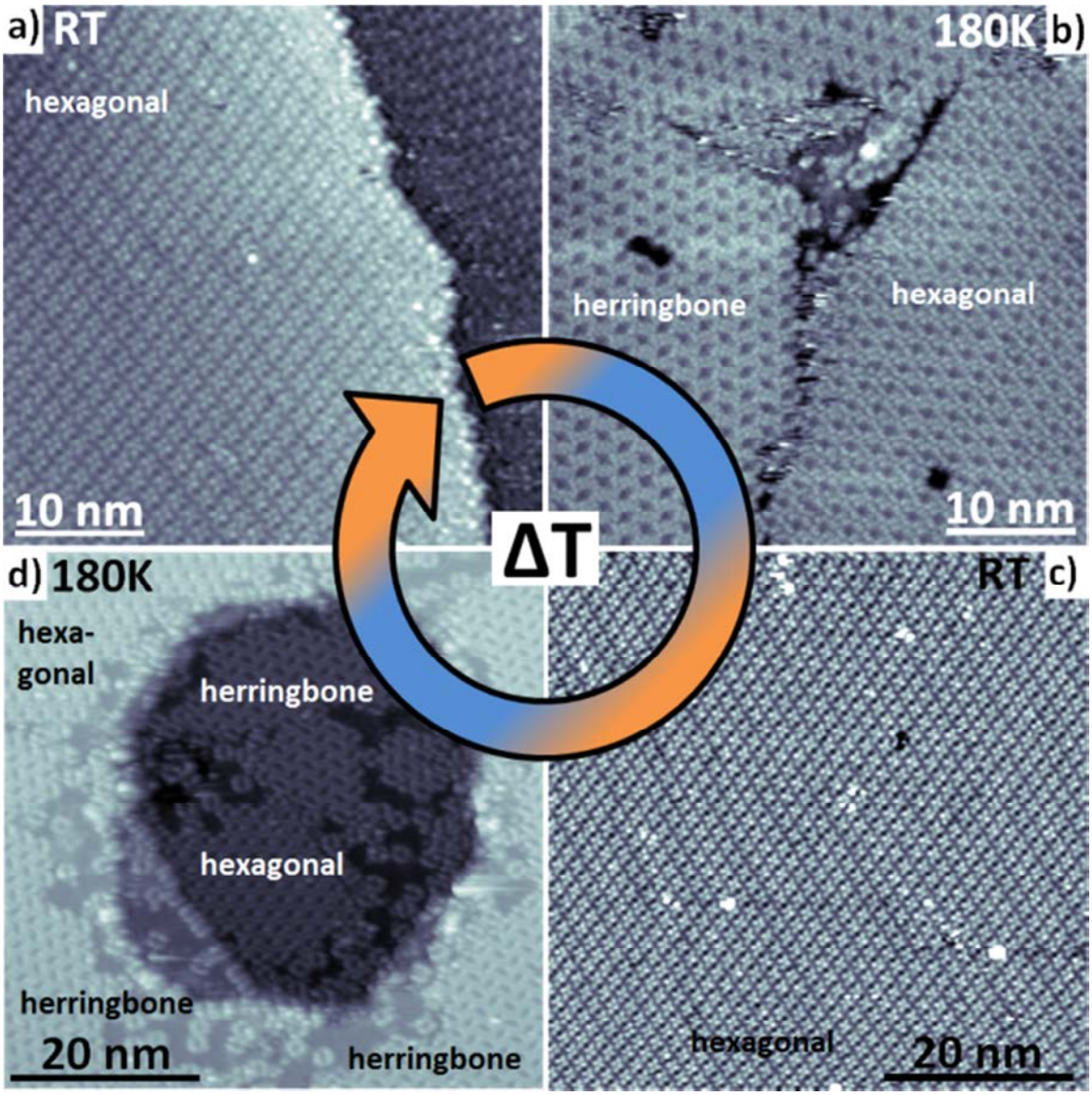

***Figure 3.15**: STM images documenting the temperature dependent reversible phase transition between herringbone and hexagonal phase. (a) and (c): pure hexagonal phases recorded at RT (U = +1.30 V, I = 30 pA). (b) and (d): coexistence of hexagonal and herringbone phase recorded at 180 K (b) U = +1.26 V, I = 23 pA; d) U =-0.66V, I = 29 pA).*

Due to the similarity of the hexagonal and the herringbone phase, the stabilization of the supramolecular arrangement is realized via intermolecular van der Waals interactions in both cases. However, there are some important differences: While in the hexagonal arrangement each molecule can interact with 16 neighboring *tert*-butyl groups, the number increases to 20

for the herringbone arrangement. In addition, for the herringbone arrangement the average distance between neighboring *tert*-butyl groups is reduced by ~1 Å. The higher packing density, the increased number of interactions and the reduced average distance suggest the herringbone arrangement to be the energetically favorable one.

A comparison of the results for CoTTBPP on Cu(111) and Ag(111)[56] shows some similarities, but also some differences: While on Ag(111) four different structures were found, only two of them are present on Cu(111). Although the overall appearances of the hexagonal and the herringbone phases are similar on both substrates, the size of the unit cell and the intramolecular conformations are different. These differences are caused by the different interaction of the molecules with the different substrates. For the hexagonal conformation, the smaller twist angle on Cu(111) (10° vs. 45° on Ag(111)) results in a reduced distance to the substrate by about 1 Å, suggesting stronger attractive interactions between the molecules and Cu(111) than for Ag(111). For the herringbone structures, a direct comparison of the results on Cu(111) and Ag(111) is not valid as in ref. [56] the herringbone structure was obtained by thermal desorption of multilayers at elevated temperatures and no investigations below RT were conducted.

In conclusion, the supramolecular structures formed by CoTTBPP on Cu(111) are primarily stabilized by van der Waals forces between *tert*-butyl groups of neighboring molecules. In addition the formation of the hexagonal and the herringbone structure is a fully reversible, temperature dependent process. Further a strong dependency of the appearance of the central Co atom on the tunneling parameters was found.

4 Summary

In the present STM study, different tetrapyrrolic adsorbates, that are, 2HTPP, 2HTPPc, 2HTTBPP, CuTTBPP, CoTTBPP, were investigated on a Cu(111) surface. Thereby it was found that small variations of the molecular theme on the same substrate significantly influence the adsorption behavior.

For 2HTPP on Cu(111), the formation of a novel, complex checkerboard-type superstructure was found at higher coverages, with half of the molecules in direct contact to the surface and the other half elevated from the surface, bridging the gaps between the lower first layer molecules. While the orientations of the checkerboard domains and the conformation of the first layer molecules are in line with the observations for low coverages, the conformation of the second layer molecules is similar to the multilayer ones. Although the adsorption of 2HTPP on Cu(111) is dominated by adsorbate-substrate interactions, the checkerboard structure is stabilized by attractive intermolecular interactions in form of T-type interactions and π-π stacking interactions at the same time.

The investigation of the adsorption behavior of 2HTPPc on Cu(111) revealed that the molecules tend to form supramolecular arrangements consisting of rows oriented along the main crystallographic directions of the substrates. Two types of rows can be distinguished: highly ordered ones, where all molecules are oriented in the same direction, and less ordered ones, where two different orientations are found. While within the highly ordered rows the situation appears to be static, the molecules in the less ordered rows frequently alter between the two orientations at RT. Right after deposition, a metastable situation is found with preferentially one less ordered row separating two highly ordered ones, which changes over time to a situation where two less ordered rows separate two highly ordered ones. This initial dynamic rearrangement is explained by strong cooperative effects and an energetically more favorable situation after the change, to a large extent caused by a better registry to the substrate. Overall, the unusual adsorption behavior of 2HTPPc at room temperature can be characterized as a mixture of supramolecular order and structural dynamics.

For 2HTTBPP on Cu(111) two thermally induced morphological and chemical transformations were found. First, at temperatures above 330 K, the transition from the initial bimodal structure to the monomodal so-called hex A arrangement is observed. This was

explained by a stabilization of the supramolecular arrangement due to a better interlocking of the peripheral *tert*-butyl groups. At higher temperatures and/or prolonged heating times, 2HTTBPP undergoes a transition to the so-called hex B phase, accompanied by the self-metalation with Cu substrate atoms to CuTTBPP. This massive structural change upon metalation, in which the molecules literally pop up from the surface, can be explained by reduced molecule-substrate interactions after metalation.

The adsorption behavior of CoTTBPP on Cu(111) again differs from the ones discussed above. For CoTTBPP, a reversible phase transition from a hexagonal to a herringbone arrangement occurs upon cooling the sample from RT to 180 K. Since this transition is accompanied by a compression of the structure, i.e. a lower molecular density for the herringbone arrangement, it is in line with a conventional freezing process. The higher stability of the hexagonal structure at RT is explained by entropic contributions lowering the free Gibbs energy. The investigation of the intramolecular conformation revealed two significantly different conformations for the hexagonal and the herringbone arrangement: For the hexagonal phase, a saddle-shaped distortion of the macrocycle is found, while in the herringbone phase a bowl shaped conformation is found, that is, all four pyrrole groups oriented to one side of the macrocycle and the four *tert*-butyl-phenyl groups to the opposite side. A comparison to Ag(111) reveals a ~1 Å smaller molecule-substrate distance indicating more attractive molecule-substrate interactions on Cu(111). For the bias dependence of the appearance in STM of CoTTBPP on Cu(111) in the hexagonal phase, it was found that only within a small negative bias voltage window (-0.44 to -0.22 V) the appearance is dominated by a central protrusion. For other bias voltages (at least in the range from -1.3 to +1.3 V), the appearance is dominated by the actual topographic height of the organic parts of the molecule.

Overall, it is shown that the complex interplay of intermolecular and molecule-substrate interactions and resulting adsorption behavior of porphyrinoids is influenced to a very large extent by the different modifications of the molecules, like attached peripheral substituents, presence and type of central metal atom, or the constitution of the macrocycle. To sum up, the adsorption behavior for porphyrinoids is determined by a complex interplay of different contribution and it is thus very difficult to generalize and predict the adsorption behavior.

5 Zusammenfassung

In der vorliegenden STM Arbeit wurden unterschiedliche tetrapyrrolische Adsorbate auf einer Cu(111) Oberflache untersucht, nämlich 2HTPP, 2HTPPc, 2HTTBPP, CuTTBPP und CoTTBPP. Dabei hat sich gezeigt dass kleine Unterschiede im molekularen Thema das Adsorptionsverhalten auf dem gleichen Substrat entscheidend beeinflussen.

Für 2HTPP auf Cu(111) wurde, bei höherer Bedeckung, die Ausbildung einer neuartigen, komplexen, schachbrettartigen Struktur beobachtet, bei welcher die eine Hälfte der Moleküle im direkten Kontakt mit der Oberfläche ist, wohingegen die andere Hälfte erhöht ist und die Lücken zwischen den Erstlagenmolekülen überbrückt. Während die Ausrichtung der Schachbrettdomänen und die Konformation der Erstlagenmoleküle sich mit den Erkenntnissen für niedrige Bedeckungen decken, gleicht die Konformation der Zweitlagenmoleküle derer der Multilagenmoleküle. Obwohl das Adsorptionsverhalten von 2HTPP auf Cu(111) von Adsorbat-Substrat-Wechselwirkungen dominiert wird, wird die Schachbrettstruktur zugleich durch attraktive intermolekulare T-type und π-π-Stapel Wechselwirkungen stabilisiert.

Die Untersuchung des Adsorptionsverhaltens von 2HTPPc auf Cu(111) hat gezeigt, dass die Moleküle dazu neigen supramolekulare Anordnungen auszubilden, welche aus, entlang der kristallographischen Vorzugsrichtungen des Substrats ausgerichteten Reihen bestehen. Dabei können zwei Arten von Reihen unterschieden werden, nämlich die hoch geordneten Reihen, in welchen alle Moleküle gleich ausgerichtet sind, und die weniger geordneten Reihen, in denen zwei unterschiedliche Ausrichtungen auftreten. Während die Situation in den hoch geordneten statisch zu sein scheint, wechseln die Moleküle in den weniger geordneten Reihen bei Raumtemperatur häufig zwischen den beiden Orientierungen. Unmittelbar nach der Abscheidung ist eine metastabile Situation zu finden, bei der zwei hoch geordnete Reihen meist von einer weniger geordneten Reihe getrennt werden. Mit der Zeit ändert sich dies hin zu einer Situation, bei der zwei weniger geordnete Reihen zwei hoch geordnete trennen. Diese anfänglich dynamische Umordnung lässt sich durch starke kooperative Effekte und einer energetisch günstigeren Situation nach der Umordnung erklären, welche weitestgehend durch eine bessere Registrierung zum Substrat erzielt wird. Allgemein kann das ungewöhnliche Adsorptionsverhalten von 2HTPPc bei Raumtemperatur als eine Mischung aus supramolekularer Ordnung und struktureller Dynamik charakterisiert werden.

Im Falle von 2HTTBPP auf Cu(111) wurden zwei thermisch induzierte morphologische und chemische Transformationen gefunden. Zuerst ist, bei Temperaturen über 330 K, der Übergang der anfänglich bimodalen Struktur zur monomodalen, sogenannten hex A Anordnung zu beobachten. Dies wurde durch die Stabilisierung der supramolekularen Anordnung auf Grund der besseren Verzahnung der peripheren *tert*-butyl Gruppen erklärt. Bei höheren Temperaturen und/oder längeren Heizdauern, vollzieht 2HTTBPP die Umwandlung zur sogenannten hex B Phase. Dies geht einher mit der Selbstmetallierung mit Cu Substratatomen zu CuTTBPP. Diese gravierende strukturelle Veränderung während der Metallierung, bei der die Moleküle buchstäblich von der Oberfläche emporschnellen, kann durch die verringerten Molekül-Substrat-Wechselwirkungen nach der Metallierung erklärt werden.

Das Adsorptionsverhalten von CoTTBPP auf Cu(111) unterscheidet sich erneut von den bereits diskutierten. Im Falle von CoTTBPP tritt ein reversibler Phasenübergang von einer hexagonalen zu einer herringbone Anordnung auf, wenn die Probe von Raumtemperatur auf 180 K abgekühlt wird. Dies deckt sich mit einem konventionellen Gefrierprozess, da der beobachtete Übergang von einer Kompression der Struktur begleitet wird, d.h. die Moleküldichte der herringbone Anordnung ist geringer. Die größere Stabilität der hexagonalen Struktur bei Raumtemperatur wird durch entropische Beiträge erklärt, welche die Gibbs'sche freie Energie verringert. Die Untersuchung der intramolekularen Konformation ergab zwei signifikant unterschiedliche Konformationen für die hexagonale und die herringbone Anordnung: Bei der hexagonalen Phase wurde eine sattelartige Verbiegung des Makrozyklus bestimmt, wohingegen bei der herringbone Phase eine schüsselartige Konformation vorliegt, d.h. alle vier Pyrrol-Gruppen sind auf die eine Seite des Makrozyklus geneigt und die vier *tert*-butyl-Gruppen auf die andere. Der Vergleich mit Ag(111) ergab einen um ~1 Å geringeren Molekül-Substrat-Abstand, was auf attraktivere Molekül-Substrat-Wechselwirkungen im Falle von Cu(111) hindeutet. Im Bezug auf die Spannungsabhängigkeit der Erscheinung von CoTTBPP auf Cu(111) in der hexagonalen Phase im STM hat sich gezeigt, dass nur in einem kleinen negativen Spannungsfenster (-0.44 bis -0.22 V) die Erscheinung von einer zentralen Erhebung dominiert wird. Bei anderen Spannungen (zumindest im Bereich zwischen -1.3 und +1.3 V) wird die Erscheinung durch die tatsächliche topographische Höhe der organischen Teile des Moleküls bestimmt.

Insgesamt wurde gezeigt, dass das komplexe Zusammenspiel von intermolekularen und Molekül-Substrat-Wechselwirkungen, sowie das resultierende Adsorptionsverhalten von

Porphyrinoiden weitestgehend beeinflusst wird durch die unterschiedlichen Modifikationen der Moleküle, wie periphere Substituenten, Anwesenheit und Typ eines zentralen Metallatoms, oder dem Aufbau des Makrozyklus. Abschließend ist zu sagen, dass das Adsorptionsverhalten von Porphyrinoiden von einem komplizierten Zusammenspiel unterschiedlicher Beiträge bestimmt wird und es deshalb sehr schwierig ist dies zu verallgemeinern und das Adsorptionsverhalten vorherzusagen.

6 Literature

[1] G. M. Whitesides, *Nanoscience, Nanotechnology, and Chemistry*, *Small*, 2005, **1**, 172-179.

[2] H. W. Du, X. Lin, Z. M. Xu and D. W. Chu, *Electric double-layer transistors: a review of recent progress*, *Journal of Materials Science*, 2015, **50**, 5641-5673.

[3] T. R. Pan and W. Wang, *From Cleanroom to Desktop: Emerging Micro-Nanofabrication Technology for Biomedical Applications*, *Annals of Biomedical Engineering*, 2011, **39**, 600-620.

[4] D. Vuillaume, *Molecular-scale electronics*, *Comptes Rendus Physique*, 2008, **9**, 78-94.

[5] C. G. You, C. M. Han, X. G. Wang, Y. R. Zheng, Q. Y. Li, X. L. Hu and H. F. Sun, *The progress of silver nanoparticles in the antibacterial mechanism, clinical application and cytotoxicity*, *Molecular Biology Reports*, 2012, **39**, 9193-9201.

[6] F. Hui and C. Debiemme-Chouvy, *Antimicrobial N-Halamine Polymers and Coatings: A Review of Their Synthesis, Characterization, and Applications*, *Biomacromolecules*, 2013, **14**, 585-601.

[7] J. Drelich, B. W. Li, B. Villeneuve and P. Bowen, *Inexpensive mineral copper materials with antibacterial surfaces*, *Surface Innovations*, 2013, **1**, 15-26.

[8] M. J. Hanus and A. T. Harris, *Nanotechnology innovations for the construction industry*, *Progress in Materials Science*, 2013, **58**, 1056-1102.

[9] S. Banerjee, D. D. Dionysiou and S. C. Pillai, *Self-cleaning applications of TiO2 by photo-induced hydrophilicity and photocatalysis*, *Applied Catalysis B-Environmental*, 2015, **176**, 396-428.

[10] G. E. Moore, *Cramming more components onto integrated circuits*, *Electronics*, 1965, **38**, 114-117.

[11] G. Binnig and H. Rohrer, *Surface imaging by scanning tunneling microscopy*, *Ultramicroscopy*, 1983, **11**, 157-160.

[12] G. Binnig, H. Rohrer, C. Gerber and E. Weibel, *Surface Studies by Scanning Tunneling Microscopy*, *Physical Review Letters*, 1982, **49**, 57-61.

[13] H. Marbach, *Habilitation Thesis*, FAU Erlangen-Nürnberg, Erlangen, 2010.

[14] L. R. Milgrom, *The colour of Life*, Oxford University Press, Oxford, 1997.

[15] G. M. Whitesides, J. P. Mathias and C. T. Seto, *Molecular self-assembly and nanochemistry: a chemical strategy for the synthesis of nanostructures*, *Science*, 1991, **254**, 1312-1319.

[16] J. M. Gottfried, *Surface chemistry of porphyrins and phthalocyanines*, *Surface Science Reports*, 2015, **70**, 259-379.

[17] H. Marbach, *Surface-Mediated in Situ Metalation of Porphyrins at the Solid–Vacuum Interface*, *Accounts of Chemical Research*, 2015, **48**, 2649-2658.

[18] W. Auwärter, D. Écija, F. Klappenberger and J. V. Barth, *Porphyrins at interfaces*, *Nat Chem*, 2015, **7**, 105-120.

[19] M. Gottfried and H. Marbach, in *Zeitschrift für Physikalische Chemie International journal of research in physical chemistry and chemical physics*, 2009, p. 53.

[20] W. Y. Gao and S. Q. Ma, *Beyond Custom Design of Organic Ligands: An Integrative Strategy for Metal-Organic Frameworks Design*, *Comments on Inorganic Chemistry*, 2014, **34**, 125-141.

[21] F. Klappenberger, *Two-dimensional functional molecular nanoarchitectures - Complementary investigations with scanning tunneling microscopy and X-ray spectroscopy*, *Progress in Surface Science*, 2014, **89**, 1-55.
[22] S. V. Bhosale, S. V. Bhosale, G. V. Shitre, S. R. Bobe and A. Gupta, *Supramolecular Chemistry of Protoporphyrin IX and Its Derivatives*, *European Journal of Organic Chemistry*, 2013, 3939-3954.
[23] M. Jurow, A. E. Schuckman, J. D. Batteas and C. M. Drain, *Porphyrins as molecular electronic components of functional devices*, *Coordination Chemistry Reviews*, 2010, **254**, 2297-2310.
[24] J. Otsuki, *STM studies on porphyrins*, *Coordination Chemistry Reviews*, 2010, **254**, 2311-2341.
[25] S. Mohnani and D. Bonifazi, *Supramolecular architectures of porphyrins on surfaces: The structural evolution from 1D to 2D to 3D to devices*, *Coordination Chemistry Reviews*, 2010, **254**, 2342-2362.
[26] S. Yoshimoto and N. Kobayashi, in *Functional Phthalocyanine Molecular Materials*, ed. J. Jiang, Springer-Verlag Berlin, Berlin, 2010, pp. 137-167.
[27] H.-J. Schneider, *Interactions in Supramolecular Complexes Involving Arenes: Experimental Studies*, *Accounts of Chemical Research*, 2013, **46**, 1010-1019.
[28] P. Bhyrappa, C. Arunkumar and B. Varghese, *Influence of Mixed Substituents on the Macrocyclic Ring Distortions of Free Base Porphyrins and Their Metal Complexes*, *Inorganic Chemistry*, 2009, **48**, 3954-3965.
[29] M. O. Senge, C. J. Medforth, T. P. Forsyth, D. A. Lee, M. M. Olmstead, W. Jentzen, R. K. Pandey, J. A. Shelnutt and K. M. Smith, *Comparative Analysis of the Conformations of Symmetrically and Asymmetrically Deca- and Undecasubstituted Porphyrins Bearing Meso-Alkyl or -Aryl Groups*, *Inorganic Chemistry*, 1997, **36**, 1149-1163.
[30] M. O. Senge, *New trends in photobiology*, *Journal of Photochemistry and Photobiology B: Biology*, 1992, **16**, 3-36.
[31] J. Brede, M. Linares, S. Kuck, J. Schwöbel, A. Scarfato, S. H. Chang, G. Hoffmann, R. Wiesendanger, R. Lensen, P. H. J. Kouwer, J. Hoogboom, A. E. Rowan, M. Bröring, M. Funk, S. Stafström, F. Zerbetto and R. Lazzaroni, *Dynamics of molecular self-ordering in tetraphenyl porphyrin monolayers on metallic substrates*, *Nanotechnology*, 2009, **20**, 275602.
[32] F. Davis and S. P. J. Higson, *Biofuel cells—Recent advances and applications*, *Biosensors and Bioelectronics*, 2007, **22**, 1224-1235.
[33] F. Rosei, M. Schunack, Y. Naitoh, P. Jiang, A. Gourdon, E. Laegsgaard, I. Stensgaard, C. Joachim and F. Besenbacher, *Properties of large organic molecules on metal surfaces*, *Progress in Surface Science*, 2003, **71**, 95-146.
[34] P. B. Messersmith and M. Textor, *Nanomaterials: Enzymes on nanotubes thwart fouling*, *Nat Nano*, 2007, **2**, 138-139.
[35] C. J. Baddeley, *Fundamental Investigations of Enantioselective Heterogeneous Catalysis*, *Topics in Catalysis*, 2003, **25**, 17-28.
[36] F. Buchner, I. Kellner, W. Hieringer, A. Görling, H.-P. Steinrück and H. Marbach, *Ordering aspects and intramolecular conformation of tetraphenylporphyrins on Ag(111)*, *Phys. Chem. Chem. Phys.*, 2010, **12**, 13082-13090.
[37] W. Auwärter, A. Weber-Bargioni, A. Riemann, A. Schiffrin, O. Gröning, R. Fasel and J. V. Barth, *Self-assembly and conformation of tetrapyridyl-porphyrin molecules on Ag(111)*, *The Journal of Chemical Physics*, 2006, **124**, 194708.

[38] F. Buchner, E. Zillner, M. Röckert, S. Gläßel, H.-P. Steinrück and H. Marbach, *Substrate-Mediated Phase Separation of Two Porphyrin Derivatives on Cu(111), Chemistry – A European Journal*, 2011, **17**, 10226-10229.

[39] W. Auwärter, F. Klappenberger, A. Weber-Bargioni, A. Schiffrin, T. Strunskus, C. Wöll, Y. Pennec, A. Riemann and J. V. Barth, *Conformational Adaptation and Selective Adatom Capturing of Tetrapyridyl-porphyrin Molecules on a Copper (111) Surface*, *Journal of the American Chemical Society*, 2007, **129**, 11279-11285.

[40] M. Eichberger, M. Marschall, J. Reichert, A. Weber-Bargioni, W. Auwärter, R. L. C. Wang, H. J. Kreuzer, Y. Pennec, A. Schiffrin and J. V. Barth, *Dimerization Boosts One-Dimensional Mobility of Conformationally Adapted Porphyrins on a Hexagonal Surface Atomic Lattice*, *Nano Letters*, 2008, **8**, 4608-4613.

[41] G. Rojas, X. Chen, C. Bravo, J. H. Kim, J. S. Kim, J. Xiao, P. A. Dowben, Y. Gao, X. C. Zeng, W. Choe and A. Enders, *Self-Assembly and Properties of Nonmetalated Tetraphenyl-Porphyrin on Metal Substrates*, *Journal of Physical Chemistry C*, 2010, **114**, 9408-9415.

[42] F. Buchner, J. Xiao, E. Zillner, M. Chen, M. Röckert, S. Ditze, M. Stark, H.-P. Steinrück, J. M. Gottfried and H. Marbach, *Diffusion, Rotation, and Surface Chemical Bond of Individual 2H-Tetraphenylporphyrin Molecules on Cu(111)*, *The Journal of Physical Chemistry C*, 2011, **115**, 24172-24177.

[43] D. Heim, K. Seufert, W. Auwärter, C. Aurisicchio, C. Fabbro, D. Bonifazi and J. V. Barth, *Surface-Assisted Assembly of Discrete Porphyrin-Based Cyclic Supramolecules*, *Nano Letters*, 2010, **10**, 122-128.

[44] T. A. Jung, R. R. Schlittler and J. K. Gimzewski, *Conformational identification of individual adsorbed molecules with the STM*, *Nature*, 1997, **386**, 696-698.

[45] F. Buchner, K. Comanici, N. Jux, H.-P. Steinrück and H. Marbach, *Polymorphism of Porphyrin Molecules on Ag(111) and How to Weave a Rigid Monolayer*, *The Journal of Physical Chemistry C*, 2007, **111**, 13531-13538.

[46] M. Lepper, L. Zhang, M. Stark, S. Ditze, D. Lungerich, N. Jux, W. Hieringer, H.-P. Steinrück and H. Marbach, *Role of Specific Intermolecular Interactions for the Arrangement of Ni(II)-5, 10, 15, 20-Tetraphenyltetrabenzoporphyrin on Cu(111)*, *The Journal of Physical Chemistry C*, 2015, **119**, 19897-19905.

[47] N. A. Rakow and K. S. Suslick, *A colorimetric sensor array for odour visualization*, *Nature*, 2000, **406**, 710-713.

[48] B. R. Takulapalli, G. M. Laws, P. A. Liddell, J. Andréasson, Z. Erno, D. Gust and T. J. Thornton, *Electrical Detection of Amine Ligation to a Metalloporphyrin via a Hybrid SOI-MOSFET*, *Journal of the American Chemical Society*, 2008, **130**, 2226-2233.

[49] L. Schmidt-Mende, W. M. Campbell, Q. Wang, K. W. Jolley, D. L. Officer, M. K. Nazeeruddin and M. Grätzel, *Zn-Porphyrin-Sensitized Nanocrystalline TiO2 Heterojunction Photovoltaic Cells*, *ChemPhysChem*, 2005, **6**, 1253-1258.

[50] I. Mochida, K. Suetsugu, H. Fujitsu and K. Takeshita, *Enhanced catalytic activity of cobalt tetraphenylporphyrin on titanium dioxide by evacuation at elevated temperatures for intensifying the complex-support interaction*, *The Journal of Physical Chemistry*, 1983, **87**, 1524-1529.

[51] J. Nowakowski, C. W?ckerlin, J. Girovsky, D. Siewert, T. A. Jung and N. Ballav, *Porphyrin metalation providing an example of a redox reaction facilitated by a surface reconstruction*, *Chemical Communications*, 2013, **49**, 2347-2349.

[52] F. Buchner, K. Flechtner, Y. Bai, E. Zillner, I. Kellner, H.-P. Steinrück, H. Marbach and J. M. Gottfried, *Coordination of Iron Atoms by Tetraphenylporphyrin Monolayers*

and Multilayers on Ag(111) and Formation of Iron-Tetraphenylporphyrin, *The Journal of Physical Chemistry C*, 2008, **112**, 15458-15465.

[53] F. Buchner, I. Kellner, H.-P. Steinrück and H. Marbach, *Modification of the Growth of Iron on Ag(111) by Predeposited Organic Monolayers*, *Zeitschrift Fur Physikalische Chemie-International Journal of Research in Physical Chemistry & Chemical Physics*, 2009, **223**, 131-144.

[54] A. Kretschmann, M.-M. Walz, K. Flechtner, H.-P. Steinrück and J. M. Gottfried, *Tetraphenylporphyrin picks up zinc atoms from a silver surface*, *Chemical Communications*, 2007, 568-570.

[55] W. Auwärter, A. Weber-Bargioni, S. Brink, A. Riemann, A. Schiffrin, M. Ruben and J. V. Barth, *Controlled Metalation of Self-Assembled Porphyrin Nanoarrays in Two Dimensions*, *ChemPhysChem*, 2007, **8**, 250-254.

[56] F. Buchner, V. Schwald, K. Comanici, H.-P. Steinrück and H. Marbach, *Microscopic Evidence of the Metalation of a Free-Base Porphyrin Monolayer with Iron*, *ChemPhysChem*, 2007, **8**, 241-243.

[57] J. M. Gottfried, K. Flechtner, A. Kretschmann, T. Lukasczyk and H.-P. Steinrück, *Direct Synthesis of a Metalloporphyrin Complex on a Surface*, *Journal of the American Chemical Society*, 2006, **128**, 5644-5645.

[58] R. González-Moreno, C. Sánchez-Sánchez, M. Trelka, R. Otero, A. Cossaro, A. Verdini, L. Floreano, M. Ruiz-Bermejo, A. García-Lekue, J. Á. Martín-Gago and C. Rogero, *Following the Metalation Process of Protoporphyrin IX with Metal Substrate Atoms at Room Temperature*, *The Journal of Physical Chemistry C*, 2011, **115**, 6849-6854.

[59] C. M. Doyle, S. A. Krasnikov, N. N. Sergeeva, A. B. Preobrajenski, N. A. Vinogradov, Y. N. Sergeeva, M. O. Senge and A. A. Cafolla, *Evidence for the formation of an intermediate complex in the direct metalation of tetra(4-bromophenyl)-porphyrin on the Cu(111) surface*, *Chemical Communications*, 2011, **47**, 12134-12136.

[60] K. Diller, F. Klappenberger, M. Marschall, K. Hermann, A. Nefedov, C. Wöll and J. V. Barth, *Self-metalation of 2H-tetraphenylporphyrin on Cu(111): An x-ray spectroscopy study*, *The Journal of Chemical Physics*, 2012, **136**, 014705.

[61] S. Ditze, M. Stark, M. Drost, F. Buchner, H.-P. Steinrück and H. Marbach, *Activation Energy for the Self-Metalation Reaction of 2H-Tetraphenylporphyrin on Cu(111)*, *Angewandte Chemie International Edition*, 2012, **51**, 10898-10901.

[62] M. Röckert, S. Ditze, M. Stark, J. Xiao, H.-P. Steinrück, H. Marbach and O. Lytken, *Abrupt Coverage-Induced Enhancement of the Self-Metalation of Tetraphenylporphyrin with Cu(111)*, *J. Phys. Chem. C*, 2013, **118**, 1661.

[63] M. Röckert, M. Franke, Q. Tariq, S. Ditze, M. Stark, P. Uffinger, D. Wechsler, U. Singh, J. Xiao, H. Marbach, H.-P. Steinrück and O. Lytken, *Inside Cover: Coverage- and Temperature-Dependent Metalation and Dehydrogenation of Tetraphenylporphyrin on Cu(111) (Chem. Eur. J. 29/2014)*, *Chemistry – A European Journal*, 2014, **20**, 8810-8810.

[64] S. Haq, F. Hanke, M. S. Dyer, M. Persson, P. Iavicoli, D. B. Amabilino and R. Raval, *Clean Coupling of Unfunctionalized Porphyrins at Surfaces To Give Highly Oriented Organometallic Oligomers*, *Journal of the American Chemical Society*, 2011, **133**, 12031-12039.

[65] M. Chen, X. Feng, L. Zhang, H. Ju, Q. Xu, J. Zhu, J. M. Gottfried, K. Ibrahim, H. Qian and J. Wang, *Direct Synthesis of Nickel(II) Tetraphenylporphyrin and Its Interaction with a Au(111) Surface: A Comprehensive Study*, *The Journal of Physical Chemistry C*, 2010, **114**, 9908-9916.

[66] T. E. Shubina, H. Marbach, K. Flechtner, A. Kretschmann, N. Jux, F. Buchner, H.-P. Steinrück, T. Clark and J. M. Gottfried, *Principle and Mechanism of Direct Porphyrin Metalation: Joint Experimental and Theoretical Investigation*, *Journal of the American Chemical Society*, 2007, **129**, 9476-9483.

[67] G. Di Santo, C. Sfiligoj, C. Castellarin-Cudia, A. Verdini, A. Cossaro, A. Morgante, L. Floreano and A. Goldoni, *Changes of the Molecule–Substrate Interaction upon Metal Inclusion into a Porphyrin*, *Chemistry – A European Journal*, 2012, **18**, 12619-12623.

[68] G. Di Santo, C. Castellarin-Cudia, M. Fanetti, B. Taleatu, P. Borghetti, L. Sangaletti, L. Floreano, E. Magnano, F. Bondino and A. Goldoni, *Conformational Adaptation and Electronic Structure of 2H-Tetraphenylporphyrin on Ag(111) during Fe Metalation*, *The Journal of Physical Chemistry C*, 2011, **115**, 4155-4162.

[69] F. Buchner, K. G. Warnick, T. Wölfle, A. Görling, H.-P. Steinrück, W. Hieringer and H. Marbach, *Chemical Fingerprints of Large Organic Molecules in Scanning Tunneling Microscopy: Imaging Adsorbate-Substrate Coupling of Metalloporphyrins*, *J. Phys. Chem. C*, 2009, **113**, 16450-16457.

[70] K. Flechtner, A. Kretschmann, L. R. Bradshaw, M.-M. Walz, H.-P. Steinrück and J. M. Gottfried, *Surface-Confined Two-Step Synthesis of the Complex (Ammine)(meso-tetraphenylporphyrinato)-zinc(II) on Ag(111)*, *The Journal of Physical Chemistry C*, 2007, **111**, 5821-5824.

[71] A. Weber-Bargioni, J. Reichert, A. P. Seitsonen, W. Auwärter, A. Schiffrin and J. V. Barth, *Interaction of Cerium Atoms with Surface-Anchored Porphyrin Molecules*, *The Journal of Physical Chemistry C*, 2008, **112**, 3453-3455.

[72] D. Écija, W. Auwärter, S. Vijayaraghavan, K. Seufert, F. Bischoff, K. Tashiro and J. V. Barth, *Assembly and Manipulation of Rotatable Cerium Porphyrinato Sandwich Complexes on a Surface*, *Angewandte Chemie International Edition*, 2011, **50**, 3872-3877.

[73] A. Goldoni, C. A. Pignedoli, G. Di Santo, C. Castellarin-Cudia, E. Magnano, F. Bondino, A. Verdini and D. Passerone, *Room Temperature Metalation of 2H-TPP Monolayer on Iron and Nickel Surfaces by Picking up Substrate Metal Atoms*, *ACS Nano*, 2012, **6**, 10800-10807.

[74] M. Röckert, M. Franke, Q. Tariq, D. Lungerich, N. Jux, M. Stark, A. Kaftan, S. Ditze, H. Marbach, M. Laurin, J. Libuda, H.-P. Steinrück and O. Lytken, *Insights in Reaction Mechanistics: Isotopic Exchange during the Metalation of Deuterated Tetraphenyl-21,23D-porphyrin on Cu(111)*, *The Journal of Physical Chemistry C*, 2014, **118**, 26729-26736.

[75] C. Burker, A. Franco-Canellas, K. Broch, T. L. Lee, A. Gerlach and F. Schreiber, *Self-Metalation of 2H-Tetraphenylporphyrin on Cu(111) Studied with XSW: Influence of the Central Metal Atom on the Adsorption Distance*, *Journal of Physical Chemistry C*, 2014, **118**, 13659-13666.

[76] C. C. Wang, Q. T. Fan, Y. Han, J. I. Martinez, J. A. Martin-Gago, W. J. Wang, H. X. Ju, M. J. Gottfried and J. F. Zhu, *Metalation of tetraphenylporphyrin with nickel on a TiO2(110)-1 x 2 surface*, *Nanoscale*, 2016, **8**, 1123-1132.

[77] R. Young, J. Ward and F. Scire, *The Topografiner: An Instrument for Measuring Surface Microtopography*, *Review of Scientific Instruments*, 1972, **43**, 999-1011.

[78] N. Yao and Z. L. Wang, *Handbook of Microscopy for Nanotechnology*, Springer, New York, 2005.

[79] R. Wiesendanger, *Scanning Probe Microscopy and Spectroscopy*, Cambridge University Press, Cambridge, 1994.

[80] P. K. Hansma and J. Tersoff, *Scanning tunneling microscopy*, *Journal of Applied Physics*, 1987, **61**, R1-R24.
[81] K. Comanici, F. Buchner, K. Flechtner, T. Lukasczyk, J. M. Gottfried, H.-P. Steinrück and H. Marbach, *Understanding the Contrast Mechanism in Scanning Tunneling Microscopy (STM) Images of an Intermixed Tetraphenylporphyrin Layer on Ag(111)*, *Langmuir*, 2008, **24**, 1897-1901.
[82] I. Horcas, R. Fernández, J. M. Gómez-Rodríguez, J. Colchero, J. Gómez-Herrero and A. M. Baro, *WSXM: A software for scanning probe microscopy and a tool for nanotechnology*, *Review of Scientific Instruments*, 2007, **78**, 013705.
[83] J. W. Steed and J. L. Atwood, *Supramolecular Chemistry*, Wiley & Sons, Chichester, 2009.
[84] G. P. Moss, in *Pure and Applied Chemistry*, 1987, p. 779.
[85] F. Moresco, G. Meyer, K.-H. Rieder, J. Ping, H. Tang and C. Joachim, *TBPP molecules on copper surfaces: a low temperature scanning tunneling microscope investigation*, *Surface Science*, 2002, **499**, 94-102.
[86] F. Moresco, G. Meyer, K.-H. Rieder, H. Tang, A. Gourdon and C. Joachim, *Conformational Changes of Single Molecules Induced by Scanning Tunneling Microscopy Manipulation: A Route to Molecular Switching*, *Physical Review Letters*, 2001, **86**, 672-675.
[87] S. Ditze, M. Stark, F. Buchner, A. Aichert, N. Jux, N. Luckas, A. Görling, W. Hieringer, J. Hornegger, H.-P. Steinrück and H. Marbach, *On the Energetics of Conformational Switching of Molecules at and Close to Room Temperature*, *Journal of the American Chemical Society*, 2014, **136**, 1609-1616.
[88] A. Weber-Bargioni, W. Auwärter, F. Klappenberger, J. Reichert, S. Lefrançois, T. Strunskus, C. Wöll, A. Schiffrin, Y. Pennec and J. V. Barth, *Visualizing the Frontier Orbitals of a Conformationally Adapted Metalloporphyrin*, *ChemPhysChem*, 2008, **9**, 89-94.
[89] R. Lindner, PhD thesis, FAU Erlangen-Nürnberg, Erlangen, 2004.
[90] F. Buchner, PhD thesis, FAU Erlangen-Nürnberg, Erlangen, 2010.
[91] *UHV 300 User´s Guide*, RHK Technologies Inc., Rochester Hills, Michigan USA.
[92] K. Besocke, *An easily operable scanning tunneling microscope*, *Surface Science*, 1987, **181**, 145-153.
[93] Y. Bai, F. Buchner, I. Kellner, M. Schmid, F. Vollnhals, H.-P. Steinrück, H. Marbach and J. M. Gottfried, *Adsorption of cobalt (II) octaethylporphyrin and 2H-octaethylporphyrin on Ag(111): new insight into the surface coordinative bond*, *New Journal of Physics*, 2009, **11**.
[94] F. Buchner, K. Seufert, W. Auwärter, D. Heim, J. V. Barth, K. Flechtner, J. M. Gottfried, H.-P. Steinrück and H. Marbach, *NO-Induced Reorganization of Porphyrin Arrays*, *ACS Nano*, 2009, **3**, 1789-1794.
[95] Y. Bai, F. Buchner, M. T. Wendahl, I. Kellner, A. Bayer, H.-P. Steinrück, H. Marbach and J. M. Gottfried, *Direct metalation of a phthalocyanine monolayer on Ag(111) with coadsorbed iron atoms*, *Journal of Physical Chemistry C*, 2008, **112**, 6087-6092.
[96] M. O. Sinnokrot and C. D. Sherrill, *High-accuracy quantum mechanical studies of pi-pi interactions in benzene dimers*, *Journal of Physical Chemistry A*, 2006, **110**, 10656-10668.
[97] E. G. Cox, D. W. J. Cruickshank and J. A. S. Smith, *The crystal structure of benzene at −3° C*, *Proc. R. Soc. London. Ser. A. Math. Phys. Sci.*, 1958, **247**, 1−21.
[98] G. Rojas, S. Simpson, X. M. Chen, D. A. Kunkel, J. Nitz, J. Xiao, P. A. Dowben, E. Zurek and A. Enders, *Surface state engineering of molecule-molecule interactions*, *Physical Chemistry Chemical Physics*, 2012, **14**, 4971-4976.

[99] J. Xiao, S. Ditze, M. Chen, F. Buchner, M. Stark, M. Drost, H.-P. Steinrück, J. M. Gottfried and H. Marbach, *Temperature-Dependent Chemical and Structural Transformations from 2H-tetraphenylporphyrin to Copper(II)-Tetraphenylporphyrin on Cu(111), J. Phys. Chem. C*, 2012, **116**, 12275-12282.

[100] T. Kumagai, F. Hanke, S. Gawinkowski, J. Sharp, K. Kotsis, J. Waluk, M. Persson and L. Grill, *Controlling intramolecular hydrogen transfer in a porphycene molecule with single atoms or molecules located nearby*, *Nat. Chem.*, 2014, **6**, 41-46.

[101] T. Kumagai, F. Hanke, S. Gawinkowski, J. Sharp, K. Kotsis, J. Waluk, M. Persson and L. Grill, *Thermally and vibrationally induced tautomerization of single porphycene molecules on a Cu(110) surface, Phys. Rev. Lett.*, 2013, **111**, 246101.

[102] H. Yanagi, H. Mukai, K. Ikuta, T. Shibutani, T. Kamikado, S. Yokoyama and S. Mashiko, *Molecularly Resolved Dynamics for Two-Dimensional Nucleation of Supramolecular Assembly*, *Nano Lett.*, 2002, **2**, 601-604.

[103] S. K. Burley and G. A. Petsko, *Aromatic-Aromatic Interaction - a Mechanism of Protein-Structure Stabilization*, *Science*, 1985, **229**, 23-28.

[104] T. Wölfle, A. Görling and W. Hieringer, *Phys. Chem. Chem. Phys.*, 2008, **10**, 5739.

[105] T. Terui, T. Kamikado, Y. Okuno, H. Suzuki and S. Mashiko, *STM investigation of porphyrin isomers on metal substrates*, *Current Applied Physics*, 2004, **4**, 148-151.

[106] L. Smykalla, P. Shukrynau, C. Mende, T. Ruffer, H. Lang and M. Hietschold, *Interplay of hydrogen bonding and molecule-substrate interaction in self-assembled adlayer structures of a hydroxyphenyl-substituted porphyrin*, *Surf. Sci.*, 2014, **628**, 132-140.

[107] J. Brede, M. Linares, R. Lensen, A. E. Rowan, M. Funk, M. Bröring, G. Hoffmann and R. Wiesendanger, *Adsorption and conformation of porphyrins on metallic surfaces, J. Vac. Sci. Technol., A*, 2009, **27**, 799-804.

[108] W. Auwärter, K. Seufert, F. Klappenberger, J. Reichert, A. Weber-Bargioni, A. Verdini, D. Cvetko, M. Dell'Angela, L. Floreano, A. Cossaro, G. Bavdek, A. Morgante, A. P. Seitsonen and J. V. Barth, *Site-specific electronic and geometric interface structure of Co-tetraphenyl-porphyrin layers on Ag(111), Phys. Rev. B*, 2010, **81**, 245403.

[109] L. Zhang, M. Lepper, M. Stark, D. Lungerich, N. Jux, W. Hieringer, H.-P. Steinrück and H. Marbach, *Self-assembly and coverage dependent thermally induced conformational changes of Ni(ii)-meso-tetrakis (4-tert-butylphenyl) benzoporphyrin on Cu(111), PCCP*, 2015, **17**, 13066-13073.

[110] T. Wölfle, A. Görling and W. Hieringer, *Conformational flexibility of metalloporphyrins studied by density-functional calculations*, *PCCP*, 2008, **10**, 5739-5742.

7 Appendix

7.1 List of Abbreviations

DFT	density functional theory
fcc	face-centered cubic
HOMO	highest occupied molecular orbital
LDOS	local density of states
LEED	low energy electron diffraction
NEXAFS	near edge X-ray absorption fine structure
QMS	quadrupole mass spectrometer
RT	room temperature
STM	scanning tunneling microscopy
STS	scanning tunneling spectroscopy
TPBP	tetraphenybenzoporphyrin
TPD	temperature programmed desorption
TPP	tetrephenylporphyrin
TPPc	tetraphenylporphycene
TPyP	tetrapyridylporphyrin
TTBPP	tetrakisditertbutylphenylporphyrin
UHV	ultra-high vacuum
XPS	X-ray photoelectron spectroscopy

7.1 List of Figure Raw Data

Figure 2.1c	100118_02	Figure 3.10a	130213_00011
Figure 3.2a	090717_0093	Figure 3.10b	130219_00029
Figure 3.2b	110615_0200	Figure 3.11a	140204_00080
Figure 3.2c	111222_0046	Figure 3.11b	140210_00045
Figure 3.2d	111223_0053	Figure 3.11c	100303_0060
Figure 3.2e	090717_0085-0156	Figure 3.11d	100219_0061
	(average frame)	Figure 3.12a	100209_0058
Figure 3.2f	110615_0195-0245	Figure 3.12b	100209_0060
	(average frame)	Figure 3.12c, e	100209_0060
Figure 3.2g	111222_0006-0065	Figure 3.12d,f	100209_0060
	(average frame)	Figure 3.12i, k	100303_0060
Figure 3.2h	111223_0048-0099	Figure 3.12l, m	100303_0060
	(average frame)	Figure 3.12o, p	100219_0047
Figure 3.3a, b	110616_0484	Figure 3.12q, r	100219_0047
Figure 3.3c, d	111223_0312	Figure 3.13a	110228_0047
Figure 3.4c	110616_0484	Figure 3.13b	110228_0067
Figure 3.5a	111223_0169	Figure 3.13c	110316_0128
Figure 3.5b	120102_0031	Figure 3.13d	110309_0113
Figure 3.6a	130212_00199	Figure 3.13e	110328_0041
Figure 3.6b	130201_00118	Figure 3.14a-d	110316_0090
Figure 3.7	130214_00014	Figure 3.14e-h	110323_0009
Figure 3.8	130214_00025	Figure 3.15a	110328_0049
Figure 3.9a	130214_00044	Figure 3.15b	110324_0034
Figure 3.9b	130214_00045	Figure 3.15c	110328_0129
Figure 3.9c	130214_00046	Figure 3.15d	110308_0084

7.2 Curriculum Vitae

MICHAEL Werner STARK

Geboren am 20. März 1985 in Ansbach

Promotion

seit 06/2010	am Lehrstuhl für physikalische Chemie II der
	Friedrich-Alexander-Universität Erlangen-Nürnberg (FAU)

Studium

06/2010	Abschluss Master of Science
10/2008 – 06/2010	Masterstudium Molecular Nano Science an der FAU
10/2008	Abschluss Bachelor of Science
10/2005 – 09/2008	Bachelorstudium Molecular Nano Science an der FAU

Schulische Ausbildung

06/2004	Erwerb der allgemeinen Hochschulreife
09/1995 – 06/2004	Reichsstadtgymnasium Rothenburg
08/1991 – 07/1995	Grundschule (Schillingsfürst)

7.3 Acknowledgment

Hereby, I would like to thank and acknowledge all persons who supported me throughout my thesis and who contributed to the presented results.

In particular, I am grateful to my supervisors Prof. Dr. Hans-Peter Steinrück, for giving me the opportunity to work at his chair, for the great support and the always fruitful discussions, and PD Dr. Hubertus Marbach for interesting, valuable discussions, input with helpful ideas, and for support in other ways.

For second assessment I thank Prof. Dr. Alexander Schneider.

Special thanks to the STM-Team, Dr. Florian Buchner, Dr. Stefanie Ditze, Dr. Liang Zhang, Michael Lepper, and Martin Drost, for creating such a pleasant and creative working atmosphere.

For good and fruitful collaborations, I would like to thank our cooperation partners:

The “Scienta-Team”, Dr. Ole Lytken, Dr. Michael Röckert, and Min Chen (Chair of Physical Chemistry II at the Friedrich- Alexander-Universität Erlangen-Nürnberg) for XPS measurements

Prof. Dr. Norbert Jux, Wolfgang Brenner, and Dominik Lungerich (Chair of Organic Chemistry II at the Friedrich-Alexander-Universität Erlangen-Nürnberg) for the synthesis of molecules.

For technical support and help in maintenance and improvement of our setup, I gratefully acknowledge Hans-Peter Bäumler, Bernd Kreß, Friedhold Wölfel and all the members of the mechanical workshop.

Further I gratefully thank all members of the Chair of Physical Chemistry II for the great working atmosphere.

Finally, I would like to thank my family for all the support I got in manifold ways, not only throughout my thesis, but also throughout my studies.

Co-Authorship statement:

In the framework of this thesis substantial novel results were conducted in collaboration with different Departments of the Friedrich-Alexander-Universität Erlangen-Nürnberg. Publication P3 presents a combined STM and XPS study and therefore I share first authorship with Michael Röckert who did the XPS measurements.

7.4 Publications

[P1] **Coverage Dependent Disorder–Order Transition of 2H-Tetraphenylporphyrin on Cu(111)**
M. Stark, S. Ditze, M. Drost, F. Buchner, H.-P. Steinrück, and H. Marbach,
Langmuir, 29 (12), **2013**, 4104–4110

[P2] **Supramolecular order and structural dynamics: A STM study of 2H-tetraphenylporphycene on Cu(111)**
M. Stark, J. Träg, S. Ditze, W. Brenner, N. Jux, H.-P. Steinrück and H. Marbach,
J. Chem. Phys. 142, **2015**, 101925

[P3] **Massive conformational changes during thermally induced self-metalation of 2H-tetrakis-(3,5-di-tert-butyl)-phenylporphyrin on Cu(111)**
M. Stark*, S. Ditze, M. Lepper, L. Zhang, H. Schlott, F. Buchner, M. Röckert*, M. Chen, O. Lytken, H.-P. Steinrück and H. Marbach,
Chem. Commun., 50, **2014**, 10225—10228

[P4] **Reversible thermally induced phase transition in ordered domains of Co(II)-5,10,15,20-tetrakis-(3,5-di-tert-butylphenyl)-porphyrin on Cu(111)**
M. Stark, S. Ditze, M. Thomann, D. Lungerich, N. Jux, H.-P. Steinrück, H. Marbach,
Surf. Sci., In Press, Corrected Proof

* These authors contributed equally to this contribution and share first author ship.

P1

Langmuir

Article

pubs.acs.org/Langmuir

Coverage Dependent Disorder–Order Transition of 2H-Tetraphenylporphyrin on Cu(111)

Michael Stark, Stefanie Ditze, Martin Drost, Florian Buchner,[†] Hans-Peter Steinrück, and Hubertus Marbach*

Lehrstuhl für Physikalische Chemie II and Interdisciplinary Center for Molecular Materials (ICMM), Universität Erlangen-Nürnberg, Egerlandstraße 3, D-91058 Erlangen, Germany

Supporting Information

ABSTRACT: In this study, we investigate the peculiar coverage dependent supramolecular arrangement of 2H-tetraphenylporhpyrin (2HTPP) on Cu(111) with scanning tunneling microscopy at room-temperature. At low coverage, "slow" diffusion of individual 2HTPP molecules along the close-packed atomic rows of the substrate is observed, and no supramolecular ordering occurs. However, at higher coverage, the formation of ordered, checkerboard-like domains is found, with two molecules per unit cell at different distances from the surface. This behavior is attributed to a complex interplay of site specific molecule–substrate interaction, mainly the strong interaction between the iminic N atoms and Cu substrate atoms, with intermolecular T-type and π–π interactions.

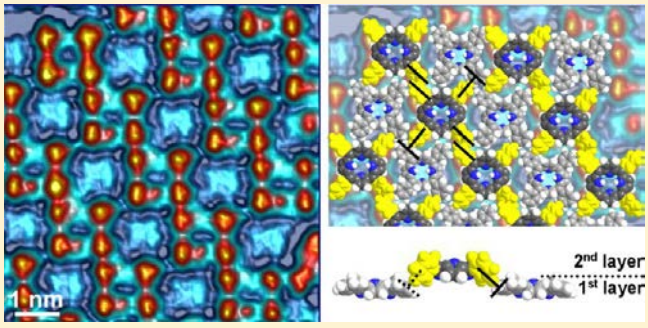

INTRODUCTION

The application of large organic molecules in multi component devices, e.g., in sensors, is a rapidly growing field in research and technology. In this context, understanding the self-assembly of corresponding molecular building blocks on well-defined surfaces is a key issue that allows for tailoring the properties of supramolecular structures.[1,2] Due to their pivotal importance as main functional building blocks for many processes in nature, porphyrins appear to be very promising candidates for such devices: their central cavity can be functionalized quite easily but at the same time their rigid, but not inflexible backbone remains intact. Long-range order of porphyrins and related molecules and the formation of supramolecular structures is in many cases triggered by intermolecular interactions and their interplay/competition with molecule–substrate interactions.[3−6] The key for understanding these properties is a detailed characterization of the adsorption behavior of the involved molecules. Scanning tunneling microscopy (STM) has proven to be a very powerful tool for the investigation and determination of supramolecular structures and to some extent also intramolecular conformations of large organic molecules on solid surfaces under ultrahigh vacuum (UHV) conditions.[1,2,7−10] Herein, we report on the adsorption behavior of free base 2H-tetraphenylporphyrin (2HTPP) on Cu(111) at room temperature (RT). The behavior of these molecules at low coverage, i.e., in the submonolayer range, has already been investigated in detail.[11,12] We will therefore now focus on higher coverages, where a transition from a disordered phase of individually adsorbed molecules to a long-range ordered supramolecular structure occurs.

RESULTS AND DISCUSSION

Previous studies of metallo-tetraphenylporphyrins (MTPPs) on hexagonal metal single crystal surfaces revealed that the molecules tend to adsorb coplanar to the surface and to form square ordered islands on the (111) terraces.[4,7,13−21] For these arrangements, the molecule–substrate interactions seem to be of minor importance and the formation of the quadratic lattice is dominated by molecule–molecule interactions.[3,4] Thereby, the attractive intermolecular interactions are realized via the phenyl side groups of the porphyrins. In these two-dimensional square arrangements, each molecule is oriented such that the outermost C–H group of the phenyl side groups of one molecule points edge-to-face toward the center of the π-system of a phenyl side group of a neighboring molecule.[3,4] This so-called T-type interaction is schematically shown in Figure 1c and is most common for tetraphenylporphyrins on metals. Typically, the plane of phenyl groups is found to be rotated relative to the plane of the macrocycle by angles, α_{ph}, of about 60° (c.f., Figure 1a).[3,7] Alternatively, a second type of interaction between the phenyl side groups of neighboring molecules is conceivable, namely a π–π interaction (also denoted as π–π stacking), which is schematically shown in Figure 1b.[22,23] For this aromatic interaction, the π-systems of

Received: November 24, 2012
Revised: February 20, 2013
Published: February 25, 2013

   dx.doi.org/10.1021/la3046753 | *Langmuir* 2013, 29, 4104–4110

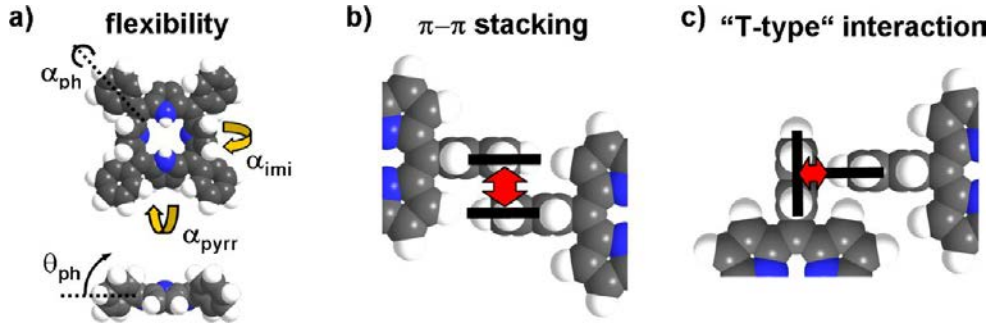

Figure 1. (a) A model of 2HTPP showing the flexibility and the saddle shaped distortion of the molecule. The angles that determine the conformation of the molecule are labeled, too. (b and c) Show schematic drawings of the two types of interaction of the phenyl side groups of 2HTPP.

the phenyl groups of two neighboring molecules have to overlap in a geometry, in which they are oriented almost parallel.

Another important factor for the adsorption behavior of TPPs is their rigid, aromatic backbone, the macrocycle, which exhibits certain degrees of flexibility (a corresponding model is shown in Figure 1a): α_{ph} describes the angle by which the phenyl ring is rotated around the C−C-bond between the phenyl ring and the porphyrin macrocycle; 0° corresponds to the phenyl ring being in plane with the macrocycle. θ_{ph} is the angle by which the C−C-bond between the macrocycle and the phenyl ring is tilted out of the porphyrin plane. Finally, α_{py} and α_{im} describe the angles by which the aminic and the iminic pyrrole rings are tilted out of the porphyrin plane, respectively.[12] With these four parameters, it is possible to describe the molecular conformation of the adsorbed TPP molecules.

So far, all studies on TPPs on different fcp (111) coinage metal surfaces reported on structures where the plane of the porphyrin macrocycle is parallel to the substrate surface. Typically, the molecules display a so-called saddle-shape conformation: thereby, two opposite pyrrole rings are bent upward out of the porphyrin plane, while the other two are bent downward, and the phenyl rings are rotated out of the porphyrin plane. This deformation mainly occurs due the fact that the attractive interaction with the substrate leads to a rotation of the phenyl groups toward a more planar arrangement (small value of α_{ph}), leading to steric repulsion between the *ortho*- and *β*-H atoms of the molecules.[3,11]

When adsorbing 2HTPP on Ag(111), individual isolated molecules cannot be imaged with conventional STM at RT and, starting already at submonolayer coverages, the formation of islands with the above-mentioned quadratic lattice is found.[3] Interestingly, on Cu(111) a very different and unusual behavior is observed: Already at very low coverages, 2HTPP can be imaged at RT as individual molecules that do not form any supramolecular structure; this is evident from Figure 2a, where each molecule appears as two longish parallel (rod-like) protrusions, with a dark region in between, which we denote as "molecular axis". This axis corresponds to the aminic pyrrole axis of the molecule and is aligned along the close-packed rows of the substrate. The molecules slowly diffuse along these directions, as can be deduced from the one-dimensional elongation of the molecules in the average frame of an STM movie depicted in Figure 2e. The energy barriers for migration and rotation were determined to be $E_m = 0.71 \pm 0.08$ eV and $E_r = 1.28 \pm 0.12$ eV, respectively.[11] At RT, the thermal energy of the molecules is sufficient to overcome the migration barrier, but typically not the rotation barrier; at this coverage, this is possible only by increasing the temperature.[11] The just described adsorption behavior has been reported before and has been attributed to a pronounced and highly site specific adsorbate−substrate interaction. At the moment, it is still not clear whether this adsorption geometry is due to charge transfer from the molecule to the substrate as proposed by Rojas et al.,[24,25] or/and due to the special conformation of the molecule caused by strong attractive interactions between Cu substrate atoms and the N atoms of the iminic pyrrole rings pointing toward the surface.[11]

This study now addresses the adsorption behavior of 2HTPP on Cu(111) at higher coverage, that is when intermolecular interactions also come into play. Figure 2b shows a typical image of the surface of the single crystal after deposition of 0.009 ML 2HTPP (1 ML stands for 1 molecule per surface atom; for illustration: one full layer CuTPP on Cu(111) in the well-ordered quadratic lattice would correspond to a coverage of 0.033 ML). The appearance of each 2HTPP molecule as two parallel rod-like protrusions still exists, but the four phenyl side groups of the molecule appear somewhat more prominent than for the isolated molecules at low coverage. Nevertheless, no supramolecular ordered structure is formed yet and the molecules are still oriented along the high symmetry substrate directions. Increasing the coverage reduces the free surface area (Figure 2b), which means that the free one-dimensional movement of the molecules is hindered. The molecules are lying almost flat on the surface with a tilt angle of the phenyl rings of only 20°,[12] which does not allow for T-type attractive intermolecular interactions between different molecules.[6] Due to repulsion between neighboring molecules at too small distances, their average diffusion length is reduced. Upon collision between molecules, sufficient momentum can be transferred to allow some of the molecules to overcome the energy barrier E_r for changes of the diffusion direction from one densely packed substrate row to another even at RT. This is evident from Figure 2f, where some of the molecules change the direction of one-dimensional motion, as is seen in the average frame of an STM movie (the corresponding full movie (movie M2) can be found in the SI).

When the total coverage of the surface exceeds a value of 0.020 ML, molecules with increased apparent height in STM are observed (see Figure 2c and also Figures S1 and S2 of the SI). These molecules will be referred to as second layer molecules in the following. They do not exhibit the parallel rod-like shape of the first layer molecules, but appear as four (red)

dx.doi.org/10.1021/la3046753 | *Langmuir* 2013, 29, 4104−4110

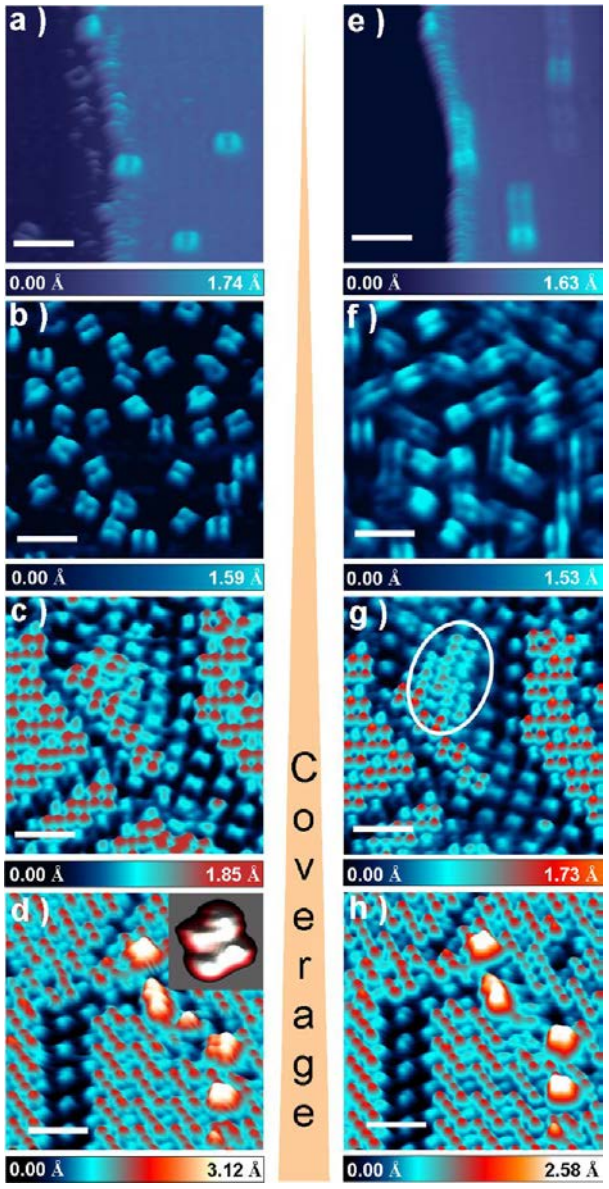

Figure 2. Constant current STM images of 2HTPP on Cu(111) at different coverages; the turquoise molecules represent first layer molecules, the red ones second layer molecules and the white ones third layer molecules. (a) Isolated molecules at very low coverage (U_{bias} = −1.49 V, I_{set} = 30 pA), (b) slightly increased coverage compared to (a) with 0.009 ML 2HTPP (U_{bias} = −0.193 V, I_{set} = 11 pA), (c) formation of checkerboard structure involving first and second layer molecules (U_{bias} = −1.05 V, I_{set} = 30 pA), (d) surface nearly completely covered with checkerboard domains and some third layer molecules present (U_{bias} = +1.35 V, I_{set} = 22 pA), (e) average frame of a 39 image (13 min) STM movie, where 1D diffusion is visible (U_{bias} = −1.49 V, I_{set} = 30 pA), (f) average frame of a 51 image (22 min) STM movie, where besides the 1D diffusion rotation of the molecules is visible (U_{bias} = −193 mV, I_{set} = 11 pA), (g) average frame of a 60 image (23 min) STM movie, where the dynamics of the checkerboard structure is visible. The white oval marks a region where frequent molecular movements occur during the movie (U_{bias} = −1.05 V, I_{set} = 30 pA), (h) average frame of a 26 image (10 min) STM movie; here the average frame is identical to each of the single frames of the movie (U_{bias} = +1.35 V, I_{set} = 22 pA). (a–d) are individual frames of the movies averaged in (e–h). The scale bars correspond to 4 nm. The color scale bars for each image are given below the corresponding image. The corresponding full movies (movies M1–4) can be found in the Supporting Information, SI.

protrusions in Figure 2c. Each protrusion is attributed to one phenyl side group of a 2HTPP molecule. We find these second layer molecules initially only on flat regions of the Cu crystal, i.e., not on typical nucleation sites like step edges and defects. This behavior will become understandable when discussing the interactions stabilizing this adsorption geometry (see below).

Further increase of the coverage leads to the formation of a well-ordered structure, as depicted in Figures 2c,d,g,h and 3. This structure has been observed before by Rojas et al.,[24] but was neither analyzed nor yet interpreted. Within this structure, the second layer molecules (4 red protrusions per molecule, indicated by the solid circle in Figure 3) arrange together with the first layer molecules (turquoise, indicated by the dashed circle in Figure 3) in a checkerboard-like structure, where one second layer molecule is surrounded by four first layer ones and vice versa. This superstructure has a rectangular unit cell with lattice vectors a = 2.12 ± 0.03 nm and b = 1.74 ± 0.05 nm and an angle of γ = 90° ± 5°, as shown in Figure 3. As evident from Figure 3, all molecules within one checkerboard domain are oriented in the same direction, which means that the molecule axes formed by the aminic pyrrole rings are parallel for both, first layer and second layer molecules. Note that this molecular axis is the one given by the dark regions in between the two bright rods of the first layer appearance of the molecules. This direction is tilted 30° left or right of the longer lattice vector a of the unit cell (60° of the shorter one b) as depicted in Figure 3 and Figure S1 of the SI. The detailed analysis reveals the existence of three different domains, rotated by 60°, with two chiral orientations each (see Figure S1 of the SI). The azimuthal rotation of the pyrrole–pyrrole axis (molecular axis) by 30° off the long lattice axis allows only for three possible orientations which 2HTPP molecules can adopt. This is in line with the observation that individual 2HTPP molecules are oriented solely along the three close packed substrate rows, due to the strong site-specific interaction with the substrate. Assuming that this adsorption behavior persists for first layer molecules of the checkerboard domains, it is possible to draw the close packed substrate rows as orange lines in Figure 3d. In this image, every porphyrin molecule adopts an equivalent position relative to the indicated substrate row. This seems to be true not only for the first layer molecules, but also for the second layer ones. However, neighboring molecules are not located over the same densely packed substrate row (orange line) of the substrate: along the long checkerboard domain lattice vector a there is a displacement of four rows, and along the short lattice vector b there is a displacement of six rows.

As a next step, we discuss the arrangement of the molecules within the checkerboard structure. The key information required in this context is the number of molecules per unit cell. Two arrangements, which are schematically shown in Figure 4a and b appear to be possible: (1) one, where a second layer molecule sits on top of a first layer one (porphyrin "sandwich", Figure 4a) and (2) one, where a second layer molecule bridges four first layer molecules (Figure 4b); in the latter arrangement, there would be a void below the second layer molecule. One first hint in the latter direction is the observation that in the STM images in Figure 3, there is no indication for the presence of molecules below second layer ones: This can best be seen in Figure 3c, where the tip contrast was adjusted to image the first layer molecules of the checkerboard structure best. In this image, the first layer molecules exhibit their typical parallel rod-like shape, i.e., protrusions at the position of the phenyl rings and at the two

dx.doi.org/10.1021/la3046753 | Langmuir 2013, 29, 4104–4110

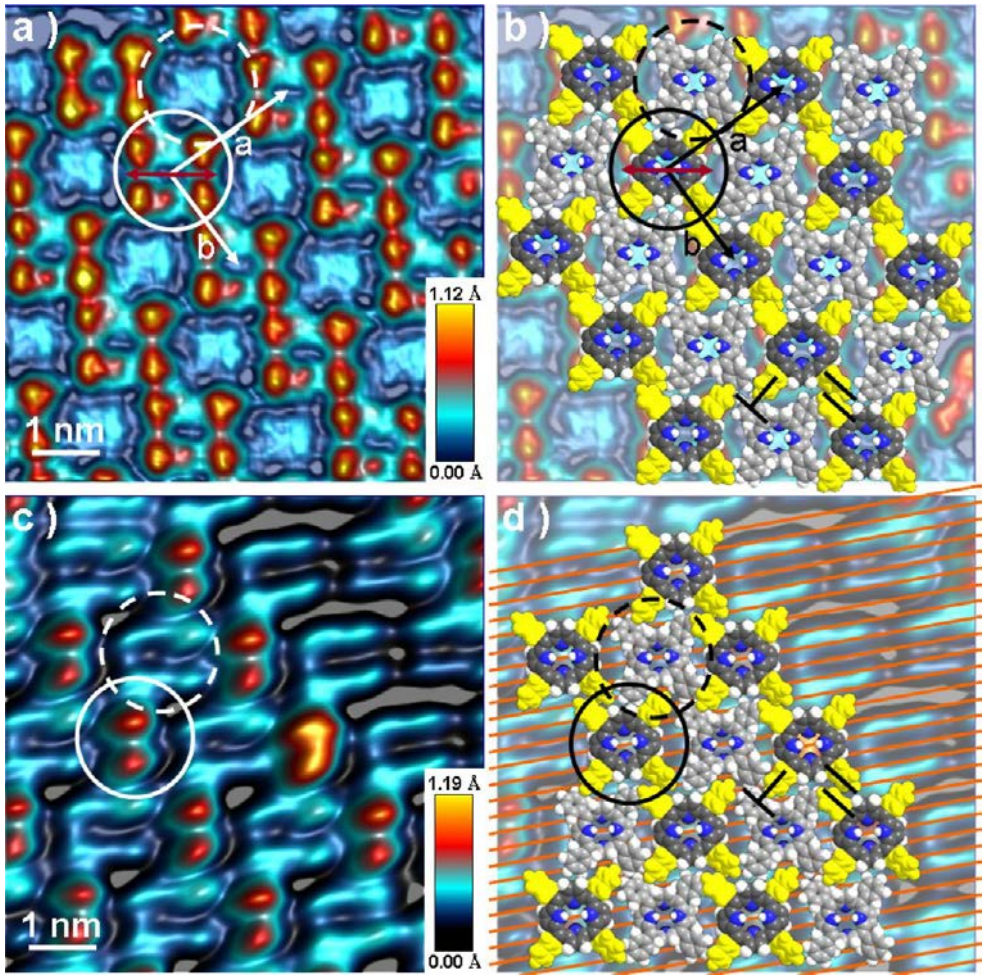

Figure 3. Constant current STM images of a checkerboard domain in (a, b) "normal" contrast (U_{bias} = −1.14 V, I_{set} = 46 pA) and (c, d) in a contrast adjusted to depict the turquoise first layer molecules with their typical two parallel rod like shape (U_{bias} = −0.92 V, I_{set} = 19 pA). (b) and (d) show superimposed scaled space filling models to the STM images. The model visualizes the stabilization of the checkerboard structure by T-type interactions (indicated by a black T) and $\pi-\pi$-stacking (black parallel lines). The solid circles mark a second layer molecule and the dashed circles a 1st layer one. The orange lines in (d) represent neighboring close packed atomic rows of the substrate in one high symmetry direction.

the pyrrole groups bent away from the surface. At the same time, the second layer molecules appear as two red spots originating from their iminic pyrrole rings indicating a considerable deformation of the macrocycle. In particular, there are no protrusions anticipated for the "sandwich" structure at the phenyl positions of a corresponding first layer molecule underneath the second layer one. In addition, the apparent height difference (see Figure S2 of the SI) of the first and second layer molecules of the checkerboard structure yields a value of ∼0.8 Å. This difference was found to be independent of the bias in the investigated bias voltage range from −1.14 to +1.00 V, indicating that the topographical contrast dominates the appearance in STM. This compares to the apparent height of an isolated 2HTPP molecule on the pristine Cu(111) of ∼1.4 Å in the same bias voltage range. Considering the underlying conductive Cu substrate, this value can be regarded as a lower limit for the corresponding height difference of a 2HTPP molecule on a corresponding closed layer of porphyrins (note that the pure topographic height difference would be ∼3−5 Å, depending on the orientation of the phenyl groups). Therefore, the value of ∼0.8 Å for the height difference indicates a position of the second layer molecules somewhat elevated relative to the first layer molecules, but probably not as high as one would expect for a "sandwich" complex with one molecule on top of the other. Therefore, the "sandwich" geometry (c.f., Figure 4b) can be safely ruled out. Instead, we propose that the second layer molecules bridge neighboring first layer molecules. In this arrangement, the phenyl group of a second layer molecule establishes a T-type interaction with an underlying phenyl ring of a first layer molecule (see for details below). This type of bridging can also be considered to contribute strongly to the observed supramolecular order in the checkerboard structure.

Additional evidence for the proposed bridging structure stems from the total coverage required to form a fully covered surface: deposition of about 0.030 ML of 2HTPP results in a surface covered with checkerboard domains and in between the different domains a few third layer molecules (white) can be observed as shown in Figure 5a. Nominally, a surface covered with one closed checkerboard domain with the bridging structure would correspond to a coverage of 0.030 ML, while 0.045 ML would be required for the "sandwich" structure (i.e., with first layer molecules also below the second layer molecules). From the coverage in Figure 5a, we thus conclude that the molecules have to be adsorbed in a bridging structure. This observation is evidenced by annealing the deposited layer

dx.doi.org/10.1021/la3046753 | *Langmuir* 2013, 29, 4104−4110

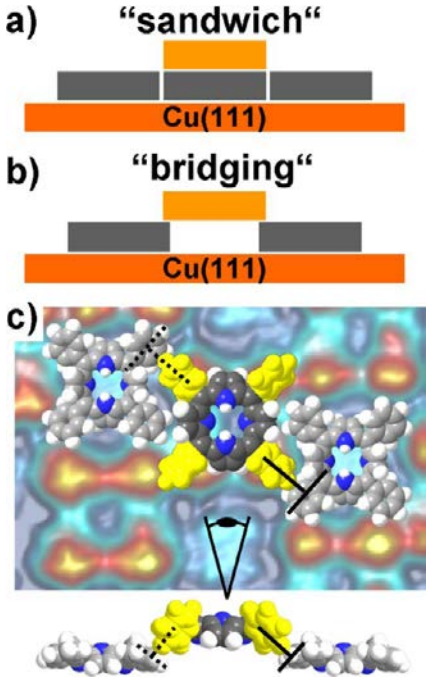

Figure 4. Parts (a) and (b) schematically show the two possible arrangements of 2HTPP molecules in checkerboard domains. Part (c) gives a top and a side view of scaled models of the 1st and 2nd layer molecules in the checkerboard structure highlighting the T-type interactions.

for 33 min to 400 K. Recent studies proved that such an annealing procedure leads to in situ metalation of the free based porphyrin with Cu substrate atoms to CuTPP.[12,24,26,27] In Figure 5, the structural change during metalation is shown: the 2HTPP structure of Figure 5a changes to a structure with large quadratic monolayer islands of CuTPP and some nonmetalated 2HTPP molecules in between in Figure 5b. The formation of square ordered islands was described earlier and is due to the different intramolecular conformation of the CuTPP, i.e. with the phenyl rings in an orientation allowing for T-type interactions of neighboring molecules.[26] In Figure 5b, the yellow/red structures represent CuTPP molecules while the turquoise structures, especially in the marked region, represent remaining 2HTPPs. The determination of the coverage after metalation yields a value of 0.028 ML which (within the margin of error) clearly proves that the 2HTPP molecules must be arranged in the bridging geometry within the checkerboard structure. (Note that no desorption occurs upon heating to 400 K.[26]) A comparison of the molecular density of 2HTPP molecules of a checkerboard domain (unit cell 2.12 ± 0.03 × 1.74 ± 0.05 nm^2 for 2 molecules, 0.54 mol/nm^2) to the quadratic structures of CuTPP on Cu(111) (1.29 ± 0.05 × 1.36 ± 0.05 nm^2 for 1 molecule,[4] 0.58 mol/nm^2) and CoTPP on Cu(111) (1.35 ± 0.05 × 1.35 ± 0.05 nm^2 for 1 molecule,[6] 0.55 mol/nm^2) shows almost identical packing density, within the margin of errors.

In order to obtain further insight, space filling models of the molecules were superimposed to the experimental STM images of the checkerboard structure in Figure 3: the yellow species represent the second layer molecules (indicated by the solid circle) and the light gray species the first layer molecules (indicated by the dashed circles). For the intermolecular conformations of the first and second layer molecules in the checkerboard structure, we used the intramolecular conformations determined by Diller et al.[12] for submonolayer 2HTPP on Cu(111) (α_{ph} = 20°, α_{py} = 40°, and α_{im} = 60°) and multilayer 2HTPP molecules (α_{ph} = 55−60°, α_{py} = 40° and α_{im} = 40°), respectively. This approach appears reasonable since the interaction for the two species in the double-decker layer should correspond to these two cases (first layer/submonolayer = strong interaction with substrate, second layer/multilayer = weaker interaction). The excellent agreement of the superimposed structure with the STM image supports the choice of these intramolecular conformations. Note that the assumed intramolecular geometry for the second layer molecules is very similar to the one of metalated TPPs like CuTPP. Nevertheless, Figure S2 of the SI shows a height difference of 0.8 Å between a second and a first layer 2HTPP, while CuTPP appears to be only 0.5 Å higher than a first layer 2HTPP. This is an additional

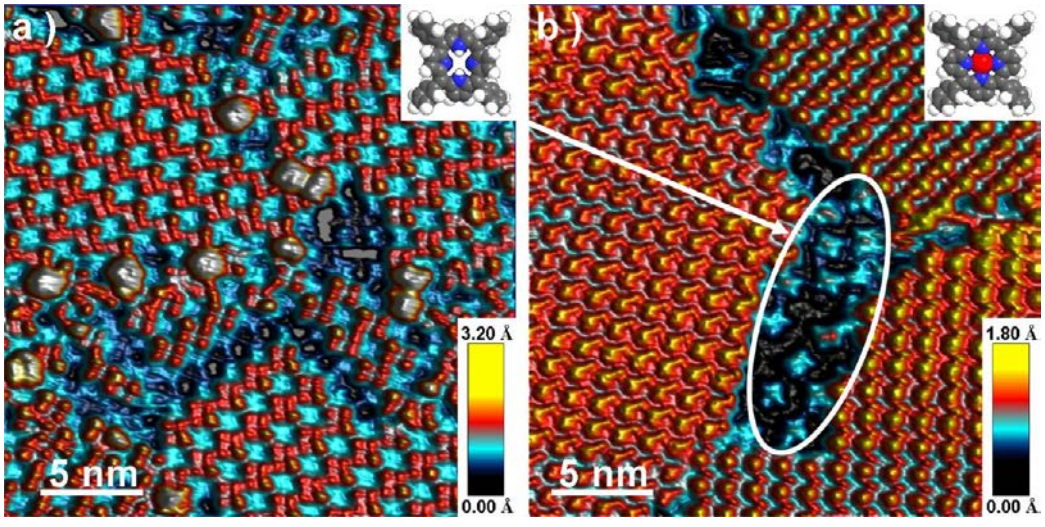

Figure 5. Constant current STM image of 0.030 ML 2HTPP on Cu(111) (a) before and (b) after annealing to 400 K. (a) 2HTPP in first (turquoise), second (red) and third layer (white) (U_{bias} = 1.35 V, I_{set} = 22 pA), (b) the metalated CuTPP (red and yellow) form square ordered islands with molecule−molecule distances of ∼1.30 nm. The turquoise molecules especially in the region marked with the white oval are residual nonmetalated 2HTPPs (U_{bias} = −1.05 V, I_{set} = 28 pA).

dx.doi.org/10.1021/la3046753 | *Langmuir* 2013, 29, 4104−4110

hint for the proposed bridging geometry of the checkerboard domains, as it evidences that the intramolecular conformation of the second layer molecules can not be the only reason for its elevated appearance in STM. Inspection of the model in Figure 3 reveals that the second layer molecules are arranged such that the phenyl groups of neighboring molecules along the short lattice direction, *b*, are oriented almost parallel, with only a small intersecting angle between the planes of the two phenyl rings. This geometry suggests that the supramolecular structure within the second layer is stabilized via $\pi-\pi$-stacking interactions. The other two phenyl groups of the second layer molecules are oriented along the long lattice vector, *a*, with an orientation relative to the phenyl groups of the first layer molecules similar to that observed for T-type interactions: within two-dimensional T-type structures known in the literature[3,4] one phenyl C−H-group in *para*-position points perpendicular toward the phenyl ring of a neighboring molecule. In the checkerboard structure the same orientation is observed, albeit with one phenyl C−H-group in the *meta*-position of a second layer molecule pointing perpendicular toward the phenyl ring of a neighboring first layer molecule. For better understanding the top and side view of the scaled molecular models based on the STM data is shown in Figure 4c. Thus, we conclude that the checkerboard structure is stabilized by $\pi-\pi$-stacking between second layer molecules and T-type interactions between first and second layer molecules. Information on the stability of the checkerboard structure at RT can be derived from Figure 2g, which shows the average frame of a 60 image STM movie. From the sharp appearance of the first layer molecules and most second layer molecules, it is obvious that the checkerboard domains are very stable in position and orientation. Only at the lower coordinated boundaries of the checkerboard domains, attachment and detachment of single second layer molecules can be observed. This can be seen best in the region marked with the white oval in Figure 2g, where the molecules appear less intense than normal second layer ones and furthermore their typical shape with four protrusions is smeared out.

Finally, at coverages higher than ∼0.030 ML, molecules in the third layer can be observed, as depicted in Figure 2d, where they are identified as white spots in between checkerboard domains. The inset in this figure shows a magnification of a third layer molecule, which clearly shows that the molecules in higher layers maintain the four spot appearance of the second layer ones. The first molecules of the third layer appear in the void locations in between the checkerboard domains, which is expected. However, the ordering of the molecules and the checkerboard structure is not continued above the second layer and there is no regular supramolecular structure found for higher layers. Concerning the dynamics of third layer molecules, all molecules observed appear to be pinned; this is evident from Figure 2h, which shows the average frame of an STM movie, which is practically identical to each single frame of the movie (c.f., Figure 2d). Thus, no diffusion occurs at RT.

CONCLUSIONS

We present a detailed analysis of the formation of a complex checkerboard-type superstructure of 2HTPP on Cu(111) with half of the molecules in direct contact with the substrate and half of them in the second layer bridging the gaps between the first layer molecules. This unusual checkerboard structure is found when increasing the coverage from the submonolayer range to higher coverages. At low coverages, a disordered layer with a very specific adsorption behavior for 2HTPP is observed and the situation is dominated by adsorbate−substrate interactions. In contrast, the checkerboard structure is stabilized by attractive molecule−molecule interactions, in form of T-type interactions and $\pi-\pi$ stacking interactions at the same time.

EXPERIMENTAL SECTION

All experiments and sample preparations were performed in a two chamber UHV-system, at a background pressure in the low 10^{-10} mbar regime. The microscope is an RHK UHV VT STM 300 with RHK SPM 100 electronics. All given voltages are referred to the sample and the images have been taken in constant current mode at RT. Moderate filtering (Gaussian smooth, background subtraction) has been applied for noise reduction. The Cu(111) single crystal was purchased from MaTeck and 2HTPP with a specified purity of 98% from Porphyrin Systems. The preparation of the clean substrate surface was done by repeated cycles of Ar^+-ion sputtering (500 eV) and annealing up to 850 K. The porphyrin layers were prepared by thermal sublimation from a home-built Knudsen cell at ∼620 K with a deposition rate of ∼0.003 ML per minute onto the substrate held at RT. The deposition rate was determined by counting the deposited molecules in STM, yielding the actual molecular density. With this value, the deposition rate can be estimated. The higher coverages were determined considering the estimated deposition rate in combination with the corresponding evaporation time. The values were confirmed by again counting the CuTPP molecules in STM after metalation.

ASSOCIATED CONTENT

Supporting Information

Additional information on the orientation of the checkerboard domains and the apparent heights of the different molecular species occurring are available as pdf and time lapse movies related to Figure 2 are available in QuickTime format. This material is available free of charge via the Internet at http://pubs.acs.org.

AUTHOR INFORMATION

Corresponding Author

*Phone: +49 (0)9131/85-27316; fax: +49 (0)9131/85-28867; e-mail: marbach@chemie.uni-erlangen.de.

Present Address

[†]Helmholtz Institut Ulm and Institut für Oberflächenchemie und Katalyse, Universität Ulm, Albert-Einstein Allee 47, D-89069 Ulm, Germany.

Notes

The authors declare no competing financial interest.

ACKNOWLEDGMENTS

The authors thank the German Science Foundation (DFG) for financial support through SFB 583 and the Excellence Cluster "Engineering of Advanced Materials" granted to the University of Erlangen-Nürnberg.

REFERENCES

(1) De Feyter, S.; De Schryver, F. C. Two-dimensional supramolecular self-assembly probed by scanning tunneling microscopy. *Chem. Soc. Rev.* **2003**, *32* (3), 139−150.

(2) Barth, J. V. Molecular architectonic on metal surfaces. *Annu. Rev. Phys. Chem.* **2007**, *58*, 375−407.

(3) Buchner, F.; Kellner, I.; Hieringer, W.; Görling, A.; Steinrück, H.-P.; Marbach, H. Ordering aspects and intramolecular conformation of tetraphenylporphyrins on Ag(111). *Phys. Chem. Chem. Phys.* **2010**, *12* (40), 13082−13090.

(4) Brede, J.; Linares, M.; Kuck, S.; Schwobel, J.; Scarfato, A.; Chang, S. H.; Hoffmann, G.; Wiesendanger, R.; Lensen, R.; Kouwer, P. H. J.;

Hoogboom, J.; Rowan, A. E.; Broring, M.; Funk, M.; Stafstrom, S.; Zerbetto, F.; Lazzaroni, R. Dynamics of molecular self-ordering in tetraphenyl porphyrin monolayers on metallic substrates. *Nanotechnology* **2009**, *20*, 275602.
(5) Buchner, F.; Kellner, I.; Steinrück, H.-P.; Marbach, H. Modification of the growth of iron on Ag(111) by predeposited organic monolayers. *Z. Phys. Chem.* **2009**, *223* (1−2), 131−144.
(6) Buchner, F.; Zillner, E.; Röckert, M.; Gläßel, S.; Steinrück, H.-P.; Marbach, H. Substrate-mediated phase separation of two porphyrin derivatives on Cu(111). *Chem.—Eur. J.* **2011**, *17* (37), 10226−10229.
(7) Buchner, F.; Warnick, K. G.; Wölfle, T.; Görling, A.; Steinrück, H.-P.; Hieringer, W.; Marbach, H. Chemical fingerprints of large organic molecules in scanning tunneling microscopy: imaging adsorbate-substrate coupling of metalloporphyrins. *J. Phys. Chem. C* **2009**, *113* (37), 16450−16457.
(8) Weber-Bargioni, A.; Reichert, J.; Seitsonen, A. P.; Auwärter, W.; Schiffrin, A.; Barth, J. V. Interaction of cerium atoms with surface-anchored porphyrin molecules. *J. Phys. Chem. C* **2008**, *112* (10), 3453−3455.
(9) Scudiero, L.; Barlow, D. E.; Hipps, K. W. Physical properties and metal ion specific scanning tunneling microscopy images of metal(II) tetraphenylporphyrins deposited from vapor onto gold (111). *J. Phys. Chem. B* **2000**, *104* (50), 11899−11905.
(10) Barth, J. V. Fresh perspectives for surface coordination chemistry. *Surf. Sci.* **2009**, *603* (10−12), 1533−1541.
(11) Buchner, F.; Xiao, J.; Zillner, E.; Chen, M.; Röckert, M.; Ditze, S.; Stark, M.; Steinrück, H.-P.; Gottfried, J. M.; Marbach, H. Diffusion, rotation, and surface chemical bond of individual 2H-tetraphenylporphyrin molecules on Cu(111). *J. Phys. Chem. C* **2011**, *115* (49), 24172−24177.
(12) Diller, K.; Klappenberger, F.; Marschall, M.; Hermann, K.; Nefedov, A.; Wöll, C.; Barth, J. V. Self-metalation of 2H-tetraphenylporphyrin on Cu(111): An X-ray spectroscopy study. *J. Chem. Phys.* **2012**, *136*, 014705.
(13) Bai, Y.; Buchner, F.; Kellner, I.; Schmid, M.; Vollnhals, F.; Steinrück, H.-P.; Marbach, H.; Gottfried, J. M. Adsorption of cobalt (II) octaethylporphyrin and 2H-octaethylporphyrin on Ag(111): New insight into the surface coordinative bond. *New J. Phys.* **2009**, *11*, 125004.
(14) Buchner, F.; Flechtner, K.; Bai, Y.; Zillner, E.; Kellner, I.; Steinrück, H.-P.; Marbach, H.; Gottfried, J. M. Coordination of iron atoms by tetraphenylporphyrin monolayers and multilayers on Ag(111) and formation of iron-tetraphenylporphyrin. *J. Phys. Chem. C* **2008**, *112* (39), 15458−15465.
(15) Shubina, T. E.; Marbach, H.; Flechtner, K.; Kretschmann, A.; Jux, N.; Buchner, F.; Steinrück, H.-P.; Clark, T.; Gottfried, J. M. Principle and mechanism of direct porphyrin metalation: Joint experimental and theoretical investigation. *J. Am. Chem. Soc.* **2007**, *129* (30), 9476−9483.
(16) Buchner, F.; Comanici, K.; Jux, N.; Steinrück, H.-P.; Marbach, H. Polymorphism of porphyrin molecules on Ag(111) and how to weave a rigid monolayer. *J. Phys. Chem. C* **2007**, *111* (36), 13531−13538.
(17) Buchner, F.; Schwald, V.; Comanici, K.; Steinrück, H.-P.; Marbach, H. Microscopic evidence of the metalation of a free-base porphyrin monolayer with iron. *Chemphyschem* **2007**, *8* (2), 241−243.
(18) Buchner, F.; Seufert, K.; Auwärter, W.; Heim, D.; Barth, J. V.; Flechtner, K.; Gottfried, J. M.; Steinrück, H.-P.; Marbach, H. NO-induced reorganization of porphyrin arrays. *ACS Nano* **2009**, *3* (7), 1789−1794.
(19) Auwärter, W.; Weber-Bargioni, A.; Brink, S.; Riemann, A.; Schiffrin, A.; Ruben, M.; Barth, J. V. Controlled metalation of self-assembled porphyrin nanoarrays in two dimensions. *Chemphyschem* **2007**, *8* (2), 250−254.
(20) Auwärter, W.; Weber-Bargioni, A.; Riemann, A.; Schiffrin, A.; Gröning, O.; Fasel, R.; Barth, J. V. Self-assembly and conformation of tetrapyridyl-porphyrin molecules on Ag(111). *J. Chem. Phys.* **2006**, *124*, 194708.
(21) Jung, T. A.; Schlittler, R. R.; Gimzewski, J. K. Conformational identification of individual adsorbed molecules with the STM. *Nature* **1997**, *386* (6626), 696−698.
(22) Cox, E. G.; Cruickshank, D. W. J.; Smith, J. A. S. The crystal structure of benzene at −3° C. *Proc. R. Soc. London. Ser. A. Math. Phys. Sci.* **1958**, *247* (1248), 1−21.
(23) Sinnokrot, M. O.; Sherrill, C. D. High-accuracy quantum mechanical studies of $\pi-\pi$ interactions in benzene dimers. *J. Phys. Chem. A* **2006**, *110* (37), 10656−10668.
(24) Rojas, G.; Simpson, S.; Chen, X. M.; Kunkel, D. A.; Nitz, J.; Xiao, J.; Dowben, P. A.; Zurek, E.; Enders, A. Surface state engineering of molecule−molecule interactions. *Phys. Chem. Chem. Phys.* **2012**, *14* (14), 4971−4976.
(25) Rojas, G.; Chen, X.; Bravo, C.; Kim, J. H.; Kim, J. S.; Xiao, J.; Dowben, P. A.; Gao, Y.; Zeng, X. C.; Choe, W.; Enders, A. Self-assembly and properties of nonmetalated tetraphenyl-porphyrin on metal substrates. *J. Phys. Chem. C* **2010**, *114* (20), 9408−9415.
(26) Xiao, J.; Ditze, S.; Chen, M.; Buchner, F.; Stark, M.; Drost, M.; Steinrück, H.-P.; Gottfried, J. M.; Marbach, H. Temperature-dependent chemical and structural transformations from 2H-tetraphenylporphyrin to copper(II)-tetraphenylporphyrin on Cu(111). *J. Phys. Chem. C* **2012**, *116* (22), 12275−12282.
(27) Ditze, S.; Stark, M.; Drost, M.; Buchner, F.; Steinrück, H.-P.; Marbach, H. Activation energy for the self-metalation reaction of 2H-tetraphenylporphyrin on Cu(111). *Angew. Chem., Int. Ed.* **2012**, *51* (43), 10898−10901.

Coverage dependent disorder-order transition of 2H-tetraphenylporphyrin on Cu(111)

*Michael Stark, Stefanie Ditze, Martin Drost, Florian Buchner†, Hans-Peter Steinrück, and Hubertus Marbach**

Lehrstuhl für Physikalische Chemie II and Interdisciplinary Center for Molecular Materials (ICMM), Universität Erlangen-Nürnberg, Egerlandstraße 3, D-91058 Erlangen, Germany.

†current address: Helmholtz Institut Ulm und Institut für Oberflächenchemie und Katalyse, Universität Ulm, Albert-Einstein Allee 47, D-89069 Ulm, Germany

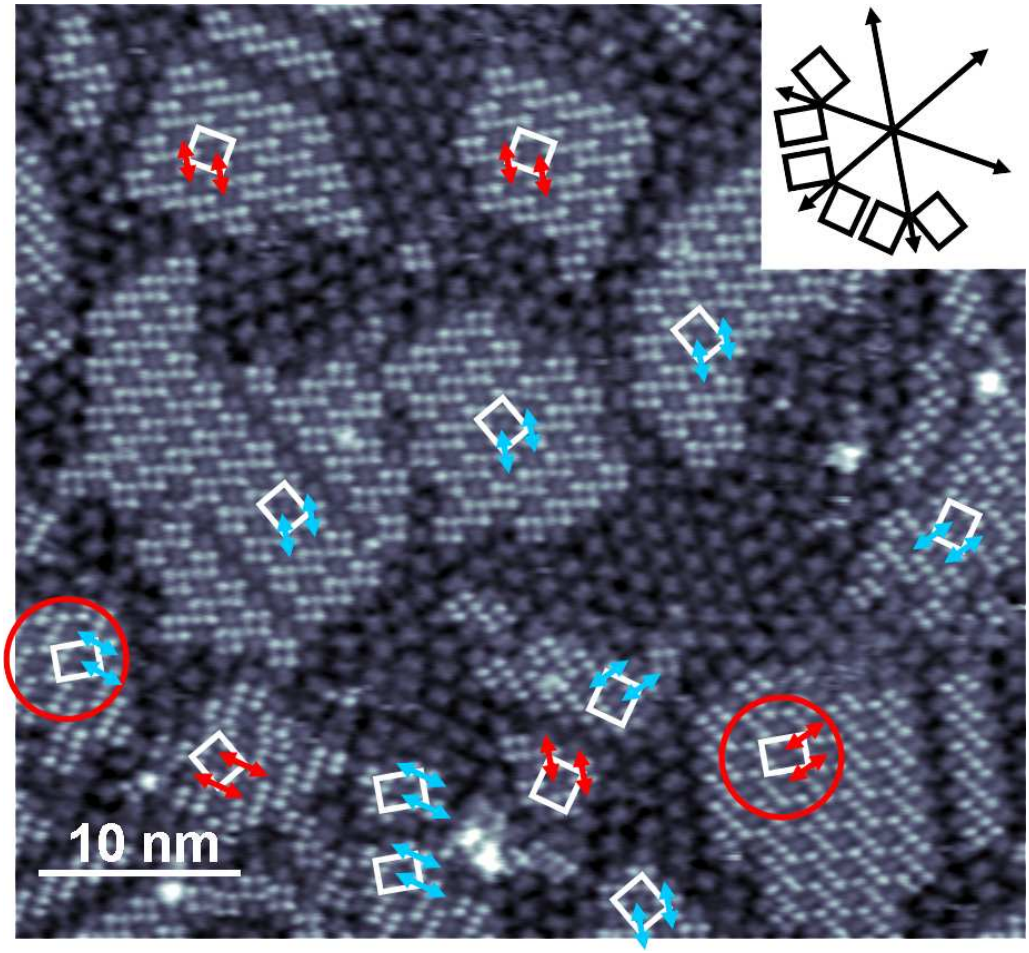

Figure S1. Constant current STM image of differently oriented checkerboard domains of 2HTPP on Cu(111) (U_{bias} = -1.01 V, I_{set} = 30 pA). The unit cells of the different domains are indicated by the white rectangles. The red and blue double-pointed arrows represent the pyrrole-pyrrole axis of the molecules within each domain. In the domains with red arrows there is the pyrrole-pyrrole axis of the molecules tilted 30° to the left of the longer lattice vector of the domain, whereas the blue arrows indicate domains with molecules tilted 30° left. The red circles mark a pair of chiral checkerboard domains with equally oriented unit cells, but differently oriented molecules. The double-pointed arrows occur pointing only in

three directions according to the substrate lattice. The sketch in the upper right corner shows the occurring three different orientations of the molecules (double-pointed arrows) and the resulting unit cells of the checkerboard domains (rectangles).

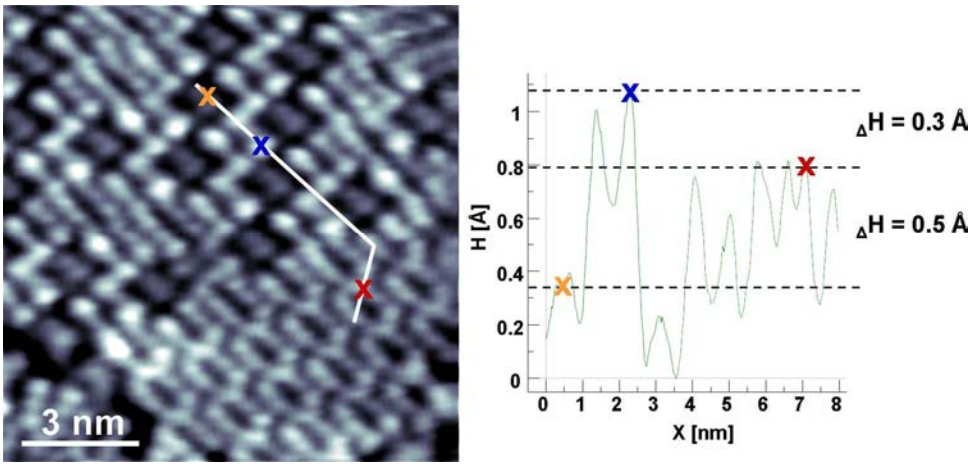

Figure S2. Constant current STM image and corresponding height profile for the determination of the differences in apparent height between 1st layer 2HTPP molecules (orange cross), 2nd layer 2HTPP molecules (blue cross) within a checkerboard domain and CuTPP (red cross) within a CuTPP domain. Note that the apparent heights of the 2HTPP molecules with direct contact to the substrate can not be determined due to the impossibility to determine a reliable substrate level for such high coverages. The tunneling parameters are: U_{bias} = -0.93 V, I_{set} = 20 pA.

Movie M1. 39 image (13 min) STM movie showing the slow unidirectional movement of individual 2HTPP molecules at RT along the close packed rows of the Cu(111) substrate. (U_{bias} = -1.49 V, I_{set} = 30 pA, size: $(17\ nm)^2$)

Movie M2. 51 image (22 min) STM movie where besides the 1D diffusion of 2HTPP on Cu(111) also frequent changes in the diffusion direction of the molecules are observable at RT. (U_{bias} = -193 mV, I_{set} = 11 pA, size: $(17\ nm)^2$)

Movie M3. 60 image (23 min) STM movie where the dynamics of the checkerboard structure at RT, formed by 2HTPP on Cu(111) is visible. (U_{bias} = -1.05 V, I_{set} = 30 pA, size: $(17\ nm)^2$)

Movie M4. 26 image (10 min) STM movie of 0.03 ML 2HTPP on Cu(111) at RT. The movie reveals a three-layered structure where all 2HTPP molecules keep their positions during the whole movie. (U_{bias} = +1.35 V, I_{set} = 22 pA, size: $(17\ nm)^2$)

P2

Supramolecular order and structural dynamics: A STM study of 2H-tetraphenylporphycene on Cu(111)

Michael Stark,[1,2] Johannes Träg,[1,2] Stefanie Ditze,[1,2] Wolfgang Brenner,[3] Norbert Jux,[3] Hans-Peter Steinrück,[1,2] and Hubertus Marbach[1,2,a)]
[1]*Lehrstuhl für Physikalische Chemie II, Universität Erlangen-Nürnberg, Egerlandstr. 3, 91058 Erlangen, Germany*
[2]*Interdisciplinary Center for Molecular Materials (ICMM), Universität Erlangen-Nürnberg, Henkestr. 42, 91054 Erlangen, Germany*
[3]*Lehrstuhl für Organische Chemie II, Universität Erlangen-Nürnberg, Henkestr. 42, 91054 Erlangen, Germany*

(Received 5 December 2014; accepted 4 February 2015; published online 24 February 2015)

The adsorption of 2H-tetraphenylporphycene (2HTPPc) on Cu(111) was investigated by scanning tunneling microscopy (STM). At medium coverages, supramolecular ordered islands are observed. The individual 2HTPPc molecules appear as two pairs of intense protrusions which are separated by an elongated depression. In the islands, the molecules are organized in rows oriented along one of the close packed Cu(111) substrate rows; the structure is stabilized by T-type interactions of the phenyl substituents of neighboring molecules. Two types of rows are observed, namely, highly ordered rows in which all molecules exhibit the same orientation, and less ordered rows in which the molecules exhibit two perpendicular orientations. Altogether, three different azimuthal orientations of 2HTPPc are observed within one domain, all of them rotated by 15° ± 1° relative to one closed packed Cu direction. The highly ordered rows are always separated by either one or two less ordered rows, with the latter structure being the thermodynamically more stable one. The situation in the islands is highly dynamic, such that molecules in the less ordered rows occasionally change orientation, also complete highly ordered rows can move. The supramolecular order and structural dynamics are discussed on the basis of the specific molecule-substrate and molecule-molecule interactions. © *2015 AIP Publishing LLC.* [http://dx.doi.org/10.1063/1.4908268]

INTRODUCTION

The engineering of functional nano-devices increasingly relies on the self-assembly of large organic building blocks.[1,2] This requires a detailed knowledge of the underlying processes, which allows for the controlled surface-confined formation of functional supramolecular architectures from suitable molecules. Therefore, it is of fundamental importance to understand the relevant mechanisms, that is, to identify the driving forces for the self-assembly of the involved molecular species. In this context, the specific contributions of molecule-substrate and molecule-molecule interactions are of major interest.

Porphyrinoids are particularly well suited as molecular building blocks, due to their intrinsic functionalities and rigid structural theme, which often trigger long range order on surfaces.[3] In this regard, scanning tunneling microscopy (STM) is a powerful tool for the analysis of the supramolecular arrangement, the intramolecular conformation, and also the electronic structure of large organic molecules adsorbed on (semi-)conductive surfaces.[1,2,4,5] For example, extensive STM investigations were performed for various tetraphenylporphyrins (TPPs) on different surfaces; these studies enabled to identify the contributions of molecule-molecule and molecule-substrate interactions.[6–18] Numerous studies report that on flat surfaces, porphyrinoids form long range ordered supramolecular structures, with the porphyrin macrocycle parallel to the surface plain.[14,18–30] Generally, the self-assembly of these molecules is determined by a subtle balance between molecule-molecule and molecule-substrate interactions.[15] Therefore, the choice of the actual peripheral ligands, the substrate, and the nature of the porphyrin center (e.g., free-base or metalated) can be regarded as a suitable route to tailor molecular architectures in a bottom up approach.[3]

2H-tetraphenylporphyrin (2HTPP) on Cu(111) has been reported to be an adsorption system with extraordinary strong molecule-substrate interactions. For this system, one observes isolated, individual molecules on the surface at room temperature (RT), due to the strong chemical interaction of the iminic nitrogen atoms of the porphyrin with Cu atoms from the substrate.[15,17,31]

After variations of the peripheral ligands and the metal center, we now expand our investigations to a modified macrocycle, namely, to 2H-tetraphenylporphycene (2HTPPc) on Cu(111). 2HTPPc is a structural isomer of 2HTPP; for comparison, the two molecular species are displayed in Fig. 1. Recent low temperature STM studies of "bare" porphycene molecules (that is, without phenyl ligands) on a Cu(110) surface revealed an adsorption geometry with the macrocycle parallel to the surface plane and strong interactions between the iminic N and the Cu substrate atoms.[32,33]

a)Author to whom correspondence should be addressed. Electronic mail: hubertus.marbach@fau.de

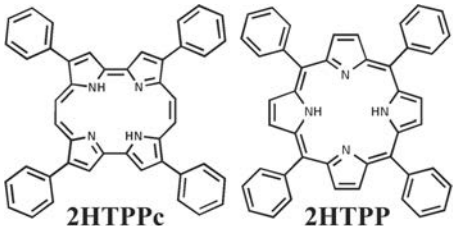

FIG. 1. 2HTPPc and its structural isomer 2HTPP.

EXPERIMENTAL

All experiments and sample preparation were performed in a two chamber ultra-high vacuum (UHV) system, at a background pressure in the low 10^{-10} mbar regime. The microscope is an RHK UHV VT STM 300 with RHK SPM 100 electronics. All given voltages are referred to the sample, and the images have been acquired in constant current mode at RT. The Cu(111) single crystal was purchased from MaTeck and the 2HTPP material with a specified purity of 98% from Porphyrin Systems.

The 2,7,12,17-tetraphenylporphycene was synthesized via a modification[34] of Vogel's[35] and Nonell's[36] original procedures. In particular, the formation of the respective pyrrole was carried out following Matsumoto's[37] synthesis of pyrroles by reacting two equivalents of ethyl isocyanoacetate with benzaldehyde in the presence of Diazabicycloundecen. The subsequent iodination with iodine monochloride[38] gave the desired iodopyrrole in nearly quantitative yield.

The preparation of the clean substrate surface was done by repeated cycles of Ar^+-ion sputtering (500 eV) and annealing up to 850 K. The porphycene layers were prepared by thermal sublimation from a home-built Knudsen cell at ~580 K onto the substrate held at RT. The STM data were processed (moderate high pass filtering and Gaussian smooth) with WSxM software.[39]

RESULTS AND DISCUSSION

After deposition of small amounts of 2HTPPc on the Cu(111) surface, step decoration is observed, as shown in Fig. 2(a). Such an adsorption behavior is common for similar systems, e.g., for 2HTPP on Ag(111).[14] It indicates that step sites are energetically favorable due to an increased coordination at the lower side of the step; thus, at low coverage, adsorption is dominated by molecule-substrate interactions at the steps. In addition, the step decoration indicates that 2HTPPc molecules are mobile on the terraces. The "excess" molecules diffuse too fast on the surface to be imaged with the STM. The fact that no islands are formed indicates that no sufficient attractive molecule-molecule interactions are present to realize a mutual stabilization and the formation of supramolecular arrangements at room temperature.[14,15,40]

At higher 2HTPPc coverages, two-dimensional islands are observed on the Cu terraces, as is evident from Figure 2(b). Note that in addition to 2HTPPc, 2HTPP molecules are coadsorbed on the surface. The latter are known to appear as two elongated parallel protrusions, which are oriented

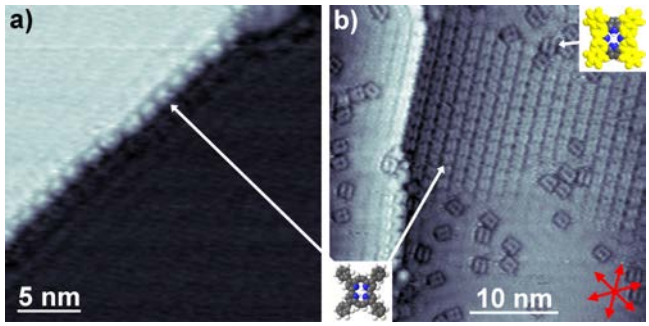

FIG. 2. (a) Constant current STM image of a low coverage of 2HTPPc on Cu(111), displaying step decoration ($U_{bias} = -0.77$ V, $I_{set} = 30$ pA); (b) medium coverage of 2HTPPc (lower left inlay) with co-deposited 2HTPP (top right inlay) on Cu(111). 2HTPPc forms islands, while 2HTPP adsorbs mainly as individual isolated molecules; their azimuthal orientation (red arrows) indicates the directions of the close packed Cu(111) substrate rows ($U_{bias} = -1.14$ V, $I_{set} = 30$ pA).

along the close packed atomic rows of the Cu(111) substrate and thus indicate the main crystallographic directions of the surface (red arrows).[15,41] The inspection of the 2HTPPc island reveals that it is composed of molecular rows along one of the main crystallographic directions. In addition, the surface regions with no islands appear with increased apparent height in STM, that is, with a similar brightness than the molecules in the islands. This observation is explained with fast diffusing molecules which form a 2D gas phase, as previously reported for similar adsorption systems.[14,15,40,42] In this regard, the supramolecular assembly into islands can be interpreted as a condensation process.[15,40] On the one hand, the molecule-substrate interaction (surface corrugation) is too weak to stabilize individual molecules at room temperature, and thus they cannot be imaged by STM. On the other hand, the formation of the two-dimensional islands indicates that attractive molecule-molecule interactions can lead to a mutual stabilization in a supramolecular ordered structure. In order to further elucidate the arrangement of 2HTPPc within the islands, the appearance of an individual molecule in STM has to be clarified first.

Fig. 3 shows a close up STM image of one molecule incorporated in a two-dimensional island; in the right part of the figure, the same image is shown with a scaled overlay of a space filling model of 2HTPPc. The molecule appears as two pairs of intense protrusions which are separated by

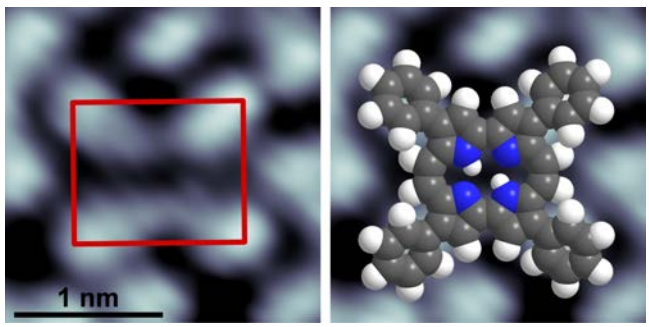

FIG. 3. Close up constant current STM image of one 2HTPPc molecule (left) and the same image overlaid with the corresponding scaled space filling model (right) ($U_{bias} = -229$ mV, $I_{set} = 30$ pA).

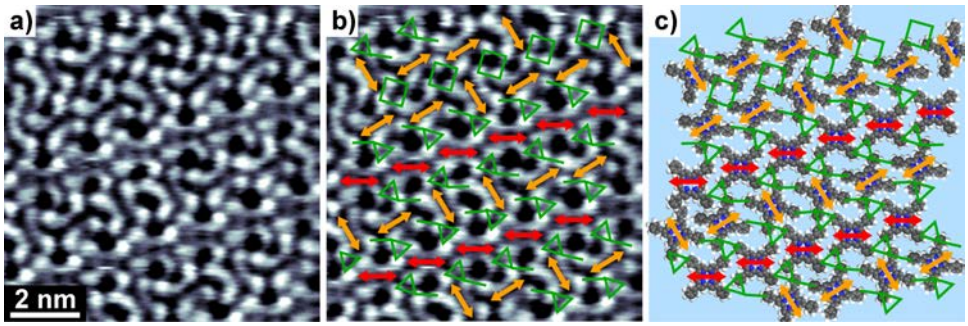

FIG. 4. Constant current STM image of a typical supramolecular 2HTPPc assembly. The molecules in the highly ordered rows are indicated by red arrows and the ones of the less ordered rows with orange arrows. The intermolecular T-type interactions are indicated by the green squares and rectangles, giving rise to the two different structural motives. For further illustration, the arrangement is shown with space filling models ($U_{bias} = -229$ mV, $I_{set} = 30$ pA).

an elongated depression through the center of the molecule. The latter depression will be referred to as the molecular axis in the following. Each pair of protrusions is linked by a less intense bow shaped protrusion. The absence of tunneling bias dependent changes (in the range of −1.5 V to +1.0 V) is a strong indication that the appearance in STM mainly reflects the topography of the 2HTPPc molecule. Under this assumption, from the lower apparent height of the ethylene bridges as compared to the pyrrole rings, a slight kinking of the molecule by ∼5° is estimated. The measurement of the dimensions of one molecule in the STM images yields a rectangular shape, with distances between the intensity maxima of the four protrusions of 0.93 ± 0.01 nm for the shorter and 0.98 ± 0.02 nm for the longer side. The resulting aspect ratio of 1.05 is in good agreement with the value of 1.08 obtained from a gas phase model of 2HTPPc, which was optimized with the MM2 force field calculation method implemented in *Chem & Bio 3D*. In this model, the long side of the molecule is formed by the two directly linked pyrrole groups, while the short side is formed by the ethylene bridge in-between two pyrrole groups. With this model, it is possible to attribute the features in the STM image to the different parts of the molecule: The four intense protrusions in the periphery of the molecule are caused by the four phenyl groups of the 2HTPPc. The less intense links between these protrusions are assigned to the pyrrole groups, and the central cavity represents the molecular axis intersecting the ethylene bridges, as depicted in the right panel of Fig. 3. As discussed above, we deduced a slight kinking of the molecule of ∼5° along this axis.

With the knowledge of the appearance of individual 2HTPPc molecules, the detailed analysis of the supramolecular arrangement within the islands is conducted in the following. A representative micrograph is depicted in Figure 4(a). To illustrate the orientation of the individual molecules, their molecular axes are indicated with arrows in Figure 4(b). The inspection of the STM image reveals a peculiar adsorption behavior: the molecules are organized in a combination of highly ordered rows, where all molecules are oriented identically (red arrows), and less ordered rows, where different azimuthal molecular orientations are observed (orange arrows). In the highly ordered rows, the molecular axes of all molecules are rotated by 15° ± 1° relative to the direction of the molecular row, and thus also 15° ± 1° relative to a close packed substrate direction. Within a domain, all molecules in highly ordered rows are oriented identically, e.g., rotated 15° ± 1° clockwise relative to one of the close packed substrate directions. As expected, one also finds the corresponding mirror domains in which the molecules in the highly ordered rows are rotated 15° ± 1° counterclockwise. In the less ordered rows (orange arrows), two different orientations exist, with the molecules either rotated by −15° ± 1° or 75° ± 1° with respect to the direction of the molecular row. Considering the threefold symmetry of the substrate lattice, all molecules adopt orientations of 15° ± 1° with respect to one of the three high symmetry directions of the substrate. The two molecular orientations in the less ordered rows occur in a ratio very close to 1:1 (i.e., 233:217 for 450 analyzed molecules), indicating that both orientations are energetically equivalent.

The analysis of the distribution of different rows in an island shows that highly ordered rows are never found directly next to each other, but always are separated by one or two less ordered rows. To understand this peculiar supramolecular arrangement, it is important to consider the specific contributions of molecule-substrate and molecule-molecule interactions. So far, it is apparent that the interactions between the molecules and the substrate drive the orientation of the molecules (15° in respect to a close packed atomic row of the substrate). If that would be the only contribution to the ordering of the molecules, one would anticipate all six possible orientations (15° clockwise and counterclockwise to close packed Cu row) in one domain, which is obviously not the case. The actual restriction to three orientations within one domain must therefore be due to intermolecular interactions. The molecule-molecule distance along the ordered and less ordered rows is 1.46 ± 0.06 nm, which is in the order of the size of a molecule. The given distance is obviously not an integer multiple of the atomic distances of the Cu substrate in the corresponding directions and thus is incommensurate or higher-order commensurate. Thus, the intermolecular interactions must occur between the phenyl groups of neighboring molecules. Simple π-π-stacking[43,44] can be ruled out, since the geometry of the phenyl groups in the STM images in Figure 4 does not fit this type of interaction. Instead, we propose T-type interactions, which were previously found to be the main contribution to intermolecular interactions in similar adsorption systems.[14,18,25] Burley *et al.* reported typical distances of 4.5–7 Å and intersection angles of 50°–90° for T-type interactions in

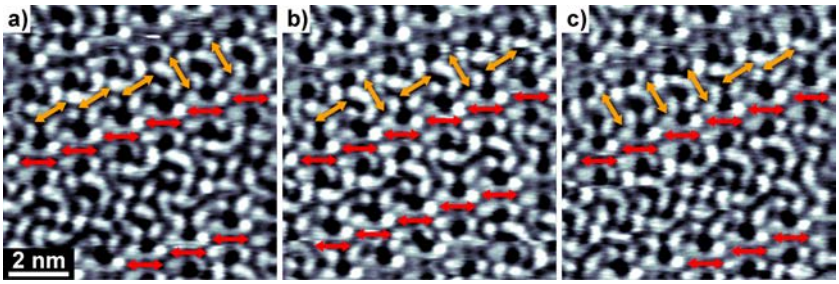

FIG. 5. Three consecutive STM images with red arrows indicating the orientation of the molecules in higher ordered rows and orange arrows for the less ordered ones. From (a) to (c) each less ordered molecule indicated changes its orientation once. Additionally, the distance between the higher ordered rows (red arrows) changes from (a) to (b) and from (b) to (c) ($U_{bias} = -229$ mV, $I_{set} = 30$ pA, $\Delta t = 14$ s).

biomolecules.[45] Close inspection of the supramolecular structure in Figure 4(c) reveals two main motives concerning the arrangement of the phenyl substituents of neighboring 2HTPPc molecules: (1) At the junctions of highly ordered and less ordered rows, a triangular T-type arrangement plus one additional T-type interaction is identified as indicated in Figs. 4(b) and 4(c) by a triangle with one leg. The distances of the centers of the phenyl rings of 5.0–6.5 Å and the intersection angle of 60° are in the parameter range for stable T-type interactions.[45] (2) At the junctions of two less ordered rows, a rectangular T-type arrangement is found, as indicated by the squares in Figs. 4(b) and 4(c). Here, the distances are in the range of 5.5–6.5 Å and the intersection angle is 90°.

The situation of 2HTPPc molecules between the ordered domains is dynamic. As outlined above, a 2D gas phase of fast diffusing 2HTPPc coexists with the ordered islands, which overall are stable with respect to their orientation and position. However, there is a rapid exchange of molecules from the periphery of the molecular islands and the 2D gas phase. This can be observed by the changes and blurred shape of the domain boundaries (see Fig. 2(b)).

Interestingly, we also observe a highly dynamic behavior within the 2HTPPc domains: while the molecules in the highly ordered rows always have the same orientation, the molecules in the less ordered rows occasionally switch between the two observed orientations at RT. This is evident from Fig. 5 in which three consecutively acquired STM images are depicted: The molecules in the highly ordered row in the middle of the image (red arrows) always exhibit the same orientation; however, some molecules in the neighboring less ordered row (orange arrows) change their orientation from image to image. Figure 5 also documents another remarkable dynamic aspect of the 2HTPPc islands, namely, the (occasional) systematic rearrangement of whole rows: in the successive images in Fig. 5, the two highly ordered rows (red arrows) are initially separated by two less ordered rows (a), then by one (b), and finally again by two (c). From this observation, it is evident that massive rearrangements also of molecules in the highly ordered rows can occur, even though this happens rarely. In corresponding experiments conducted at a reduced temperature of 200 K, the situation is completely static, i.e., no rotation of individual molecules or rearrangement of whole rows is observed. This clearly evidences that the observed dynamic behavior is thermally induced. It is also important to emphasize that we always observed the highly ordered rows either separated by one or by two less ordered rows, and within the highly ordered rows, all molecules have an identical orientation. From the fact that all molecules in Figure 5 appear static at RT (that is, not blurred), one has to conclude that the rotation and reorganization must occur much faster than the timeframe of the STM acquisition (~14 s/image).

Interestingly, when following the dynamic behavior in an ordered island over a long time period, we observe a clear systematic trend: while shortly after deposition at RT, the highly ordered rows are predominantly separated by one less ordered row (Fig. 6(a)); after a few days, the highly ordered rows are predominantly separated by two less ordered rows (Fig. 6(b)). This observation along with the observed spontaneous rearrangements between both structures (one line vs. two lines separation) indicates that the energy difference between the two structures is rather small, and that highly ordered rows separated by one less ordered row are initially, at least partly, kinetically stabilized.

The key to understand the peculiar rearrangement behavior towards the thermodynamically more stable arrangement with highly ordered rows separated by two less ordered rows is to evaluate the distances of the highly ordered rows in the two distinct arrangements. On the one hand, highly ordered rows with one less ordered row in-between (Fig. 6(a)) are separated by 2.96 ± 0.06 nm, which corresponds to 13.5 Cu substrate rows (with a distance of 0.221 nm between neighboring closed-packed Cu substrate rows); on the other hand, highly ordered rows with two less ordered rows in-between (Fig. 6(b)) are separated by 4.44 ± 0.07 nm, which corresponds to 20.0 Cu substrate rows. Thus, for the latter case, each highly ordered molecule row is in registry with the Cu(111) substrate. We thus propose that the better registry with the substrate for the molecular arrangement with two less ordered rows between highly ordered rows is responsible for its larger thermodynamic stability. In addition, it appears likely that the quadratic T-type (90°) interaction motive is energetically favorable as compared to the triangular T-type

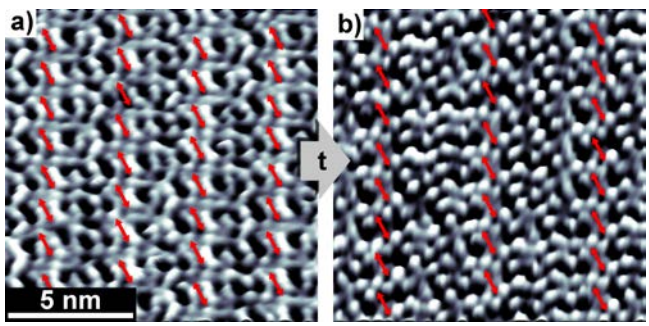

FIG. 6. Representative constant current STM images of 2HTPPc domains right after deposition ((a), $U_{bias} = -0.89$ V, $I_{set} = 30$ pA) and after storage at RT for 1 week ((b), $U_{bias} = -113$ mV, $I_{set} = 33$ pA). The molecules of the highly ordered molecular rows are indicated by red arrows.

(60°) interaction motive (see Fig. 4), which would also favor the arrangement with two less ordered rows in-between highly ordered rows, since only in this arrangement the quadratic motive appears.

An additional argument might be derived from a comparison with the adsorption of 2H-5,10,15,20-Tetrakis-(3,5-di-*tert*-butyl)-phenylporphyrin (2HTTBPP) on the same Cu(111) substrate.[46] 2HTTBPP adsorbs in alternating rows with two distinct appearances in STM which are assigned to concave and convex intramolecular conformations. From a detailed kinetic analysis of the bidirectional conformational switching of individual molecules between the two conformations around room temperature, the underlying energetics was deduced. One main finding was an entropic stabilization of the bimodal 2HTTBPP structure through rotational and probably vibrational excitation of the convex molecules. In analogy to these findings, one could speculate that the occasional rotation of 2HPPc in the less ordered rows might also yield an entropic stabilization of the corresponding aggregate, even though the effect is expected to be much smaller than for 2HTTBPP. In this picture, also the separation of the highly ordered 2HTPPc rows by two less ordered rows would mean enhanced entropic stabilization compared to the situation with only one separating less ordered row due to the larger number of rotating molecules.

Finally, there is to note that moderate thermal treatment of the structure with two less ordered rows between highly ordered rows (Fig. 6(b)) up to 450 K did not induce any changes of the arrangement. At higher temperatures, the supramolecular ordering is significantly degraded, and the uniform shape of the molecules is no longer present (not shown). This effect is most likely due to the dehydrogenation of the molecules.[31,47] Furthermore, it is interesting to mention that, in contrast to the similar 2HTPP[17,31,48] and 2HTTBPP,[47] no indication for metalation of 2HPPc with substrate atoms of the Cu(111) surface is observed up to 450 K. This is probably due to the smaller size of the central pocket for the porphycene that possibly does not allow for metalation.

SUMMARY AND CONCLUSION

We presented a detailed investigation of the peculiar adsorption behavior of 2H-tetraphenylporphycene on Cu(111). After initial step decoration, the existence of a 2D gas phase and finally two-dimensional ordered islands on the surface were found with increasing coverage. The supramolecular arrangement in the islands is composed of molecular rows along one of the three dense packed atomic rows of the substrate. Two types of molecular rows can be distinguished: first, highly ordered rows with all molecules oriented identically and the molecular axis at an angle of 15° ± 1° with respect to the molecular row; second, less ordered rows in which the 2HTPPc molecules exhibit two perpendicular orientations in a random fashion. The orientations of the individual molecules occasionally change, which corresponds to an azimuthal rotation by 90°. Another striking feature of the adsorption system is the systematic rearrangement of the sequence of neighboring molecular rows. Directly after thermal deposition of the 2HTPPc, the majority of highly ordered rows are separated by one less ordered row. However, this situation is only a transient metastable state, since with time the rows rearrange such that two highly ordered rows are separated by two less ordered rows. This peculiar rearrangement can at instances be observed reversibly in consecutively acquired images (cf. Fig. 5), indicating that the overall energy difference between the two arrangements is rather small. All dynamic changes, that is, rotation of individual molecules and rearrangement of whole molecular rows, occur in a timeframe faster than the scan speed of the STM (e.g., line acquisition time <30 ms), as concluded from the static appearance of the acquired images. The rearrangement of complete rows indicates comparably strong cooperative effects. The tendency to form the structure with highly ordered rows separated by two less ordered rows is explained by the better registry to the substrate and by the favorable geometry of the T-type interaction between less ordered rows. In addition, one might speculate that entropic stabilization might also contribute due to the rotation of molecules within the less ordered rows. Altogether, there is only little orientational order in the 2HTPPc islands: only in the highly ordered rows, all molecules have identical azimuthal orientation. Between neighboring rows, the orientational order varies, and different structural motives are found for the arrangements where one highly ordered row is separated by one or two less ordered rows. Overall, the unusual adsorption behavior of 2HTPPc at room temperature can be characterized as a mixture of supramolecular order and structural dynamics.

ACKNOWLEDGMENTS

The authors gratefully acknowledge the funding by the German Research Council (DFG) through research unit FOR 1878/funCOS, the Cluster of Excellence "Engineering of Advanced Materials" (http://www.eam.uni-erlangen.de) and by the Collaborative Research Center SFB 953 at the Friedrich-Alexander-Universitat Erlangen-Nurnberg.

[1]J. V. Barth, Annu. Rev. Phys. Chem. **58**, 375 (2007).
[2]J. V. Barth, Surf. Sci. **603**, 1533 (2009).
[3]J. M. Gottfried and H. Marbach, Z. Phys. Chem. **223**, 53 (2009).
[4]S. de Feyter and F. C. de Schryver, Chem. Soc. Rev. **32**, 139 (2003).
[5]J. K. Gimzewski and C. Joachim, Science **283**, 1683 (1999).
[6]Y. Bai, F. Buchner, I. Kellner, M. Schmid, F. Vollnhals, H.-P. Steinrück, H. Marbach, and J. M. Gottfried, New J. Phys. **11**, 125004 (2009).
[7]W. Auwärter, A. Weber-Bargioni, S. Brink, A. Riemann, A. Schiffrin, M. Ruben, and J. V. Barth, ChemPhysChem **8**, 250 (2007).
[8]A. Weber-Bargioni, W. Auwärter, F. Klappenberger, J. Reichert, S. Lefrancois, T. Strunskus, C. Wöll, A. Schiffrin, Y. Pennec, and J. V. Barth, ChemPhysChem **9**, 89 (2008).
[9]A. Weber-Bargioni, J. Reichert, A. P. Seitsonen, W. Auwärter, A. Schiffrin, and J. V. Barth, J. Phys. Chem. C **112**, 3453 (2008).
[10]T. Wölfle, A. Görling, and W. Hieringer, Phys. Chem. Chem. Phys. **10**, 5739 (2008).
[11]F. Buchner, I. Kellner, H.-P. Steinrück, and H. Marbach, Z. Phys. Chem. **223**, 131 (2009).
[12]F. Buchner, K. Flechtner, Y. Bai, E. Zillner, I. Kellner, H.-P. Steinrück, H. Marbach, and J. M. Gottfried, J. Phys. Chem. C **112**, 15458 (2008).
[13]F. Buchner, K. G. Warnick, T. Wölfle, A. Görling, H.-P. Steinrück, W. Hieringer, and H. Marbach, J. Phys. Chem. C **113**, 16450 (2009).
[14]F. Buchner, I. Kellner, W. Hieringer, A. Görling, H.-P. Steinrück, and H. Marbach, Phys. Chem. Chem. Phys. **12**, 13082 (2010).

[15]F. Buchner, E. Zillner, M. Röckert, S. Gläßel, H.-P. Steinrück, and H. Marbach, Chem. - Eur. J. **17**, 10226 (2011).
[16]F. Buchner, J. Xiao, E. Zillner, M. Chen, M. Röckert, S. Ditze, M. Stark, H.-P. Steinrück, J. M. Gottfried, and H. Marbach, J. Phys. Chem. C **115**, 24172 (2011).
[17]K. Diller, F. Klappenberger, M. Marschall, K. Hermann, A. Nefedov, C. Wöll, and J. V. Barth, J. Chem. Phys. **136**, 014705 (2012).
[18]M. Stark, S. Ditze, M. Drost, F. Buchner, H.-P. Steinrück, and H. Marbach, Langmuir **29**, 4104 (2013).
[19]T. A. Jung, R. R. Schlittler, and J. K. Gimzewski, Nature **386**, 696 (1997).
[20]T. E. Shubina, H. Marbach, K. Flechtner, A. Kretschmann, N. Jux, F. Buchner, H.-P. Steinrück, T. Clark, and J. M. Gottfried, J. Am. Chem. Soc. **129**, 9476 (2007).
[21]F. Buchner, K. Comanici, N. Jux, H.-P. Steinrück, and H. Marbach, J. Phys. Chem. C **111**, 13531 (2007).
[22]F. Buchner, V. Schwald, K. Comanici, H.-P. Steinrück, and H. Marbach, ChemPhysChem **8**, 241 (2007).
[23]F. Buchner, K. Seufert, W. Auwärter, D. Heim, J. V. Barth, K. Flechtner, J. M. Gottfried, H.-P. Steinrück, and H. Marbach, ACS Nano **3**, 1789 (2009).
[24]W. Auwärter, A. Weber-Bargioni, A. Riemann, A. Schiffrin, O. Gröning, R. Fasel, and J. V. Barth, J. Chem. Phys. **124**, 194708 (2006).
[25]J. Brede, M. Linares, S. Kuck, J. Schwöbel, A. Scarfato, S. H. Chang, G. Hoffmann, R. Wiesendanger, R. Lensen, P. H. J. Kouwer, J. Hoogboom, A. E. Rowan, M. Bröring, M. Funk, S. Stafström, F. Zerbetto, and R. Lazzaroni, Nanotechnology **20**, 275602 (2009).
[26]Y. Bai, F. Buchner, M. T. Wendahl, I. Kellner, A. Bayer, H.-P. Steinrück, H. Marbach, and J. M. Gottfried, J. Phys. Chem. C **112**, 6087 (2008).
[27]M. I. Veld, P. Iavicoli, S. Haq, D. B. Amabilino, and R. Raval, Chem. Commun. 1536 (2008).
[28]T. Sasaki, A. J. Osgood, J. L. Kiappes, K. F. Kelly, and J. M. Tour, Org. Lett. **10**, 1377 (2008).
[29]M. Koepf, J. A. Wytko, J. P. Bucher, and J. Weiss, J. Am. Chem. Soc. **130**, 9994 (2008).
[30]F. Klappenberger, A. Weber-Bargioni, W. Auwärter, M. Marschall, A. Schiffrin, and J. V. Barth, J. Chem. Phys. **129**, 214702 (2008).
[31]J. Xiao, S. Ditze, M. Chen, F. Buchner, M. Stark, M. Drost, H.-P. Steinrück, J. M. Gottfried, and H. Marbach, J. Phys. Chem. C **116**, 12275 (2012).
[32]T. Kumagai, F. Hanke, S. Gawinkowski, J. Sharp, K. Kotsis, J. Waluk, M. Persson, and L. Grill, Nat. Chem. **6**, 41 (2014).
[33]T. Kumagai, F. Hanke, S. Gawinkowski, J. Sharp, K. Kotsis, J. Waluk, M. Persson, and L. Grill, Phys. Rev. Lett. **111**, 246101 (2013).
[34]W. Brenner, J. Malig, C. Oelsner, D. M. Guldi, and N. Jux, J. Porphyrins Phthalocyanines **16**, 651 (2012).
[35]E. Vogel, M. Kocher, H. Schmickler, and J. Lex, Angew. Chem., Int. Ed. Engl **25**, 257 (1986).
[36]S. Nonell, N. Bou, J. I. Borrell, J. Teixidò, A. Villanueva, A. Juarranz, and M. Canete, Tetrahedron Lett. **36**, 3405 (1995).
[37]M. Suzuki, M. Miyoshi, and K. Matsumoto, J. Org. Chem. **39**, 1980 (1974).
[38]J. B. Paine and D. Dolphin, J. Org. Chem. **53**, 2787 (1988).
[39]I. Horcas, R. Fernández, J. M. Gómez-Rodríguez, J. Colchero, J. Gómez-Herrero, and A. M. Baro, Rev. Sci. Instrum. **78**, 013705 (2007).
[40]H. Yanagi, H. Mukai, K. Ikuta, T. Shibutani, T. Kamikado, S. Yokoyama, and S. Mashiko, Nano Lett. **2**, 601 (2002).
[41]G. Rojas, X. Chen, C. Bravo, J. H. Kim, J. S. Kim, J. Xiao, P. A. Dowben, Y. Gao, X. C. Zeng, W. Choe, and A. Enders, J. Phys. Chem. C **114**, 9408 (2010).
[42]M. Röckert, S. Ditze, M. Stark, J. Xiao, H.-P. Steinrück, H. Marbach, and O. Lytken, J. Phys. Chem. C **118**, 1661 (2013).
[43]M. O. Sinnokrot and C. D. Sherrill, J. Phys. Chem. A **110**, 10656 (2006).
[44]E. G. Cox, D. W. J. Cruickshank, and J. A. S. Smith, Proc. R. Soc. London, Ser. A **247**, 1–21 (1958).
[45]S. K. Burley and G. A. Petsko, Science **229**, 23 (1985).
[46]S. Ditze, M. Stark, F. Buchner, A. Aichert, N. Jux, N. Luckas, A. Görling, W. Hieringer, J. Hornegger, H.-P. Steinrück, and H. Marbach, J. Am. Chem. Soc. **136**, 1609 (2014).
[47]M. Stark, S. Ditze, M. Lepper, L. Zhang, H. Schlott, F. Buchner, M. Röckert, M. Chen, O. Lytken, H.-P. Steinrück, and H. Marbach, Chem. Commun. **50**, 10225 (2014).
[48]S. Ditze, M. Stark, M. Drost, F. Buchner, H.-P. Steinrück, and H. Marbach, Angew. Chem., Int. Ed. **51**, 10898 (2012).

P3

ChemComm

COMMUNICATION

View Article Online
View Journal | View Issue

Cite this: *Chem. Commun.*, 2014, **50**, 10225

Received 15th May 2014,
Accepted 13th July 2014

DOI: 10.1039/c4cc03708a

www.rsc.org/chemcomm

Massive conformational changes during thermally induced self-metalation of 2*H*-tetrakis-(3,5-di-*tert*-butyl)-phenylporphyrin on Cu(111)†

M. Stark, S. Ditze, M. Lepper, L. Zhang, H. Schlott, F. Buchner,‡ M. Röckert, M. Chen,§ O. Lytken, H.-P. Steinrück and H. Marbach*

Based on a combined scanning tunnelling microscopy and X-ray photoelectron spectroscopy study we present detailed insights into pronounced changes of long-range order and intramolecular conformation during the self-metalation of 2*H*-5,10,15,20-tetrakis-(3,5-di-*tert*-butyl)-phenylporphyrin (2HTTBPP) to CuTTBPP on Cu(111). Upon metalation, the porphyrin literally "pops up" from the surface, due to a drastically reduced molecule–substrate interaction.

A detailed understanding of the adsorption behaviour of molecular building blocks on solid surfaces is a crucial step towards the bottom-up fabrication of functional devices.[1,2] Scanning tunnelling microscopy (STM) is an especially suitable method to study the relevant elementary processes. Porphyrins are regarded as prototype functional molecular building blocks for nanotechnology applications. Recent surface science studies of porphyrins addressed their switching capabilities[3–5] and adsorption behaviour as well as surface-mediated metalation of free base porphyrins.[6] The metalation can occur with predeposited and postdeposited metal atoms, or *via* the so-called self-metalation with atoms from an underlying metal substrate.[7–10] Thereby, the free base porphyrin picks up a substrate atom and reacts to the corresponding metalloporphyrin with the release of hydrogen. Herein, we report on the self-metalation of 2HTTBPP on Cu(111), which goes along with a massive intramolecular conformational change due to reduced molecule–substrate interactions. In a vivid image, this process can be summarized as a popping up of the molecular centre from the surface.

The investigation of free base porphyrins on single crystal Cu surfaces recently received great interest, mainly due to the very strong attractive interactions of the iminic nitrogen atoms of the porphyrin macrocycle with Cu atoms from the substrate.[11–15] This interactions can give rise to very peculiar adsorption behaviours like the one observed by STM for 2HTTBPP on Cu(111), see Fig. 1a. The corresponding supramolecular structure exhibits a bimodal appearance, *i.e.* alternating bright and dark rows, which (predominantly) consist of convex and concave intramolecular conformations, respectively (see also Fig. 3a–h and discussion below).[4]

Upon heating, the bimodal supramolecular arrangement undergoes massive transformations, as depicted in Fig. 1b–d. Fig. 1b represents a transient situation after 10 minutes heating at 330 K, *i.e.* the onset of the formation of a monomodal supramolecular structure, in the following referred to as hex A. The most apparent change on the molecular level is the appearance of pronounced protrusions, which occur pairwise and increase in number with increasing heating time. In Fig. 1b, the bimodal structure is still dominating, while only very few of the peculiar protrusions are formed, preferentially at dislocations of the row structure. A fully developed hex A structure is depicted in Fig. 1c; this structure can be achieved either by prolonged heating at 330 K or by heating for 2 minutes at 360 K. After heating the sample to 450 K for 2 minutes the molecular arrangements again changes significantly and the whole surface is now covered with the structure depicted in Fig. 1d, which is referred to as hex B.

In the following, we address the origin of this thermally induced transformation from the bimodal structure into the hex A and hex B arrangements. In previous studies of different free base porphyrins on Cu surfaces, the so called self-metalation reaction was observed.[7–10] For example, on Cu(111) 2*H*-tetraphenylporphyrin (2HTPP) reacts with Cu surface atoms to CuTPP, at temperatures as low as ~390 K.[8] Therefore, one can anticipate that a similar reaction occurs for the here investigated 2HTTBPP. To find out, whether such a reaction occurs, we performed X-ray photoelectron spectroscopy (XPS). The corresponding N 1s spectra in Fig. 2 indeed evidence that the 2HTTBPP reacts to CuTTBPP: 2HTTBPP has two non-equivalent nitrogen atoms (iminic and aminic), yielding two clearly distinguishable N 1s peaks, as is evident from Fig. 2 (bottom). After heating the sample to 450 K for 2 minutes, the spectrum shows only one

Lehrstuhl für Physikalische Chemie II, Egerlandstrasse 3 and Interdisciplinary Center for Molecular Materials (ICMM), Universität Erlangen-Nürnberg, D-91058 Erlangen, Germany. E-mail: hubertus.marbach@fau.de

† Electronic supplementary information (ESI) available. See DOI: 10.1039/c4cc03708a

‡ Present address: Helmholtz Institut Ulm and Institut für Oberflächenchemie und Katalyse, Universität Ulm, Albert-Einstein Allee 11, D-89081 Ulm, Germany.

§ Present address: Fachbereich Chemie, Physikalische Chemie, Philipps-Universität Marburg, Hans-Meerwein-Straße 6, D-35032 Marburg, Germany.

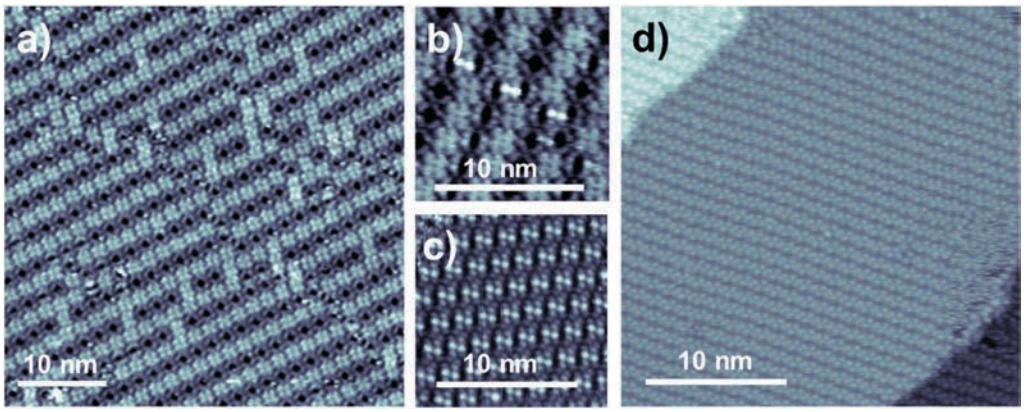

Fig. 1 Constant current RT STM images of ordered islands of a submonolayer of 2HTTBPP on Cu(111) prepared at RT, after different heat treatments: (a) bimodal appearance observed for the as prepared layer (U = +1.3 V, I = 30 pA); (b) transition phase from bimodal to monomodal hex A phase after heating for 10 minutes at 330 K (U = +1.3 V, I = 30 pA); (c) fully developed hex A phase after heating for 2 minutes at 360 K (U = +1.8 V, I = 30 pA); (d) representing monomodal hex B phase (U = −1.8 V, I = 30 pA).

peak (top spectrum), which is characteristic for the metalized porphyrin, CuTTBPP, in which all four nitrogen atoms are equally coordinated to a central Cu atom. In addition, we show two spectra after heating to lower temperatures (350 K for 210 min, and 400 K for 30 min). In these spectra, contributions from both, 2HTTBPP and CuTTBPP, are seen, and from the relative intensities the corresponding degrees of metalation can be determined, by using a fitting procedure. Comparison of the XPS data with the STM data yields the conclusion that the hex B structure consists of CuTTBPP. For the preparation conditions of the partially metalated situations shown in Fig. 2, we always observe coexisting domains in STM, in which the surface ratio covered with hex B molecules roughly resembles the degree of metalation determined in XPS.

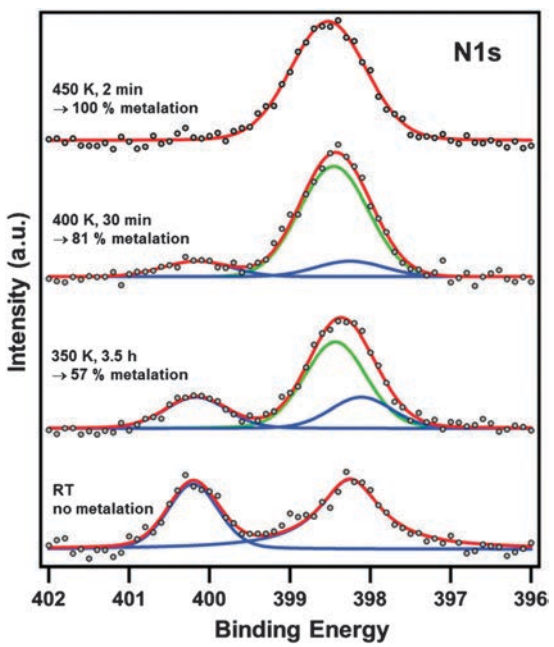

Fig. 2 N 1s XP spectra of 2HTTBPP on Cu(111), for the as prepared layer (bottom) and after the indicated heat treatments; the topmost spectrum corresponds to fully metalated CuTTBPP.

To further shed light on the nature of the observed supramolecular structures, high resolution STM micrographs of individual porphyrins were acquired and analysed. In Fig. 3, the molecular arrangements are depicted (left), along with micrographs of corresponding individual porphyrins within the arrangements with submolecular resolution (center), and the extracted intramolecular conformations (right). The conformational flexibility of TTBPP species on different substrates is well known and was reported before.[16–20] From the inspection of Fig. 3, it becomes immediately apparent that the different supramolecular arrangements go along with different intramolecular conformations. It is well established that the appearance of the individual molecules in STM is dominated by the four upper *tert*-butyl groups,[16–19] which form a rectangle as indicated in Fig. 3d, g, l and q. From the lengths of the two sides s and l of these rectangles, the intramolecular conformations can be extracted using the perimeter and aspect ratio of the latter, according to a procedure described elsewhere[4,16] (A sketch visualizing this procedure and additional information is provided in the ESI†). In a simplified model, the conformation of a molecule is described by twisting and/or tilting the phenyl rings with respect to the porphyrin plane; the corresponding twist angle is denoted as θ and the tilt angle as ϕ.[16] The full set of parameters for the supramolecular arrangements is given in Table 1. In addition the two intramolecular conformations in the bimodal phase were confirmed by STM simulations based on DFT calculations of the electronic structure.[4]

The bimodal structure in Fig. 3a was recently investigated in great detail by Ditze *et al.*: the intramolecular conformation with $\theta = 5 \pm 5^\circ$ and $\phi = 35 \pm 5^\circ$ resembles the shape of a bowl, which can either occur standing "upright" on the surface (Fig. 3c–e, concave conformation) or upside down (Fig. 3f–h, convex conformation). The supramolecular order is formed by alternating rows of molecules in the concave and convex conformations. While the concave conformation is in line with a strong attractive interaction of the iminic nitrogen atoms with the Cu substrate, the convex conformation is stabilized by entropic effects. This was derived from studying the thermally induced reversible conformational switching of 2HTTBPP in

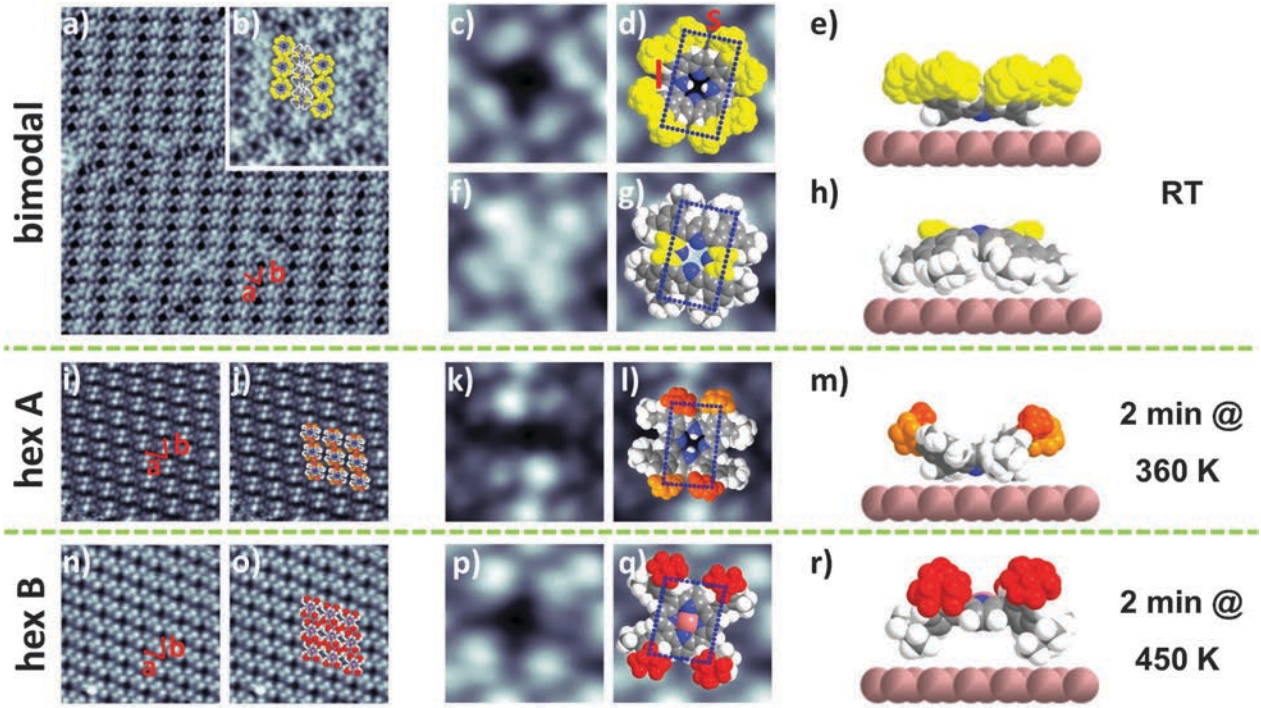

Fig. 3 Overview of the observed supramolecular porphyrin phases and the derived molecular models on Cu(111): (a–h) bimodal phase of 2HTTBPP as prepared at room temperature. (i–m) hex A phase of 2HTTBPP after heating to 360 K for 2 minutes. (n–r) representing hex B phase of CuTTBPP after thermally induced metalation reaction. The scanning parameters are: (a) U = +1.3 V, I = 30 pA; (b–g) U = +1.8 V, I = 25 pA; (i–q), U = +1.8 V, I = 30 pA; (a) 35.0 × 35.0 nm^2; (b, i, j, n, o) 13.5 × 13.5 nm^2; (c, d, f, g, k, l, p, q) 2.5 × 2.5 nm^2.

Table 1 Overview of the supramolecular and intramolecular geometrical values, as extracted from STM data; *a, b*: lattice parameters, α: angle between lattice vectors, ρ: molecular density, s_{exp} and l_{exp} experimentally determined s and l values, s_{mod} and l_{mod} s and l values of the used models, θ: the twist angle of the phenyl groups, ϕ: the corresponding tilt angle

Phase ↓	a [nm]	b [nm]	α [°]	ρ [molecules per nm^2]	s_{exp} [nm]	l_{exp} [nm]	s_{mod} [nm]	l_{mod} [nm]	θ [°]	ϕ [°]
Bimodal	1.90 ± 0.10	2.00 ± 0.06	60 ± 5	0.30	0.70 ± 0.1	1.25 ± 0.1	0.72	1.34	5 ± 5	35 ± 5
hex A	1.75 ± 0.10	1.92 ± 0.10	68 ± 5	0.32	0.57 ± 0.1	1.07 ± 0.1	0.69	1.07	35/10 ± 5	35 ± 5
hex B	1.81 ± 0.10	1.85 ± 0.05	60 ± 5	0.35	0.87 ± 0.05	1.12 ± 0.05	0.85	1.10	75 ± 5	5 ± 5

the bimodal structure.[4] Upon moderate heating, the bimodal structure transforms into the monomodal hex A structure (Fig. 3i), *i.e.* all molecules exhibit the same intramolecular conformation (Fig. 3k–m), and appear static, *i.e.* they do not show any thermally induced switching. For this conformation the position of the macrocycle is very similar to the concave conformation. The main difference between these two conformations is that the four phenyl rings are significantly twisted out of the porphyrin plane ($\theta = 35 \pm 5^\circ$) for hex A. From the close proximity of the porphyrin macrocycle to the Cu substrate (Fig. 3m) and the information from XPS that the porphyrin is not yet metalated in hex A, we conclude that the strong attractive interaction of the iminic nitrogen atoms of the free base porphyrin causes this conformation. In addition, the upper *tert*-butyl groups from the phenyl rings with the larger twist angle ($\theta = 35 \pm 5^\circ$, indicated in red in Fig. 3j, l and m) are arranged such, that they are in close proximity to their likes of molecules in the neighboring rows (Fig. 3i–k). As a consequence, the corresponding protrusions from two neighboring molecules appear with a dumbbell shape. This close proximity, together with the increased molecular density (bimodal: ρ = 0.30 molecules per nm^2, hex A: ρ = 0.32 molecules per nm^2), indicate an additional stabilizing contribution from the attractive interaction between the corresponding side groups. This interpretation is confirmed by the observations of the onset of the hex A formation (Fig. 1b), which is the formation of the pairwise protrusions between neighboring concave molecules at dislocations in the bimodal structure, already after 10 minutes at 330 K. Taking the irreversibility of the conformational change from bimodal to hex A into account, it appears that the hex A structure is energetically favorable over the bimodal arrangement, but has to overcome some activation barrier in order to be formed.

Upon further heating, the hex A structure transforms into the hex B structure, as shown in Fig. 1d and Fig. 3n and o. From the XPS data, it is evident that the free base porphyrin is transformed to CuTTBPP in the hex B arrangement. The intramolecular conformation drastically changes to a situation where the center of the porphyrin with the coordinated Cu atom is now significantly lifted above the Cu(111) surface. This interpretation is also supported by a shift of the C 1s peak in

XPS to higher binding energies, in agreement with a reduced final state screening as the molecule moves away from the surface (see Fig. S3 in ESI†). Consequently, the twist angle $\theta = 75 \pm 5^{\circ}$ changed such that the phenyl rings are almost perpendicular to the porphyrin macrocycle. At the same time, the tilt angle is also significantly reduced to $\phi = 5 \pm 5^{\circ}$. This modified molecular conformation obviously allows for attractive interactions between the side groups of neighboring CuTTBPPs, as judged by the close proximity of the corresponding protrusions (Fig. 3n and o) and the again increased molecular density of $\rho = 0.35$ molecules per nm^2. Overall, the intramolecular conformation in hex B is very similar to the one expected for the isolated molecule in the gas phase ($\theta = 70$; $\phi = 0$).[20] Obviously, the strong attractive interaction of 2HTTBPP with the substrate is almost completely switched off by the insertion of the Cu atom. As a consequence, the central part of the molecule literally pops up from the surface, resulting in a very different intramolecular conformation. In a vivid picture, the 2HTTBPP in the hex A phase behaves almost like a loaded spring which is hold by the strong attractive interactions of the iminic nitrogens with the Cu substrate and is released upon metalation.

In summary, we gained detailed insights into the thermally induced morphological and chemical transformations of 2HTTBPP on Cu(111). Starting at $\sim$330 K, the initially bimodal supramolecular structure changes to the monomodal hex A arrangement with reduced intramolecular symmetry. At higher temperatures and/or prolonged heating times, 2HTTBPP undergoes a metalation reaction with Cu substrate atoms to form CuTTBPP in the hex B phase. The observed massive structural change can be conclusively explained by reduced molecule–substrate interactions after metalation.

This work was funded by the German Research Council (DFG) through research unit FOR 1878/funCOS and the Cluster of Excellence 'Engineering of Advanced Materials' granted to the FAU Erlangen-Nürnberg.

Notes and references

1 J. V. Barth, G. Costantini and K. Kern, *Nature*, 2005, **437**, 671–679.
2 S. de Feyter and F. C. de Schryver, *Chem. Soc. Rev.*, 2003, **32**, 139.
3 W. Auwärter, K. Seufert, F. Bischoff, D. Écija, S. Vijayaraghavan, S. Joshi, F. Klappenberger, N. Samudrala and J. V. Barth, *Nat. Nanotechnol.*, 2012, **7**, 41–46.
4 S. Ditze, M. Stark, F. Buchner, A. Aichert, N. Jux, N. Luckas, A. Görling, W. Hieringer, J. Hornegger, H.-P. Steinrück and H. Marbach, *J. Am. Chem. Soc.*, 2014, **136**, 1609.
5 T. Kumagai, F. Hanke, S. Gawinkowski, J. Sharp, K. Kotsis, J. Waluk, M. Persson and L. Grill, *Nat. Chem.*, 2014, **6**, 41.
6 J. M. Gottfried and H. Marbach, *Z. Phys. Chem.*, 2009, **223**, 53.
7 K. Diller, F. Klappenberger, M. Marschall, K. Hermann, A. Nefedov, C. Woll and J. V. Barth, *J. Chem. Phys.*, 2012, **136**, 014705.
8 S. Ditze, M. Stark, M. Drost, F. Buchner, H.-P. Steinrück and H. Marbach, *Angew. Chem., Int. Ed.*, 2012, **51**, 10898.
9 M. Röckert, S. Ditze, M. Stark, J. Xiao, H.-P. Steinrück, H. Marbach and O. Lytken, *J. Phys. Chem. C*, 2014, **118**, 1661–1667.
10 R. González-Moreno, C. Sánchez-Sánchez, M. Trelka, R. Otero, A. Cossaro, A. Verdini, L. Floreano, M. Ruiz-Bermejo, A. García-Lekue, J. Á. Martín-Gago and C. Rogero, *J. Phys. Chem. C*, 2011, **115**, 6849–6854.
11 M. Eichberger, M. Marschall, J. Reichert, A. Weber-Bargioni, W. Auwärter, R. L. C. Wang, H. J. Kreuzer, Y. Pennec, A. Schiffrin and J. V. Barth, *Nano Lett.*, 2008, **8**, 4608.
12 F. Buchner, J. Xiao, E. Zillner, M. Chen, M. Röckert, S. Ditze, M. Stark, H.-P. Steinrück, J. M. Gottfried and H. Marbach, *J. Phys. Chem. C*, 2011, **115**, 24172.
13 C. M. Doyle, S. A. Krasnikov, N. N. Sergeeva, A. B. Preobrajenski, N. A. Vinogradov, Y. N. Sergeeva, M. O. Senge and A. A. Cafolla, *Chem. Commun.*, 2011, **47**, 12134.
14 G. Rojas, X. Chen, C. Bravo, J. H. Kim, J. S. Kim, J. Xiao, P. A. Dowben, Y. Gao, X. C. Zeng, W. Choe and A. Enders, *J. Phys. Chem. C*, 2010, **114**, 9408.
15 S. Haq, F. Hanke, M. S. Dyer, M. Persson, P. Iavicoli, D. B. Amabilino and R. Raval, *J. Am. Chem. Soc.*, 2011, **133**, 12031.
16 F. Buchner, K. Comanici, N. Jux, H.-P. Steinrück and H. Marbach, *J. Phys. Chem. C*, 2007, **111**, 13531.
17 T. A. Jung, R. R. Schlittler and J. K. Gimzewski, *Nature*, 1997, **386**, 696.
18 F. Moresco, G. Meyer, K. H. Rieder, H. Tang, A. Gourdon and C. Joachim, *Phys. Rev. Lett.*, 2001, **86**, 672.
19 F. Moresco, G. Meyer, K. H. Rieder, J. Ping, H. Tang and C. Joachim, *Surf. Sci.*, 2002, **499**, 94–102.
20 T. Wölfle, A. Görling and W. Hieringer, *Phys. Chem. Chem. Phys.*, 2008, **10**, 5739.

Electronic Supplementary Material (ESI) for ChemComm.

Massive conformational changes during thermally induced self-metalation of 2H-Tetrakis-(3,5-di-tert-butyl)-phenylporphyrin on Cu(111)

M. Stark,[a] S. Ditze,[a] M. Lepper,[a] L. Zhang,[a] H. Schlott,[a] F. Buchner,[a, b] M. Röckert,[a] M. Chen [a, c], O. Lytken,[a] H.-P.Steinrück,[a] and H. Marbach[a, *]

[a] Lehrstuhl für Physikalische Chemie II, Egerlandstrasse 3 and Interdisciplinary Center for Molecular Materials (ICMM), Universität Erlangen-Nürnberg, D-91058 Erlangen, Germany.

[b] Present address: Helmholtz Institut Ulm and Institut für Oberflächenchemie und Katalyse, Universität Ulm, Albert-Einstein Allee 11, D-89081 Ulm, Germany.

[c] Present address: Fachbereich Chemie, Physikalische Chemie, Philipps-Universität Marburg, Hans-Meerwein-Straße 6, D-35032 Marburg, Germany.

* Correspondence to: Hubertus Marbach, email: hubertus.marbach@fau.de

Supporting Information

Determination of the internal conformation of 2HTTBPP on Cu(111)

The appearance of TTBPP molecules is usually dominated by the peripheral tert-butyl groups such that four of them form a rectangle. The geometric shape of the rectangle (perimeter and aspect ratio of long to short side) can be used to determine the intramolecular conformation of the molecules based on the geometric considerations shown in Fig. S2. A detailed description of the estimation procedure can be found in[1].

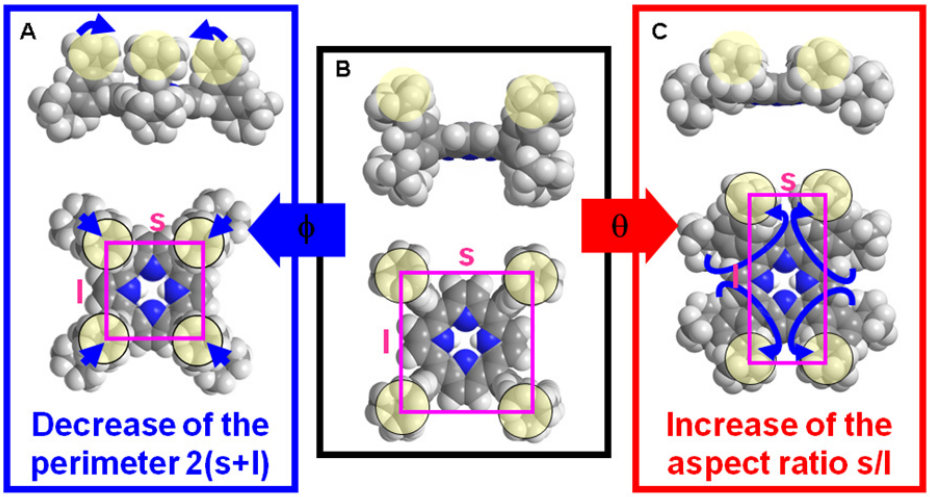

Figure S1: Scheme on how the intramolecular conformation 2HTTBPP (given by the twist angle θ and tilt angle ϕ of the peripheral phenyl groups) determines the geometry of a rectangle (purple) formed by four tert-butyl groups (yellow circles). (**B**) side view and top view of a space filling model of 2HTTBPP with the phenyl group oriented perpendicular to the plane of the poprhyrin macrocycle (twist angle θ = 90°, tilt angle ϕ = 0°). In (**C**), a possible molecular deformation is shown, with the phenyl groups rotated out of the porphyrin macrocycle plane (twist angle θ > 0°). Thereby, the quadratic arrangment of the upper tert-butyl groups (indicated by a yellow circle) changes to a rectangle, which effectively changes the aspect ratio, s/l, of the short and long sides of the rectangle. In (**A**), the phenyl groups are tilted upwards out of the plane of the poprhyrin macrocycle (tilt angle ϕ > 0°). Thereby, the distance between the upper tert-butyl groups is reduced, resulting in a decreased perimeter, 2(s+l), of the corresponing rectangle. By comparing the experimental values s_{exp} and l_{exp} extracted from high-resolution STM images with the values s_{mod} and l_{mod} measured from corresponding space filling models (CambridgeSoft, Chem3D Pro 12.0.2.1076) an estimation of twist and tilt angle is possible.

Reference

(1) Buchner, F.; Comanici, K.; Jux, N.; Steinrück, H.-P.; Marbach, H. *J. Phys. Chem. C* **2007**, *111*, 13531.

Bias voltage dependence of STM of 2HTTBPP and CuTTBPP on Cu(111)

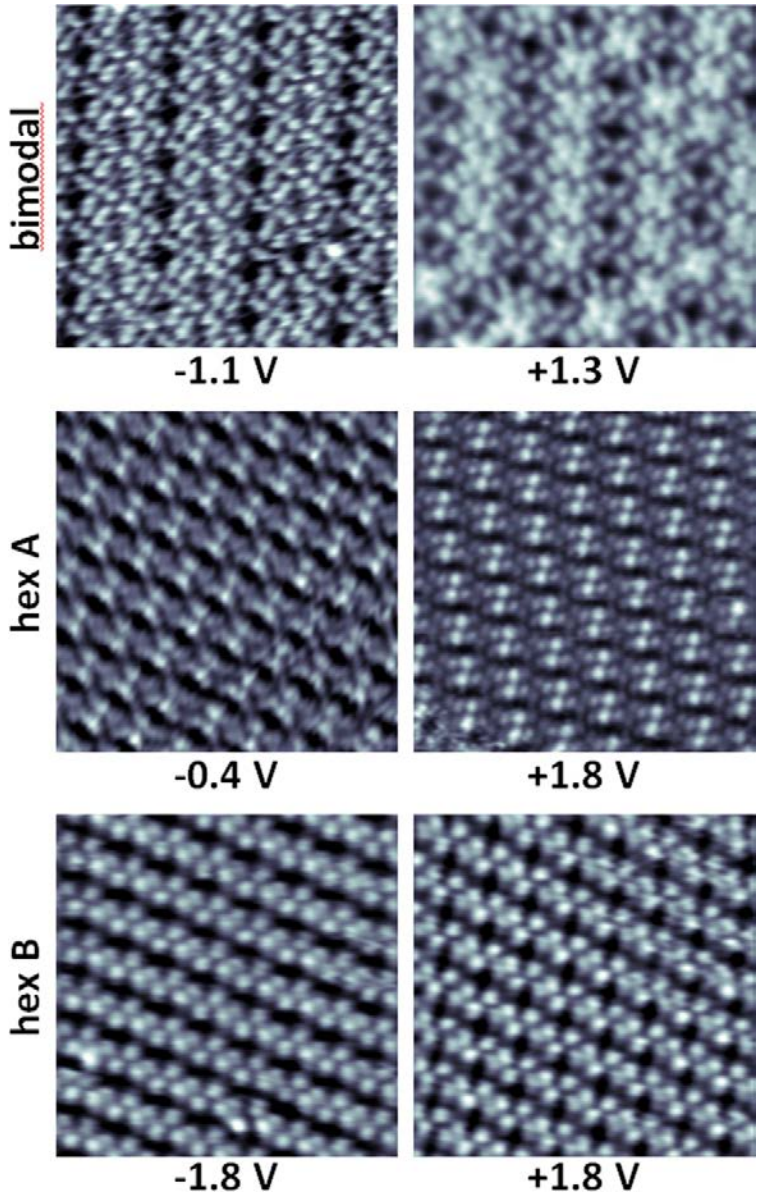

Figure S2: Set of images of bimodal, *hexA* and *hexB* domains at positive and negative bias. The appearance of the molecules is due to their upper tert-butyl groups and thus to a large extent independent of the bias voltage. All images were acquired in constant current mode with a tunneling current of 30 pA.

C 1s XP spectra

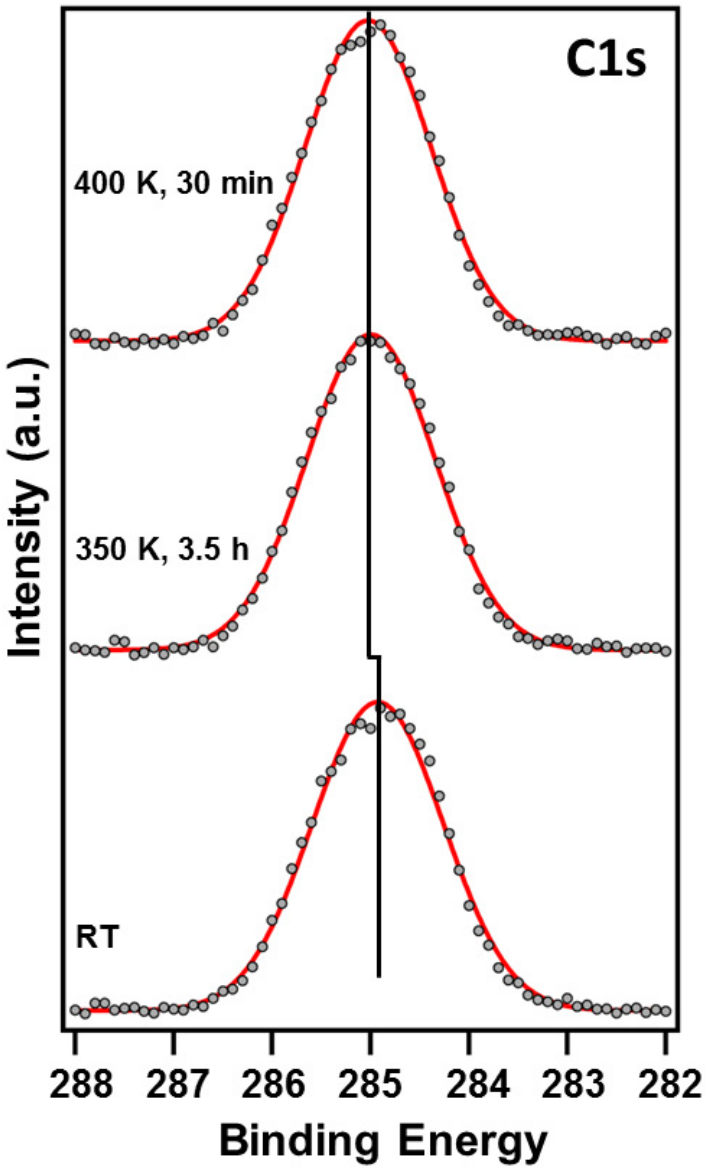

Figure S3: C 1s XP spectra of 2HTTBPP on Cu(111) for the as prepared layer (bottom) and after the indicated heat treatments; the topmost spectrum corresponds to almost fully metalated CuTTBPP (81 %, see Fig. 2). Upon metalation of 2HTTBPP, the C 1s peak shifts slightly by 0.1 eV to higher binding energies, in agreement with a reduced final state screening as the molecule moves away from the surface. The shift is accompanied by a slight narrowing of the FWHM from 1.57 to 1.51 eV.

P4

Surface Science xxx (2015) xxx–xxx

Contents lists available at ScienceDirect

Surface Science

journal homepage: www.elsevier.com/locate/susc

Reversible thermally induced phase transition in ordered domains of Co(II)-5,10,15,20-tetrakis-(3,5-di-*tert*-butylphenyl)-porphyrin on Cu(111)

Michael Stark [a,b], Stefanie Ditze [a,b], Michael Thomann [a,b], Dominik Lungerich [b,c], Norbert Jux [b,c], Hans-Peter Steinrück [a,b], Hubertus Marbach [a,b,*]

[a] Lehrstuhl für Physikalische Chemie II, Universität Erlangen-Nürnberg, Egerlandstr. 3, 91058 Erlangen, Germany
[b] Interdisciplinary Center for Molecular Materials (ICMM), Universität Erlangen-Nürnberg, Germany
[c] Lehrstuhl für Organische Chemie II, Universität Erlangen-Nürnberg, Henkestr. 42, 91054 Erlangen, Germany

ARTICLE INFO

Available online xxxx

Keywords:
Porphyrin
Scanning tunneling microscopy
Reversible phase transition
Self-assembly
Intramolecular conformation
Bias voltage dependence

ABSTRACT

We investigated the adsorption behavior of Co(II)-5,10,15,20-tetrakis-(3,5-di-*tert*-butylphenyl)-porphyrin (CoTTBPP) on Cu(111) by scanning tunneling microscopy (STM). At room temperature (RT), the coverage dependent adsorption behavior follows an expected scheme: at low coverage step decoration is found, which evolves into supramolecular domains with a hexagonal order at higher coverage. Interestingly, upon cooling the sample to 180 K the occurrence of a clearly distinguishable coexisting herringbone phase is observed. Upon heating to RT again, the herringbone phase vanishes. Thus a temperature dependent, fully reversible phase transition was observed. High resolution STM micrographs allow for the determination of the intramolecular conformations which are different for the two supramolecular arrangements. In addition, we studied the bias voltage dependent appearance of the molecule in STM and assigned a dominant contribution of the central Co at negative bias voltages close to the Fermi edge to the occupied d_z^2 orbital. Interestingly, the herringbone phase, which dominates at 180 K, exhibits a significantly higher molecular density than the monomodal hexagonal arrangement at RT, which is in line with the "normal" behavior of freezing substances.

1. Introduction

The self-assembly of molecular building blocks into highly ordered nanostructures on well-defined surfaces is a powerful approach towards the fabrication of novel functional materials with outstanding properties [1–9]. For such a bottom-up strategy, knowledge concerning the adsorption behavior of corresponding organic molecules on single-crystal metal surfaces is of fundamental importance. Therefore, this research area has become a fast growing field in surface science [2,5–7,10]. First, one gains insight into the interactions of large organic molecules and solid supports, which is a key issue for the development of functional interfaces and plays an essential role for the controlled fabrication of molecular architectures. Second, new ways open up to gain deeper insight into fundamental properties and functionalities of the utilized molecular building blocks. In this context, scanning tunneling microscopy (STM) has proven to be a powerful experimental tool [7,11–13].

One important group of organic molecules is porphyrins, which are main functional building blocks in many complex biomolecules in nature and also in technological applications, due to their versatile functionalities and distinct chemical and physical properties [14,15]. In this respect, the self-assembly of porphyrin derivatives on metal surfaces gained considerable attention, aiming to collect detailed information on their fundamental properties, like electronic structure, conformational flexibility, and inherent reactivity [4,15–28]. The adsorption behavior of porphyrins, concerning intramolecular conformation and supramolecular arrangement, strongly depends on the chemical nature and structure of the surface [5,20,29], the coverage [24], the temperature [4,27,30], the presence or absence of a metal center [4,21,31,32], and the peripheral side groups of the porphyrins [5,26,33,34]. The investigated porphyrins include tetraphenylporphyrins (TPPs) and tetrakis-(di-*tert*-butylphenyl)-porphyrins (TTBPPs), with a central metal ion (MTPP/MTTBPP) or without (2HTPP/2HTTBPP).

STM investigations of various MTPPs at room temperature (RT) basically found the same adsorption behavior for different surfaces, namely self-assembly into supramolecular square arrangements [18,20,29,35–41]. In contrast, TTBPP molecules exhibit a large variety of supramolecular arrangements, ranging from no long-range order (ZnTTBPP on Ag(100) [42]), square arrangements (PtTTBPP on Cu(100) [43], CuTTBPP on Au(110) and Cu(100) [5]) and close-packed hexagonal phases (2HTTBPP on Au(111) [44,45], 2HTTBPP and CuTTBPP on

* Corresponding author at: Lehrstuhl für Physikalische Chemie II, Universität Erlangen-Nürnberg, Egerlandstr. 3, 91058 Erlangen, Germany.
E-mail address: hubertus.marbach@fau.de (H. Marbach).

http://dx.doi.org/10.1016/j.susc.2015.11.024
0039-6028/

Cu(111) [31]) to a herringbone arrangement (CuTTBPP on Cu(111) [46]). A previous, closely related STM study of CoTTBPP on Ag(111) reported a variety of four different, partially coexisting structures, with different intramolecular conformations and supramolecular arrangements [33]. In that study, a hexagonal arrangement was found to be the energetically favorable structure in the submonolayer range upon deposition at RT, while upon heating a multilayer to elevated temperatures a herringbone phase was found after cooling down to RT.

In most cases, a specific supramolecular long range order goes along with a corresponding specific intramolecular conformation. The latter can be described by the dihedral or so-called twist angle Θ around the C–C-bonds between the phenyl rings and the porphyrin macrocycle [5] and by the tilt angle Φ of the phenyl groups relative to the porphyrin plane [47], as indicated for CoTTBPP in Fig. 1. The appearance of an individual TTBPP molecule in constant current STM at positive bias voltages is dominated by the uppermost *tert*-butyl groups, which appear as four protrusions mainly reflecting the topography of the molecule [33,46,48,49]. For Θ values close to 0°, that is, when the phenyl rings are parallel to the surface, all eight *tert*-butyl groups are visible in the STM image, resulting in eight protrusions surrounding the center of the molecule [33,46,48,49]. The intramolecular conformation of the individual molecule on a surface is generally regarded as the result of the subtle interplay of different factors like the steric repulsion between the ortho-substituents and the porphyrin macrocycle, the interactions of the molecule with next neighbor molecules, and molecule–substrate interactions or particular surface features [5,45].

In this work, we present a detailed investigation of the self-assembly and temperature-dependent conformations of CoTTBPP on Cu(111) by STM. Our experimental results demonstrate that upon deposition at RT, CoTTBPP molecules self-assemble into extended supramolecular domains of hexagonal order. Interestingly, at reduced temperature (180 K) a large fraction of the ordered domains undergoes a fully reversible phase transition to a herringbone arrangement.

2. Experimental

The experiments were performed in a two chamber UHV system, at a background pressure in the low 10^{-10} mbar regime. The microscope is an RHK UHV VT STM 300 with RHK SPM 1000 electronics. The STM images were acquired, unless noted otherwise, at RT in constant current mode with a Pt/Ir tip. The given bias voltages refer to the sample. The STM images were processed with WSxM software and moderate filtering (Gaussian smooth, linear background subtraction along the fast scan direction) was applied for noise reduction [50]. The Cu(111) single crystal was prepared by repeated cycles of Ar^+ sputtering (500 eV) and annealing to 850 K. Co(II)-tetrakis(3,5-di-*tert*-butylphenyl) porphyrin was synthesized according to standard porphyrin synthesis protocols starting from commercially available 3,5-di-*tert*-butyl benzaldehyde with a metalation degree >95%. The preparation of the porphyrin layers was done in-situ via thermal sublimation from a home-built Knudsen cell onto the substrate held at room temperature. Prior to use, the porphyrin was degassed in vacuum for 24 h at 420 K. With the evaporator at 610 K, one monolayer was deposited in 20 min. The given unit cell parameters of the long-range ordered molecular arrangements (*a, b, α*) and the values characterizing the intramolecular conformation (*s, l*) are averaged over a multitude of measurements; the denoted errors are the corresponding standard deviations.

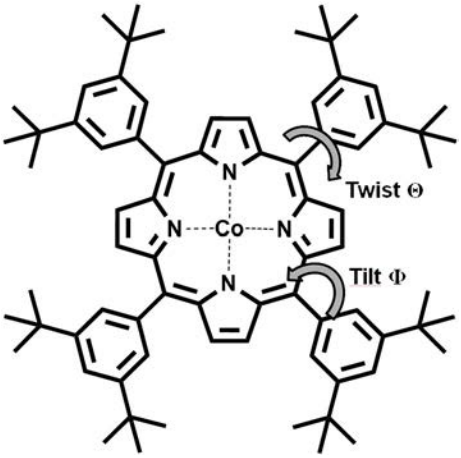

Fig. 1. Structure of CoTTBPP with tilt and twist deformations indicated.

3. Results & discussion

Upon deposition of CoTTBPP onto Cu(111) at RT, initially the step edges of the substrate are decorated with molecules. This can be explained by energetically favorable adsorption sites at the steps compared to the terraces due to the lower coordinated step atoms. Such a step decoration is shown in Fig. 2a. The actual adsorption structure can be seen best in the close-up in Fig. 2b, where one molecule appears with a central protrusion (caused by the d_z^2 orbital of the Co atom, see Fig. 5 and corresponding discussion below), surrounded by eight smaller protrusions, which are assigned to the eight *tert*-butyl groups (six are well visible, while the two on the lower side of the step are dim). The reduced intensity of the *tert*-butyl groups on the lower side of the step and the position of the Co atom right at the step edge suggest an adsorption site bridging the lower and the upper terrace [51].

On the terrace, indications for a so-called 2D gas phase are observed, which are the stripy, horizontal features along the fast scan direction in Fig. 2a, and also the elevated, noisy background in Fig. 2d. The 2D gas phase is formed by mobile molecules diffusing over the surface faster than the scanning speed of the STM tip. This observation indicates that the diffusion barrier on the terraces is small, that is, molecule–substrate interactions are not very site-specific and, therefore, individual molecules are not immobilized on the Cu(111) substrate at RT.

At higher coverages, we observe the formation of well-ordered supramolecular hexagonal arrangements, as shown in Fig. 2c and d. Since all molecular islands in a large number of STM images are in contact with at least one step edge (see e.g. lower right and top center left edges of the molecular island shown in Fig. 2d), we propose that the steps act as nucleation sites for the formation of the islands and contribute to the stabilization of the corresponding assemblies. Interestingly, some of the islands continue their long range order even across step edges (see Fig. 2c). For coverages up to one closed layer, all islands exhibit the same supramolecular hexagonal arrangement at RT (Fig. 2e). High resolution RT STM images of this hexagonal arrangement, partially overlaid with scaled CoTTBPP models, are depicted in Fig. 3a–d. At the given tunneling conditions (~1 V bias voltage), each molecule appears with a central depression surrounded by eight bright protrusions that are assigned to the eight *tert*-butyl groups of the molecule. The very similar intensity of all eight protrusions indicates a "flat" adsorption geometry of the molecule, with the plane of the phenyl substituents parallel or close to parallel to the surface. Upon close inspection, two less intense protrusions are visible in the center of the CoTTBPP, and are assigned to two upward bent pyrrole groups of the porphyrin core of the molecule. This observation is in line with a saddle-shaped distortion of the macrocycle, which is generally observed for phenyl meso-substituted porphyrin derivates [20,40,41,52,53].

By using a method described elsewhere [3,33], the intramolecular conformation of a TTBPP molecule, i.e. the tilt (Φ) out of the porphyrin plane and the twist (Θ) around the C–C-bond to the porphyrin core, can be determined for the di-*tert*-butylphenyl side-groups from the dimensions of the molecule in the STM images. In detail, that is, from the length *l* and width *s* of the rectangle that is formed by the brightest protrusions due to the topmost *tert*-butyl groups (cf. red rectangles in Fig. 3b and f); the latter are indicated in yellow in the space filling models in Fig. 3b, d, f, and h. The results are summarized in Table 1

Please cite this article as: M. Stark, et al., Reversible thermally induced phase transition in ordered domains of Co(II)-5,10,15,20-tetrakis-(3,5-di-tert-butylphenyl)-porphyrin..., Surf. Sci. (2015), http://dx.doi.org/10.1016/j.susc.2015.11.024

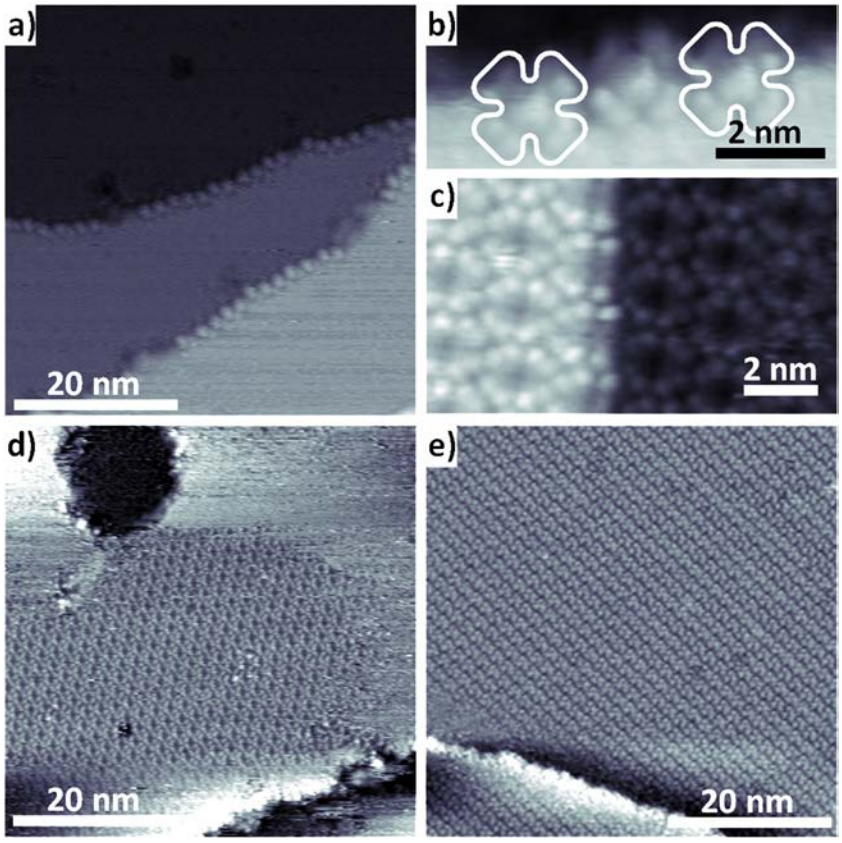

Fig. 2. Coverage dependent adsorption behavior of CoTTBPP on Cu(111): a) step decoration at low coverage (U = +1.03 V, I = 29 pA); b) close-up on three molecules decorating a step edge; the left and right molecules are indicated by the white frames (U = −0.4 V, I = 29 pA). c) close-up on a supramolecular arrangement pursuing over a step edge (U = +1.30, I = 36 pA). d) island formation at medium coverage (U = +1.22 V, I = 23 pA); e) completely covered surface at low resolution (U = +1.34 V, I = 35 pA).

and were used for the models overlaid in Fig. 3. The derived values for tilt and twist angles indicate that the molecule is almost completely flat; there is a small tilt angle of only 5° and a twist angle of only 10°. Although the visual interpretation of the STM image suggests a twist angle of 0°, height measurements of the *tert*-butyl groups (not shown) reveal that there is indeed a small height difference of about 10 ± 5 pm. This height difference reflects the pairwise counter-directional twisting of the side-groups of the molecule, i.e. neighboring side-groups are rotated in opposite directions. This is expected for a saddle shape-distorted molecule, due to the steric repulsion of the β- and *ortho*-hydrogen atoms.

As already discussed above, the molecule–substrate interactions for CoTTBPP are not site specific enough to immobilize individual molecules. Thus, the formation and stabilization of the supramolecular arrangements are proposed to be mainly driven by intermolecular interactions. From the scaled overlaid CoTTBPP models of the molecular arrangement shown in Fig. 3b, it is obvious that the *tert*-butyl groups of neighboring molecules are in close proximity. Therefore, we conclude that the interactions between neighboring molecules are mainly mediated via van der Waals forces between the *tert*-butyl groups. An illustration of the assumed interaction pattern is shown in the SI, Fig. S1.

Next, the structural evolution of CoTTBPP will be addressed: starting at RT, upon heating an almost closed CoTTBPP layer first a slight decrease in the total area covered by islands is observed, while at the same time the area associated to the 2D gas increases. Such a behavior is expected from simple thermodynamics due to an increased 2D vapor pressure. This process continues up to 440 K, where the molecular ordering is irreversibly destroyed. Most likely, dehydrogenation occurs at this temperature, which was reported to occur at similar temperatures for related systems [27,40,54]. Dehydrogenation usually starts at the sterically hindered positions, resulting in the formation of new C–C bonds while drastically changing the conformation of the molecule, no longer allowing for the mutual stabilization.

Surprisingly, upon cooling the sample to below 220 K a new supramolecular arrangement, that is, a herringbone structure forms, which coexists with the hexagonal between 180 and 220 K, as shown in Fig. 4b and d. Interestingly, the phase transition from hexagonal to herringbone arrangement upon cooling was found to be a reversible process, as documented in Fig. 4.

The ratio of both structures shifts towards the herringbone phase with reduced temperature: at ~180 K, the lowest achievable temperature in our experimental setup, 65 ± 5% of the supramolecular ordered area is in the herringbone phase, as deduced from a large number of STM images. Detailed STM images of the herringbone structure are shown in Fig. 3e–h. Again, under the given tunneling conditions, CoTTBPP appears as eight protrusions surrounding a central cavity. However, the intramolecular conformation of the molecules is clearly different from that in the hexagonal phase: While the twist angle of $\theta = 10°$ is similar, the tilt angle of $\Phi = 30°$ is much larger (c.f. Fig. 3d vs. h). This increase in tilt angle results in a smaller surface area per molecule and thus a higher molecular density (0.34 vs. 0.28 molecules/nm^2 for the hexagonal phase). The small twist angle of 10° could again be verified by an apparent height difference of 5 ± 4 pm of the associated *tert*-butyl groups. However, the central elongated protrusion at high negative bias voltage could not be observed for the herringbone conformation, suggesting that the porphyrin backbone forms a less pronounced or no saddle shape distortion. Indeed, DFT calculations for CoTTBPP on Ag(111) show a local minimum in the potential energy surface for the present combination of angles [55]. This calculated structure does not retain the saddle shaped distortion of the macrocycle, but forms a conformation, where all four pyrrole rings are tilted by 30° to

Please cite this article as: M. Stark, et al., Reversible thermally induced phase transition in ordered domains of Co(II)-5,10,15,20-tetrakis-(3,5-di-tert-butylphenyl)-porphyrin..., Surf. Sci. (2015), http://dx.doi.org/10.1016/j.susc.2015.11.024

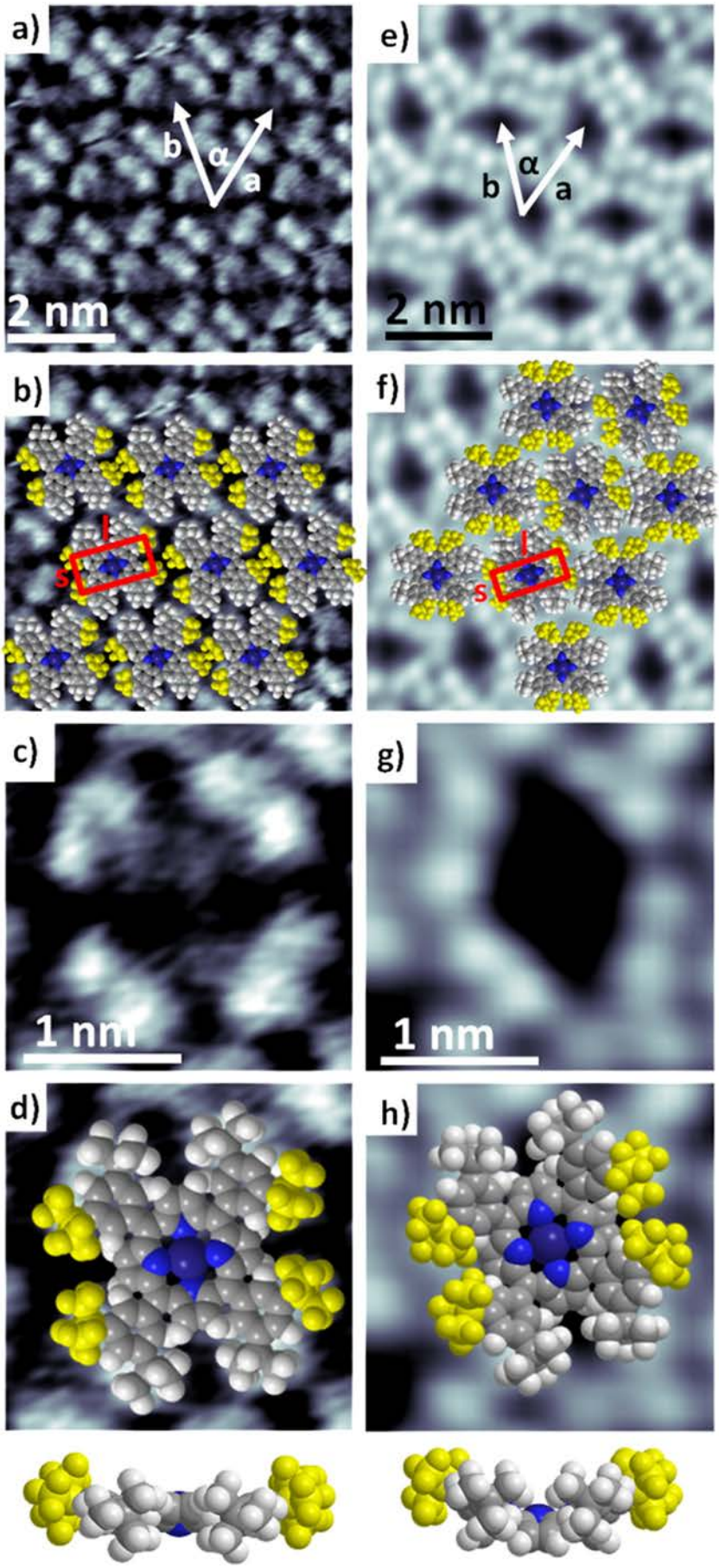

Please cite this article as: M. Stark, et al., Reversible thermally induced phase transition in ordered domains of Co(II)-5,10,15,20-tetrakis-(3,5-di-tert-butylphenyl)-porphyrin..., Surf. Sci. (2015), http://dx.doi.org/10.1016/j.susc.2015.11.024

Table 1
(Top) supramolecular and intramolecular geometrical values for the two arrangements on Cu(111), as extracted from STM data; a, b: lattice parameters of the unit cell, α: angle between lattice vectors, ρ: molecular density, l and s: experimentally determined values of the rectangle, formed by the four brightest protrusions in the STM image, θ: the twist angle of the phenyl groups, Φ: the corresponding tilt angle. (Bottom) for comparison, the corresponding parameter for Ag(111) is reproduced from reference [33].

Cu(111)	a [nm]	b [nm]	α [°]	ρ [Mol/nm^2]	l [nm]	s [nm]	θ [°]	Φ [°]
Hexagonal	1.97 ± 0.05	2.07 ± 0.05	59 ± 1	0.28	1.37 ± 0.05	0.70 ± 0.05	10	5
Herringbone	1.90 ± 0.06	1.77 ± 0.05	60 ± 1	0.34	1.25 ± 0.07	0.63 ± 0.06	10	30
Ag(111) [33]	a [nm]	b [nm]	α [°]	ρ [Mol/nm^2]	l [nm]	s [nm]	θ [°]	Φ [°]
Hexagonal (hex B)	1.89 ± 0.10	1.89 ± 0.10	60 ± 1	0.31	1.11 ± 0.07	0.70 ± 0.03	45	15
Herringbone	1.89 ± 0.05	1.89 ± 0.05	60 ± 1	0.31	1.31 ± 0.04	0.65 ± 0.04	20	5

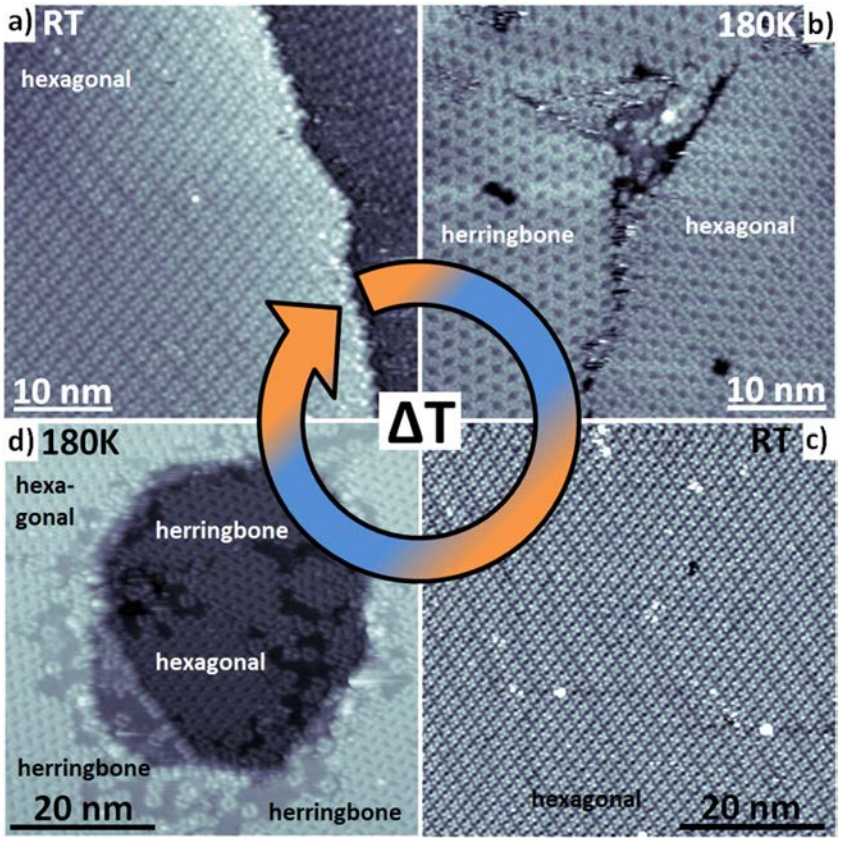

Fig. 4. STM images documenting the temperature dependent reversible phase transition of herringbone and hexagonal phase. (a) and (c): pure hexagonal phases recorded at RT (U = +1.30 V, I = 30 pA). (b) and (d): coexistence of hexagonal and herringbone phase recorded at 180 K (b) U = +1.26 V, I = 23 pA; d) U = −0.66 V, I = 29 pA).

one side of the molecule plane, while the *tert*-butylphenyl groups are tilted in the opposite direction.

The intermolecular interactions stabilizing the herringbone arrangement can be addressed via the overlaid space filling models in Fig. 3f and more detailed in Fig. S1c and d in the SI. Like for the hexagonal phase, the stabilization occurs via van der Waals interactions between the *tert*-butyl groups. However, the interaction pattern for the *tert*-butyl groups with neighboring molecules as shown in Fig. S1 in the SI suggests that the number of interactions per molecule (as deduced by counting the directly neighboring *tert*-butyl groups) varies for the two arrangements from 16 for the hexagonal to 20 for the herringbone arrangement. In addition, the average distance between these groups is reduced by ~1 Å for the herringbone arrangement compared to the hexagonal one, which is in line with the higher packing density. From the higher packing density (cf. Table 1), the larger number of interactions, and the lower formation temperature, we conclude that the herringbone arrangement is energetically favorable. In a thermodynamic picture, the larger (negative) entropic contribution at RT lowers the Gibbs free energy such that only the hexagonal phase forms at RT. Along the same lines, from a microscopic point of view, at room temperature, it is to be expected that a rotational motion of the *tert*-butyl groups is excited (e.g., see Gribble et al. [56]), that is, the *tert*-butyl groups are more or less freely rotating, which impedes a very dense packing. At low temperature, this rotation could be frozen, which would then allow for the formation of the more densely packed herringbone structure. This is in line with the rather fuzzy appearance of the

Fig. 3. High resolution STM images of the two observed arrangements at RT and at 180 K, demonstrating the different supramolecular ordering: a) hexagonal arrangement, b) overlaid with space filling models; c) single molecule of the hexagonal phase, d) overlaid with a space filling model and additional side view of the molecular conformation (a)–d): U = +1.31 V, I = 36 pA, T = RT). e) herringbone arrangement, f) overlaid with space filling models; g) single molecule of the herringbone phase, h) overlaid with a space filling model and additional side view of the molecular conformation (e)–h): U = +1.26 V, I = 23 pA, T = 180 K).

Please cite this article as: M. Stark, et al., Reversible thermally induced phase transition in ordered domains of Co(II)-5,10,15,20-tetrakis-(3,5-di-tert-butylphenyl)-porphyrin..., Surf. Sci. (2015), http://dx.doi.org/10.1016/j.susc.2015.11.024

molecules in the hexagonal phase at RT as depicted in the left column of Fig. 3, compared to the well-defined images of the herringbone phase at reduced temperature in the right column of Fig. 3.

When comparing the results for CoTTBPP on Cu(111) to those on Ag(111) [33], only two instead of four structures were found on Cu(111). Although the two structures have the same overall appearance (hexagonal and herringbone) on the two surfaces, there are significant differences concerning the size of the unit cell and the internal conformation, as is evident from Table 1, where in addition to the data for Cu(111) also the values for Ag(111) are reproduced from [33]. These differences are attributed to differences in the adsorbate–substrate interactions on Cu(111) and Ag(111). For the hexagonal conformation, the much smaller twist angle on Cu(111), that is 10° vs 45° on Ag(111) results in a distance of the CoTTBPP macrocycle to the substrate, which is about 1 Å smaller than on Ag(111); therefore one might deduce stronger attractive molecule–substrate interactions on Cu(111) than on Ag(111). Notably, the herringbone structure on Ag(111) was observed after deposition of multilayers of CoTTBPP followed by subsequent heating to elevated temperatures in order to obtain only a saturated monolayer. For the Ag(111) surface, no experiments below room temperature were performed in ref. [33] and thus no comparison of the temperature-induced changes is possible.

Finally, the bias voltage dependence of the intramolecular appearance will be discussed. As mentioned above, there is a strong dependency of the appearance of the center of the molecule, that is, the Co atom, on the tunneling conditions, due to the originally half-filled Co $3d_z^2$ orbital. A series of ST micrographs of CoTTBPP on Cu(111) in the hexagonal arrangement is shown with varying bias voltages in Fig. 5. The space

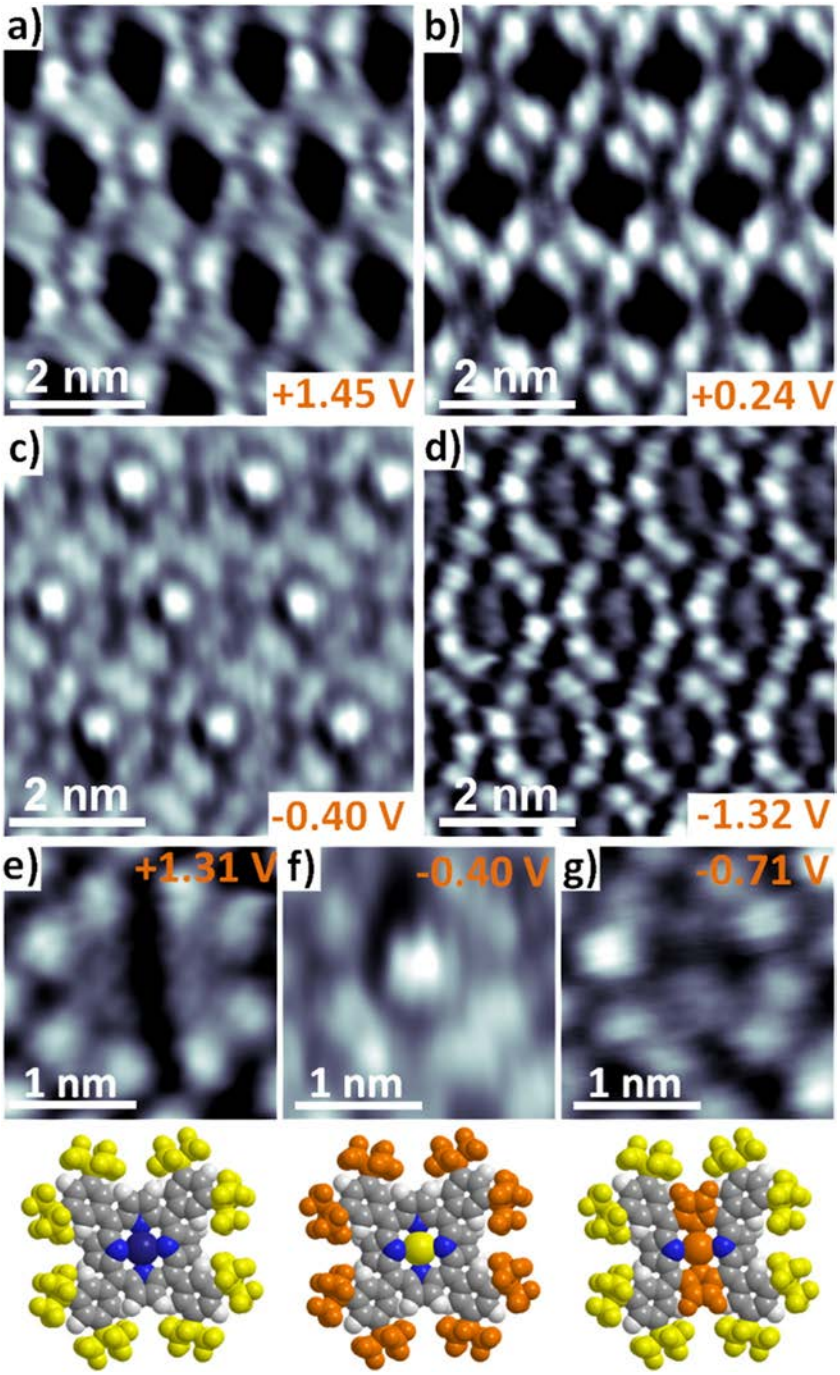

Fig. 5. Bias voltage-dependent appearance of CoTTBPP in the hexagonal phase at RT; the bias voltages are indicated in the figure (I = ~30 pA for all images).

Please cite this article as: M. Stark, et al., Reversible thermally induced phase transition in ordered domains of Co(II)-5,10,15,20-tetrakis-(3,5-di-tert-butylphenyl)-porphyrin..., Surf. Sci. (2015), http://dx.doi.org/10.1016/j.susc.2015.11.024

filling models in the lower part of Fig. 5 illustrate the different bias dependent appearances of the molecule where the orange color indicates a protrusion and the yellow color the most intense protrusion. Common features present at all voltages are the eight protrusions of the *tert*-butyl groups in the periphery of the molecule. This clearly demonstrates that the appearance of the organic periphery of porphyrinoids is to a large extent independent on the tunneling conditions and reflects the actual topography. For the center, however, a pronounced dependency on the bias voltage is observed: Above −0.44 V (Fig. 5d and g) an elongated protrusion is found in the center of the molecules which evolves into an intense protrusion between −0.44 and −0.22 V (Fig. 5c and f). At voltages larger than −0.22 V (Fig. 5a, b and e), the molecules appear with a central depression, i.e. the orbitals with Co(d_z^2) character are (almost) not involved in the tunneling process.

In order to understand this observation, the well-investigated electronic structure of CoTPP on Ag(111) will be briefly recapitulated [57]: CoTPP shows a bias dependent appearance in STM, which is explained by the specific electronic structure of the adsorbate complex. Notably, CoTPP on Ag(111) also shows a saddle shape deformation of the macrocycle. At bias voltages between −0.4 and −0.1 V, CoTPP appears with a central protrusion, which becomes elongated at voltages below −0.4 V. This behavior results from the specific electronic structure of molecule and substrate: due to the interaction with the Ag surface, the singly occupied Co(d_z^2) molecular orbital (SOMO) is shifted below the Fermi energy and is partially filled by electrons from the substrate. The resulting highest occupied molecular orbital (HOMO) of the adsorbate complex still resembles the d_z^2-orbital shape. At low negative bias voltages, this HOMO dominates the appearance in STM, and the intense, central protrusion reflects the d_z^2 character of this orbital. At lower bias voltages, also energetically lower lying orbitals contribute to the appearance in STM. These are orbitals with Co(d_{xz} and d_{yz}) character and orbitals with π character from the aromatic parts of the porphyrin backbone. The result is the elongated protrusion in the center of the molecule. Note that only two pyrrole groups are visible due to the saddle shape deformation of the molecule. To summarize these results for CoTPP on Ag(111), it was shown that the appearance in STM at small negative bias voltages is dominated by a central protrusion at the position of the Co atom, while at positive bias voltages it is dominated by the topography of the organic part of the molecule. Similar results were found for CoTPP on Cu(111) [58]. From these results, we conclude that also for CoTTBPP on Cu(111) the intensity of the Co center dominates the appearance in STM at negative bias close to the Fermi edge via an orbital-mediated tunneling process via a Co(dz^2)-Cu-orbital, induced by molecule–substrate interactions [39,57,59]. This is in very good agreement with corresponding ultra-violet photoelectron spectroscopy (UPS) results for CoTTBPP on Ag(111) [59], indicating that the interpretation obtained for these system is, indeed, valid for CoTTBPP on Cu(111) as well.

4. Conclusion

In summary, we report on the peculiar adsorption behavior of CoTTBPP on Cu(111) with the main finding that a reversible phase transition from a hexagonal arrangement to a herringbone order occurs upon cooling the sample from RT to 180 K. Thereby the herringbone structure exhibits a smaller unit cell, which intuitively is in line with a normal freezing process. We propose that the higher stability of the "expanded" hexagonal structure at RT is due to an entropic contribution, which effectively lowers the free Gibbs energy. This corroborates a recent finding in our group that entropic contributions for "larger" functional molecules around room temperature can play a decisive role and should be generally considered [3]. Within this picture, the increase of the entropic contribution can be realized by translation, rotation and vibration of the molecule as a whole or of its parts, which is indeed reflected in the noisier STM images at RT. The high resolution STM data allowed for the detailed determination of the supramolecular arrangement and the intramolecular conformation. Based on this data, it was found that the intramolecular conformations within the two observed supramolecular arrangements are significantly different, that is, the molecules in the hexagonal phase exhibit a saddle-shape conformation of the macrocycle while the ones in the herringbone order are in a conformation in which all pyrrole groups are oriented to one side of the macrocycle with the phenyl rings oriented to the opposite side. A comparison with literature values of the same CoTTBPP molecule on Ag(111) reveals that the distance of the macrocycle to the substrate is around 1 Å smaller for Cu(111). Thus it is proposed that the molecule–substrate interaction is more attractive on Cu(111) than on Ag(111). Finally, the bias dependent appearance of CoTTBPP on Cu(111) in the hexagonal phase was investigated. Only within a small negative bias voltage window (−0.44 and −0.22 V) a central protrusion is visible and dominates the appearance in STM; it is assigned to an specific orbital-mediated tunneling process via a hybrid Co(d_z^2)-Cu-orbital.

Supplementary data to this article can be found online at http://dx.doi.org/10.1016/j.susc.2015.11.024.

Acknowledgments

The authors gratefully acknowledge the funding by the German Research Council (DFG) through research unit FOR 1878/funCOS, the Cluster of Excellence "Engineering of Advanced Materials" (http://www.eam.uni-erlangen.de) and by the Collaborative Research Center SFB 953 at the Friedrich-Alexander-Universität Erlangen-Nürnberg.

References

[1] J.V. Barth, G. Costantini, K. Kern, Nature 437 (2005) 671.
[2] M. Chen, M. Röckert, J. Xiao, H.-J. Drescher, H.-P. Steinrück, O. Lytken, J.M. Gottfried, J. Phys. Chem. C 118 (2014) 8501.
[3] S. Ditze, M. Stark, F. Buchner, A. Aichert, N. Jux, N. Luckas, A. Görling, W. Hieringer, J. Hornegger, H.-P. Steinrück, H. Marbach, J. Am. Chem. Soc. 136 (2014) 1609.
[4] S. Ditze, M. Stark, M. Drost, F. Buchner, H.-P. Steinrück, H. Marbach, Angew. Chem. Int. Ed. 51 (2012) 10898.
[5] T.A. Jung, R.R. Schlittler, J.K. Gimzewski, Nature 386 (1997) 696.
[6] H.-J. Gao, L. Gao, Prog. Surf. Sci. 85 (2010) 28.
[7] F. Klappenberger, Prog. Surf. Sci. 89 (2014) 1.
[8] J.M. Gottfried, Surf. Sci. Rep. 70 (2015) 259.
[9] W. Auwärter, D. Ecija, F. Klappenberger, J.V. Barth, Nat. Chem. 7 (2015) 105.
[10] M. Chen, X.F. Feng, L. Zhang, H.X. Ju, Q. Xu, J.F. Zhu, J.M. Gottfried, K. Ibrahim, H.J. Qian, J.O. Wang, J. Phys. Chem. C 114 (2010) 9908.
[11] H. Marbach, H.-P. Steinrück, Chem. Commun. 50 (2014) 9034.
[12] J.V. Barth, Annu. Rev. Phys. Chem. 58 (2007) 375.
[13] J.K. Gimzewski, C. Joachim, Science 283 (1999) 1683.
[14] M. Jurow, A.E. Schuckman, J.D. Batteas, C.M. Drain, Coord. Chem. Rev. 254 (2010) 2297.
[15] G. Di Santo, C. Sfiligoj, C. Castellarin-Cudia, A. Verdini, A. Cossaro, A. Morgante, L. Floreano, A. Goldoni, Chem. Eur. J. 18 (2012) 12619.
[16] W. Auwärter, A. Weber-Bargioni, A. Riemann, A. Schiffrin, O. Gröning, R. Fasel, J.V. Barth, J. Chem. Phys. 124 (2006) 194708.
[17] Y. Bai, F. Buchner, I. Kellner, M. Schmid, F. Vollnhals, H.-P. Steinrück, H. Marbach, J.M. Gottfried, New J. Phys. 11 (2009) 125004.
[18] F. Buchner, K. Flechtner, Y. Bai, E. Zillner, I. Kellner, H.-P. Steinrück, H. Marbach, J.M. Gottfried, J. Phys. Chem. C 112 (2008) 15458.
[19] F. Buchner, K. Seufert, W. Auwärter, D. Heim, J.V. Barth, K. Flechtner, J.M. Gottfried, H.-P. Steinrück, H. Marbach, ACS Nano 3 (2009) 1789.
[20] F. Buchner, E. Zillner, M. Röckert, S. Gläßel, H.-P. Steinrück, H. Marbach, Chem. Eur. J. 17 (2011) 10226.
[21] K. Diller, F. Klappenberger, M. Marschall, K. Hermann, A. Nefedov, C. Wöll, J.V. Barth, J. Chem. Phys. 136 (2012) 014705.
[22] S. Ditze, M. Röckert, F. Buchner, E. Zillner, M. Stark, H.-P. Steinrück, H. Marbach, Nanotechnology 24 (2013) 115305.
[23] J.M. Gottfried, K. Flechtner, A. Kretschmann, T. Lukasczyk, H.-P. Steinrück, J. Am. Chem. Soc. 128 (2006) 5644.
[24] M. Stark, S. Ditze, M. Drost, F. Buchner, H.-P. Steinrück, H. Marbach, Langmuir 29 (2013) 4104.
[25] D.E. Barlow, K.W. Hipps, J. Phys. Chem. B 104 (2000) 5993.
[26] M. In't Veld, P. Iavicoli, S. Haq, D.B. Amabilino, R. Raval, Chem. Commun. 13 (2008) 1536.
[27] J. Xiao, S. Ditze, M. Chen, F. Buchner, M. Stark, M. Drost, H.-P. Steinrück, J.M. Gottfried, H. Marbach, J. Phys. Chem. C 116 (2012) 12275.
[28] G. Di Santo, S. Blankenburg, C. Castellarin-Cudia, M. Fanetti, P. Borghetti, L. Sangaletti, L. Floreano, A. Verdini, E. Magnano, F. Bondino, C.A. Pignedoli, M.-T. Nguyen, R. Gaspari, D. Passerone, A. Goldoni, Chem. Eur. J. 17 (2011) 14354.

Please cite this article as: M. Stark, et al., Reversible thermally induced phase transition in ordered domains of Co(II)-5,10,15,20-tetrakis-(3,5-di-tert-butylphenyl)-porphyrin..., Surf. Sci. (2015), http://dx.doi.org/10.1016/j.susc.2015.11.024

[29] J. Brede, M. Linares, S. Kuck, J. Schwöbel, A. Scarfato, S.-H. Chang, G. Hoffmann, R. Wiesendanger, R. Lensen, P.H.J. Kouwer, J. Hoogboom, A.E. Rowan, M. Bröring, M. Funk, S. Stafström, F. Zerbetto, R. Lazzaroni, Nanotechnology 20 (2009) 275602.
[30] F. Klappenberger, A. Weber-Bargioni, W. Auwärter, M. Marschall, A. Schiffrin, J.V. Barth, J. Chem. Phys. 129 (2008) 214702.
[31] M. Stark, S. Ditze, M. Lepper, L. Zhang, H. Schlott, F. Buchner, M. Röckert, M. Chen, O. Lytken, H.-P. Steinrück, H. Marbach, Chem. Commun. 50 (2014) 10225.
[32] H. Marbach, Acc. Chem. Res. 48 (2015) 2649.
[33] F. Buchner, K. Comanici, N. Jux, H.-P. Steinrück, H. Marbach, J. Phys. Chem. C 111 (2007) 13531.
[34] L. Grill, M. Dyer, L. Lafferentz, M. Persson, M.V. Peters, S. Hecht, Nat. Nanotechnol. 2 (2007) 687.
[35] F. Buchner, V. Schwald, K. Comanici, H.-P. Steinrück, H. Marbach, ChemPhysChem 8 (2007) 241.
[36] D.E. Barlow, L. Scudiero, K.W. Hipps, Langmuir 20 (2004) 4413.
[37] L. Scudiero, D.E. Barlow, U. Mazur, K.W. Hipps, J. Am. Chem. Soc. 123 (2001) 4073.
[38] W. Auwärter, A. Weber-Bargioni, S. Brink, A. Riemann, A. Schiffrin, M. Ruben, J.V. Barth, ChemPhysChem 8 (2007) 250.
[39] K. Comanici, F. Buchner, K. Flechtner, T. Lukasczyk, J.M. Gottfried, H.-P. Steinrück, H. Marbach, Langmuir 24 (2008) 1897.
[40] W. Auwärter, K. Seufert, F. Klappenberger, J. Reichert, A. Weber-Bargioni, A. Verdini, D. Cvetko, M. Dell'Angela, L. Floreano, A. Cossaro, G. Bavdek, A. Morgante, A.P. Seitsonen, J.V. Barth, Phys. Rev. B 81 (2010) 245403.
[41] F. Buchner, I. Kellner, W. Hieringer, A. Görling, H.-P. Steinrück, H. Marbach, PCCP 12 (2010) 13082.
[42] F.J. Williams, O.P.H. Vaughan, K.J. Knox, N. Bampos, R.M. Lambert, Chem. Commun. 15 (2004) 1688.
[43] H. Yanagi, H. Mukai, K. Ikuta, T. Shibutani, T. Kamikado, S. Yokoyama, S. Mashiko, Nano Lett. 2 (2002) 601.
[44] T. Terui, S. Yokoyama, H. Suzuki, S. Mashiko, M. Sakurai, T. Moriwaki, Thin Solid Films 499 (2006) 157.
[45] T. Yokoyama, S. Yokoyama, T. Kamikado, S. Mashiko, J. Chem. Phys. 115 (2001) 3814.
[46] L. Grill, I. Stass, K.-H. Rieder, F. Moresco, Surf. Sci. 600 (2006) L143.
[47] T. Kamikado, T. Sekiguchi, S. Yokoyama, Y. Wakayama, S. Mashiko, Thin Solid Films 499 (2006) 329.
[48] F. Moresco, G. Meyer, K.-H. Rieder, H. Tang, A. Gourdon, C. Joachim, Phys. Rev. Lett. 86 (2001) 672.
[49] F. Moresco, G. Meyer, K.-H. Rieder, J. Ping, H. Tang, C. Joachim, Surf. Sci. 499 (2002) 94.
[50] I. Horcas, R. Fernández, J.M. Gómez-Rodríguez, J. Colchero, J. Gómez-Herrero, A.M. Baro, Rev. Sci. Instrum. 78 (2007) 013705.
[51] T. Terui, T. Kamikado, Y. Okuno, H. Suzuki, S. Mashiko, Curr. Appl. Phys. 4 (2004) 148.
[52] L. Smykalla, P. Shukrynau, C. Mende, T. Ruffer, H. Lang, M. Hietschold, Surf. Sci. 628 (2014) 132.
[53] J. Brede, M. Linares, R. Lensen, A.E. Rowan, M. Funk, M. Bröring, G. Hoffmann, R. Wiesendanger, J. Vac. Sci. Technol. A 27 (2009) 799.
[54] L. Zhang, M. Lepper, M. Stark, D. Lungerich, N. Jux, W. Hieringer, H.-P. Steinrück, H. Marbach, PCCP 17 (2015) 13066.
[55] T. Wölfle, A. Görling, W. Hieringer, PCCP 10 (2008) 5739.
[56] G.W. Gribble, E.R. Olson, J.H. Brown, C.H. Bushweller, J. Org. Chem. 58 (1993) 1631.
[57] F. Buchner, K.G. Warnick, T. Wölfle, A. Görling, H.-P. Steinrück, W. Hieringer, H. Marbach, J. Phys. Chem. C 113 (2009) 16450.
[58] A. Weber-Bargioni, W. Auwärter, F. Klappenberger, J. Reichert, S. Lefrançois, T. Strunskus, C. Wöll, A. Schiffrin, Y. Pennec, J.V. Barth, Chem. Phys. Chem. 9 (2008) 89.
[59] T. Lukasczyk, K. Flechtner, L.R. Merte, N. Jux, F. Maier, J.M. Gottfried, H.-P. Steinrück, J. Phys. Chem. C 111 (2007) 3090.

Please cite this article as: M. Stark, et al., Reversible thermally induced phase transition in ordered domains of Co(II)-5,10,15,20-tetrakis-(3,5-di-tert-butylphenyl)-porphyrin..., Surf. Sci. (2015), http://dx.doi.org/10.1016/j.susc.2015.11.024

Reversible thermally induced phase transition in ordered domains of Co(II)-5,10,15,20-tetrakis-(3,5-di-*tert*-butylphenyl)-porphyrinon Cu(111)

Michael Stark [a,b], *Stefanie Ditze* [a,b], *Michael Thomann* [a,b], *Dominik Lungerich* [b,c], *Norbert Jux* [b,c], *Hans-Peter Steinrück* [a,b] *and Hubertus Marbach* [a,b] *

[a] Lehrstuhl für Physikalische Chemie II, Universität Erlangen-Nürnberg, Egerlandstr. 3, 91058 Erlangen, Germany.

[b] Interdisciplinary Center for Molecular Materials (ICMM) Universität Erlangen-Nürnberg, Germany.

[c] Lehrstuhl für Organische Chemie II, Universität Erlangen-Nürnberg, Henkestr. 42, 91054 Erlangen, Germany.

* Email: hubertus.marbach@fau.de

Supplementary Information:

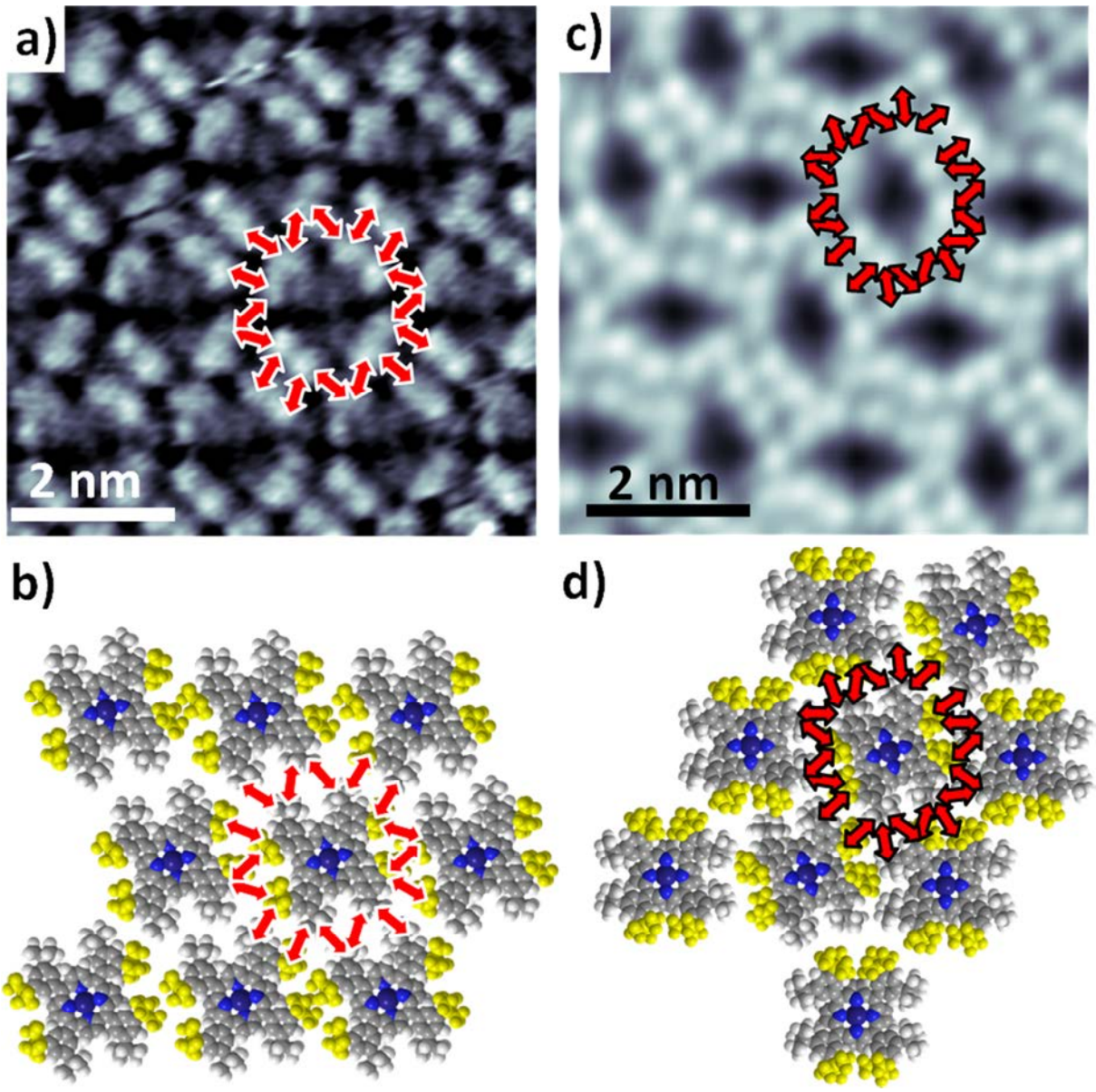

Figure S1: visualizing the postulated interaction pattern of *tert*-butyl groups of neighboring molecules for one molecule in the hexagonal (left column) and the herringbone arrangement (right column). The interactions are indicated on STM images (upper part) and molecular models (lower part) of the two arrangements. ((a): U = +1.31 V, I = 36 pA, T = RT; (b): U = +1.26 V, I = 23 pA, T = 180 K)